SANDIA REPORT

SAND95–1888 • UC–814
Unlimited Release
Printed August 1996

Yucca Mountain Site Characterization Project

Laboratory Investigation of Constitutive Property Up-Scaling in Volcanic Tuffs

Vincent C. Tidwell

Approved for public release; distribution is unlimited.

SF2900Q(8-81)

Laboratory Investigation of Constitutive Property Up-Scaling in Volcanic Tuffs

Vincent C. Tidwell
Geohydrology Department
Sandia National Laboratories
Albuquerque, New Mexico 87185

Abstract

One of the critical issues facing the Yucca Mountain site characterization and performance assessment programs is the manner in which property up-scaling is addressed. Property up-scaling becomes an issue whenever heterogeneous media properties are measured at one scale but applied at another. A research program has been established to challenge current understanding of property up-scaling with the aim of developing and testing improved models that describe up-scaling behavior in a quantitative manner. Up-scaling of constitutive rock properties is investigated through physical experimentation involving the collection of suites of gas-permeability data measured over a range of discrete scales. To date, up-scaling studies have been performed on a series of tuff and sandstone (used as experimental controls) blocks. Samples include a welded, anisotropic tuff (Tiva Canyon Member of the Paintbrush Tuff, upper cliff microstratigraphic unit), and a moderately welded tuff (Tiva Canyon Member of the Paintbrush Tuff, Caprock microstratigraphic unit). A massive fluvial sandstone (Berea Sandstone) was also investigated as a means of evaluating the experimental program and to provide a point of comparison for the tuff data.

Because unsaturated flow is of prime interest to the Yucca Mountain Program, scoping studies aimed at investigating the up-scaling of hydraulic properties under variablly saturated conditions were performed to compliment our studies of intrinsic permeability. These studies focused on matrix sorptivity, a constitutive property quantifying the capillarity of a porous medium.

i

ACKNOWLEDGMENTS

TABLE OF CONTENTS

FIGURES

TABLES

1. INTRODUCTION

Characterization of the heterogeneous, tuffaceous units at Yucca Mountain and the subsequent integration of such information into predictive models for fluid flow and radionuclide transport is a non-trivial matter. Difficulties arise for two basic reasons. First, the quantity of porous medium actually observed and/or sampled is inevitably a minute faction of the entire repository site. This gives rise to the need for models to predict material characteristics at unsampled locations. The second problem relates to the fact that material properties are seldom measured at the same scale as the computational grid block. Therefore, up-scaling models are required to transform information from the available measurement scale to the computational grid block scale. Together these limitations introduce uncertainty into Groundwater Travel Time (GWTT), Total Systems Performance Assessment (TSPA), and Technical Site Suitability (TSS) calculations. For this reason, a research program predicated on systematic physical experimentation has been established to address the second of these problems, property up-scaling.

To date, relatively little effort has been made to incorporate scaling concepts into Performance Assessment (PA) calculations. This, to a large part, is due to the lack of sufficient data for input into up-scaling models and limited experience in employing up-scaling models in applied problems of the nature of the Yucca Mountain Project. Among the PA studies that have addressed up-scaling issues is TSPA-93 (Wilson et al., 1994). In this study, input parameter distributions were scaled from the measurement to the grid block scale using a functional relation based on the square root of the correlation length scale/bed thickness ratio (Dagan, 1989). Subsequently, Rautman and Robey (1993) proposed an up-scaling model for use in PA calculations based on adaptive gridding (i.e., computational grid blocks are defined in such a way that 'neighborhoods' of porous media with like hydraulic properties are formed in efforts to minimized variability within discrete grid blocks) of heterogeneous 2- or 3-D rock property fields followed by spatial averaging of the fine scale data in each grid block. In recent GWTT calculations, up-scaling has been accomplished using power law averaging where the power coefficient was predicated on results of numerical experimentation (McKenna and Rautman, 1996).

In this section we lay the foundation for investigating up-scaling behavior of heterogeneous, porous media. We begin with a discussion of the problem to be addressed by this program followed by a brief overview of the research program and objectives. A review of pertinent up-scaling literature is then given. The review looks at both theoretical up-scaling models and the results of laboratory, field, and numerical up-scaling studies.

1.1. Purpose

Problem Statement

The continuum hypothesis of rational mechanics forms the basis of most subsurface flow and transport models. In this approach, the time and space dependence of field variables is expressed in the form of differential balance equations formulated on the precepts of mass, momentum, and energy conservation. Specific characteristics of a unique porous formation are incorporated (at least in part) into the balance equations in the form constitutive properties. The continuum hypotheses requires the constitutive properties to form a continuum; that is, vary continuously in time and space. In this sense, the fine scale variability inherent to geologic material must be effectively "smoothed out". To achieve this, constitutive properties are related not to the physical characteristics at discrete points within the porous media but to a locally averaged spatial domain.

Much difficulty would be circumvented if the constitutive variables could simply be measured at the computational grid block scale (or analysis support). However, due to technological and

computational constraints this can be rarely accomplished. For this reason, averaging rules or up-scaling models are required for transferring information at the available scale (or support) to the computational grid block scale. Again, if the correct averaging process of the particular variable under study were known the problem would be much alleviated. For example, the average porosity of a volume is simply the arithmetic average of the porosities of all the samples that constitute it. The simple arithmetic averaging process holds true for additive variables such as saturation and more generally porosity. Unfortunately, many other constitutive properties are not additive; that is the up-scaling process is not merely dependent on the volume fraction of the phase present but other characteristics of the medium as well (e.g., connectivity of the phase). It is the nature of this averaging or up-scaling process that is of interest here.

Implicit to this approach is the idea that the porous media posses a discrete hierarchy of scales (Cushman, 1990). In other words, the media can be classified in terms of discrete pore, laboratory, formation, and regional scales (Dagan, 1986) or alternatively microscopic, macroscopic, megascopic, and gigascopic (Haldorsen, 1986) scales, according to which the sample and/or analysis support is defined. Where such discrete hierarchy is lacking, theory to accommodate continuously evolving heterogeneity and its influence on the up-scaling process is necessary (Wheatcraft and Tyler, 1988, Neuman, 1990).

Project Overview and Justification

A number of theories, representing a wide diversity of approaches, have been proposed for "scaling-up" measurements; however, physical data to support these theoretical models are sparse and limited in scope (see Sections I.B. and I.C. below). Supporting physical data are needed to improve confidence in our existing up-scaling models, to bound their range of applicability relative to limiting assumptions, and to explore other readily available measures that may be diagnostic of up-scaling behavior. For these reasons, a research program founded on systematic physical experimentation has been established to challenge and imporve current understanding of up-scaling behavior. The experimental program involves the collection of gas permeability data at a number of discrete sample supports, thereby providing a direct means of investigating scaling behavior. Factors influencing scaling behavior (i.e., characteristics of the sampling strategy and porous medium) are varied in a systematic fashion to isolate relative contributions to overall scaling behavior. The acquired data are used to explore empirical up-scaling relationships and directly challenge existing up-scaling theory.

Objectives

The basic objective of this research program is to enhance fundamental understanding of up-scaling behavior through systematic physical investigation. Specifically, we are pursuing answers to the following basic questions:

- Do constitutive properties scale in a predictable and quantifiable manner; and if so, what is the nature of the scaling behavior?
- What characteristics of the geologic medium influence up-scaling behavior?
- What are the appropriate measures of up-scaling behavior (i.e., are the mean and covariance function sufficient or is there need for additional information and if so, what)?

Through improved understanding of the up-scaling process we hope to establish tighter bounds on predictions of intrinsic matrix permeability up-scaling behavior, thereby benefiting YMP PA calculations.

1.2. Theoretical Up-Scaling Models

There are a wide range of theoretical models that have been proposed for up-scaling constitutive properties. In general, such models are employed to 1) up-scale or average a suite of data to produce a single effective property value, or 2) up-scale the first two (in some cases first three) moments of the multivariate property distribution. The later of these cases is necessary when simulation of a heterogeneous property field is desired. Here, a range of up-scaling techniques are reviewed that can be employed in one or the other, or both of the modes discussed above.

Simple averaging rules (arithmetic, geometric, and harmonic) are probably the most commonly employed means for modeling up-scaling behavior. However, these averaging rules are only valid for a narrow range of aquifer/reservoir conditions. For example, Warren and Price (1961) found, by means of numerical simulation, that the geometric mean provides a good estimate of the effective permeability for a wide range of univariate distribution models when the permeability field is spatially uncorrelated. The geometric mean k_g is given by

$$k_g = \exp[1/n \sum_{i=1}^{n} \ln(k_i)] \tag{1.1}$$

where n is the sample set size and k_i are the measured permeability values. Because the geometric mean is sensitive to the low values of the distribution, a jth Winsorized mean (ranking all data then discarding the high and low values) is suggested by Jensen (1991) to reduce effects of outlier values. By manipulation of the governing flow equations, the effective permeability for an infinitely stratified system can be found. Where flow is oriented parallel to the stratification the arithmetic mean k_a, given by

$$k_a = \sum_{i=1}^{n} k_i d_i / d \tag{1.2}$$

where d_i is the thickness of a discrete bed and d is the total thickness of the system, yields the effective permeability. When flow is oriented normal to stratification the harmonic mean k_h, given by

$$k_h = \frac{d}{\sum_{i=1}^{n} d_i / k_i} \tag{1.3}$$

represents the appropriate averaging rule. In general, $k_a > k_g > k_h$.

Unfortunately, most natural systems lie somewhere in-between these extremes as do the appropriate up-scaling rules. The power law average provides a convenient means of handling this wide range of behavior. The power law average k_p is given by:

$$k_p = [1/n \sum_{i=1}^{n} k_i^{\omega}]^{1/\omega} \tag{1.4}$$

where ω is the power coefficient. With this approach the selection of an appropriate up-scaling rule is predicated on finding the power coefficient. Where flow is oriented parallel or normal to an infinitely stratified system ω is simply set to 1 or -1 to yield the arithmetic and harmonic averages, respectively. Alternatively, the geometric mean is defied as $\omega=0$, although Equation 1.4 must

3

undergo a limited expansion as it is currently defined (Deutsch, 1989). In general, empirical methods are used to determine ω. Empirical approaches for calculating ω for bimodal sand-shale sequences are given by Journel et al. (1986) and Deutsch (1989). These approaches were later extended by Desbarats (1992) for the case of log-normally distributed data.

Although geologic media do not always scale according to a simple arithmetic or harmonic average, these averaging rules can be used to help set physical limits on the effective permeability. Cardwell and Parsons (1945) establish bounds on the effective permeability for a 2-D isotropic system where infinite stratification is lacking. By conceptualizing the hydraulic conductivity field as a network of electrical resistors, Cardwell and Parsons (1945) recognized that the maximum effective permeability (k^+) is found by taking the arithmetic average of each column and then taking the harmonic mean of the arithmetic means. For flow in the same direction, the minimum bound on effective permeability (k^-) is found by reversing the arithmetic and harmonic averaging. Using these bounds (k^+ and k^-) Leloc'h (1989) and Duquerroix et al. (1993) developed expressions for the effective permeability for heterogeneous isotropic and anisotropic media, respectively.

Estimation of effective permeability for sand-shale formations is of particular concern in the petroleum industry. If the permeability of such systems can be treated as a binary distribution, the streamline (or stream tube) method (Haldorsen and Lake, 1984) can be used to calculate the effective permeability. Haldorsen and Lake (1984) used information on shale size and position to condition Monte Carlo simulations to generate realizations of sand-shale reservoirs. Using these realizations, vertical and horizontal effective permeabilities were calculated based on the streamline (or stream tube) concept. In this approach, a functional relationship between the effective permeability and the sand permeability, flow path tortuosity, and flow path geometry was developed. Begg and King (1985) subsequently modified the method to remove length and aspect ratio restrictions on the shale bodies. The method was further modified for application to 3-D problems and for layered media by Begg et al. (1985). Kasap and Lake (1990) used a similar approach to estimate the full tensorial effective block permeability for cross-bedded systems.

For an unbounded, heterogeneous medium characterized by a strong variance, Effective Media Theory (EMT) provides a means of calculating the effective permeability (Dagan 1979; 1981). In EMT the heterogeneous medium, conceptualized as a collection of randomly distributed homogenous blocks of different permeability, is replaced by a single isolated inclusion with permeability k_i, embedded in an unbounded homogenous medium of unknown permeability k_u. If the inclusion is taken to have a simple shape (i.e., sphere or ellipse) an analytic solution for the resulting head distribution can be found (which must be equivalent to that of the original heterogeneous medium). From this, the effective permeability k_{eff} of the medium can then be found by employing the self consistency requirement (i.e., the permeability of the matrix surrounding the inclusion k_u is equal to the effective permeability k_{eff}). For a spherical inclusion,

$$k_{eff} = 1 / m [\int_{\infty}^{0} \frac{f(k_i)dk_i}{(m-1)k_{eff} + k_i}]^{-1} \qquad (1.5)$$

where $f(k_i)$ is the permeability distribution function and m is the dimension of the flow domain. It should be noted that EMT is not constrained by assumptions concerning the magnitude of the variance of the permeability distribution; however, the volume over which k_{eff} is calculated must be much larger than the integral scale times the square of the coefficient of variation. Dagan (1989) extended this work to anisotropic media through the use of elliptical inclusions. Applications of this method can be found in Dykaar and Kitanidis (1992b) and Desbarats (1987).

Stochastic methods (Bakr et al., 1978; Gelhar, 1986; 1993) have received considerable attention relative to their use in calculating effective media properties. Application of such methods requires

4

an unbounded domain and uniform flow (i.e., the extent of the domain and the characteristic scale of the flow nonuniformity are much larger than the correlation length of the medium). The permeability distribution must also be a weakly stationary and ergodic random variable with a relatively small variance (just how small is still an issue of considerable debate). In this approach, the aquifer/reservoir is viewed as an ensemble of homogenous, isotropic blocks whose spatial distribution is fully characterized by its first two moments. Using small perturbation, first-order approximation of the governing stochastic differential equation, an expression for the effective permeability has been obtained. Gutjahr et al. (1978), extending the earlier work of Matheron (1967), found the effective permeability of a heterogeneous, isotropic medium to be:

$$k_{eff} = k_g[1 - \sigma_y^2 / 2] \tag{1.6}$$

in one dimension,

$$k_{eff} = k_g \tag{1.7}$$

in two dimensions, and

$$k_{eff} = k_g[1 + \sigma_y^2 / 6] \tag{1.8}$$

in three dimensions, where k_g and σ_y^2 are the geometric mean and variance of the natural log permeability distribution. An interesting result of this work is the dependence of k_{eff} on the dimensionality of the flow domain. Gelhar and Axness (1983) extended this work to a 3-D statistically anisotropic medium. In this case, the effective permeability can be expressed as:

$$k_{ii} = k_g\left[1 + \sigma_y^2(1/2 - g_{ii})\right] \tag{1.9}$$

where ii designates the components of the permeability tensor and g is a geometric factor accounting for the degree of anisotropy and orientation of flow relative to the principal permeability axes. For the case of infinite stratification and flow parallel or normal to the bedding, Equation 1.9 reduces to that of an arithmetic and harmonic mean, respectively. Indelman and Abramovich (1994) have recently shown g_{ii} to also be a function of the shape of the covariance function. Using the small perturbation approach, Dagan (1982) calculated the effective permeability for the case of a slowly varying head gradient in time and space (i.e., non-uniform flow).

A popular method used to investigate up-scaling from the microscopic to the macroscopic scale is the volume averaging method (Anderson and Jackson, 1967; Whitaker, 1967; Bear and Bachmat, 1990). Up-scaling is achieved by integrating the governing flow equations and boundary conditions at the pore scale over the macroscopic porous media. This process can be applied to sequentially larger scales assuming a discrete hierarchy exists. Where all higher moment terms arising from the averaging of the balance equations are retained, an infinite set of balance equations will be encountered. Treatment of the resulting set of equations is impractical both conceptually and computationally, hence closure must be sought using various assumptions, approximations, and order of magnitude analysis. The specific level of equation where closure is made will ultimately govern the level of accuracy of the model (Tompson and Gray, 1986).

Following the Taylor-Aris method of moments, Kitanidis (1990) derived a governing system of equations for the effective permeability of a periodic porous medium. For an n-dimensional flow domain, n uncoupled partial differential equations are solved for n unknown auxiliary functions

subject to periodic boundary conditions. Integration of the ensuing auxiliary functions over the volume of interest then yields the desired effective permeability. A numerical-spectral approach has been proposed by Dykaar and Kitanidis (1992a) to solve the resulting set of equations. Key assumptions include a periodic media, periodic boundary conditions, and gradually varying flow. In general, these assumptions are much less restrictive than that imposed by other approaches (e.g., stochastic, EMT).

Homogenization methods (Mei and Auriault, 1989; Ene, 1990) offer an alternative means of calculating the effective permeability for media exhibiting periodic structure. The concepts behind homogenization are essentially those of perturbation theory. Consider a two-scale system where the characteristic dimension of the macroscale structure T is much larger than the period τ of the fine scale structure. As the permeability is periodic so will be the associated dependent variable. For this reason the dependent variable μ is expanded by an asymptotic expansion

$$u^{\varepsilon}(x) = u^{0}(x,y) + \varepsilon u^{1}(x,y) + \varepsilon^{2} u^{2}(x,y) + ... \qquad (1.10)$$

where $\varepsilon = \tau/T$. Next, u^{ε} is substituted into the governing flow equation and like powers of ε are collected, which is usually truncated at ε^{2}. The zeroth order equation is solved and the solution inserted into the first order equation and solved. The second order equation is then averaged over a cell to form the macroscopic law. This provides the scaled forms of the governing equation and associated constitutive variables.

The renormalization group method is a statistical mechanics approach that was originally developed to determine the phase transition behavior of systems near a critical point. Real space renormalization group methods (as opposed to momentum space) provides a direct analogy to a lattice or network model of conduction (percolation models) and have found application in the up-scaling of geologic materials (King, 1989; Mohanty and Sharma, 1990; Piggott and Elsworth, 1992; Hinrichsen et al., 1993). Its implementation in real space is a recursive process of scale transformation in which features at a fine scale are integrated over to produce an effective property at successively larger scales. Transformation from one scale to another is generally accomplished through the analogy with equivalent resistor network models. Advantages include ability to handle large variances and multimodal systems. Disadvantages primarily relate to difficulties in achieving a suitable transfer function for complex systems (e.g., anisotropic systems).

Spatial averaging rules were developed in the mining industry (Journel and Huijbregts, 1978; Clark, 1977; Parker, 1979) to assist in predicting the ore grade of large selective mining units from small scale core data. The primary assumption of this approach is that up-scaling follows a simple arithmetic average and hence the mean or effective value is constant regardless of the support. According to this assumption the second moment can be calculated by a simple volume average of the point support covariance function (or semi-variogram function) at the grid block scale

$$C_{v}(h) = 1/V^{2} \int\limits_{V} dx \int\limits_{V} C_{o}(x - x') dx' \qquad (1.11)$$

where $C_{o}(x-x')$ is the point covariance function, V is the volume over which the spatial average is performed, h is the separation vector, and $C_{v}(h)$ is the volume averaged covariance function. The assumption of arithmetic up-scaling restricts application to additive properties such as porosity, saturation, and bulk density.

The simple spatial averaging approach was extended to the case of a harmonic averaging process by Desbarats (1989) and then later generalized to the spatial power-average (Desbarats, 1992; Dimitrakopoulos and Desbarats, 1993; Desbarats and Bachu, 1994). Assuming a

6

multivariate log-normal distribution with relatively low variance, the ensemble mean and variance block permeability $ln\ k_V$ are,

$$E[\ln k_V] = k_g + (\omega / 2)\gamma_{avg}(V,V) \qquad (1.12)$$

$$Var[\ln k_V] = \sigma_y^2 - \gamma_{avg}(V,V) \qquad (1.13)$$

respectively; where ω is the power coefficient and $\gamma_{avg}(V,V)$ is calculated numerically as the average value of $\gamma(h)$ (sample semi-variogram function for the fine scale data) when the extremities of the separation vector h independently sweep the block V. By assuming $\ln k_V$ is Gaussian, Equations 1.12 and 1.13 can be rewritten as:

$$E[k_V] = k_\omega \exp\left[0.5(1-\omega)\left(\sigma_y^2 - \gamma_{avg}(V,V)\right)\right] \qquad (1.14)$$

$$Var[k_V] = E[k_V]\left(\exp[\sigma_y^2 - \gamma_{avg}(V,V)] - 1\right) \qquad (1.15)$$

where $k_\omega = \exp[k_g + \omega(\sigma_y^2/2)]$. In this way, both the ensemble mean and variance block permeability are a function of the averaging volume as represented by $\gamma_{avg}(V,V)$. An interesting result is that the expression for the ensemble mean block permeability was found to be similar to that of the effective permeability derived by Gelhar and Axness (1983) for the case of an infinite field.

Rubin and Gomez-Hernandez (1990) proposed a method to up-scale permeability measurements observed at a given scale to grid block permeability values for arbitrary block sizes. The approach is predicated on the assumption of a multivariate log-normal distribution for the fine-support permeabilities. Using small perturbation methods and defining the block permeability as the ratio of the volume-averaged flux to the volume averaged head gradient the spatial distribution of the up-scaled blocks is derived, conditioned on the point measurements. Indelman and Dagan (1993) suggest a similar up-scaling approach; however, they adopt the rate of dissipation of energy (E = -q · dψ) as a basic random function instead of the pressure head ψ and the velocity q separately. The necessary conditions for flow in the up-scaled formation are; 1) the first two moments of the up-scaled E distribution must approach that of the point-scale E, and 2) the global response of the flow system must be the same for both the up-scaled block property field and point-scale property field.

Up-scaling can also be approached by purely numerical means. The inverse method (Freeze, 1975; Ababou et al., 1989; Bachu and Cuthiell, 1990; Desbarats, 1987; Kossack et al., 1990) involves numerically solving the steady-state flow equation for a particular permeability field in a simple domain. Realizations of the permeability field are generated by statistical methods which are restricted to normal, log-normal, or binary distributions and specific covariance functions. Generally, constant head boundaries are prescribed on two faces of the computational element while no-flow boundaries are specified on the other faces. However, other boundary conditions and flow geometries may be applied to minimize dependence of the calculated effective properties on characteristics of the flow field (Lasseter et al., 1986). The statistical moments of the up-scaled permeability field can then be extracted though Monte Carlo simulations or from a single realization provided that the ergodicity requirements are satisfied. Use of inverse methods in applied up-scaling problems is limited due to the excessive, sometimes insurmountable computational requirements.

7

A central issue to up-scaling is the selection of an appropriate scale or support at which to measure and/or calculate an effective media property. In general, some notion of an representative elementary volume (REV) is offered as a guide to defining the appropriate support (Hassanizadeh and Gray, 1979; Bear, 1972). The classical definition of an REV requires indifference of its geometrical character regardless of the physical nature of the effective property (i.e., permeability or saturation) or its position in time or space. The REV is selected such that it is large with respect to the fine scale detail of the porous medium but small enough to qualify as a mathematical neighborhood about its centroid at the macroscopic scale. The REV concept has been recognized as being unnecessarily restrictive and impossible to physically define or verify (Baveye and Sposito, 1984). As an alternative, Baveye and Sposito (1984) introduce the relativist concept in which macroscopic effective properties are defined as convolution products of microscopic properties with weighting functions that represent appropriate measuring instruments. In this way, volume integration is defined operationally in terms of the sample size, rather than a REV. Cushman (1984, 1986) builds on the relativist approach in an effort integrate the concepts of measurement, scale, and heterogeneity. In these papers the concept of an ideal instrument is introduced. An ideal instrument is defined by its ability to filter the effects of high frequency noise (heterogeneity) on a volume averaged property while preserving the signature of low frequency structure.

In general, each of the aforementioned theories assume the porous media exhibits a discrete hierarchy of scales (i.e., a finite correlation length exists). However, it has been realized that not all porous media behave in such manner, but rather exhibit a continuous hierarchy of scales or evolving heterogeneity (i.e., infinite correlation length). While there are many ways that heterogeneity can evolve (as a function of scale), the most convenient conceptual model is fractal. A number of researchers have found geologic materials to display fractal characteristics. Fractal behavior was noted for the case of sandstone porosity by Katz and Thompson (1985), soil properties by Burrough (1983), fracture networks by Barton and Larsen (1985), and reservoir porosity by Hewett (1986). Fractal concepts have also been used to explain the basic transport processes of diffusion (Sapoval et al., 1985) and macroscopic dispersion (Hewett, 1986; Wheatcraft and Tyler, 1988). Neuman (1990; 1994) provides one of the few instances in which fractal concepts have been used to model permeability up-scaling.

1.3. Up-Scaling Studies

A number of physical and numerical investigations have been conducted to study up-scaling of constitutive properties. In general, the physical experiments are limited by the number of samples collected and/or by the number of different sample supports investigated. Another common problem is the use of different measurement techniques at different sample supports, which makes it difficult to determine whether the measured behavior is due to up-scaling or simply differences in the sampling technique. A problem common to both the physical and numerical studies is the lack of systematic experimentation; that is, the studies are limited to a single rock type, soil, or heterogeneous random field.

Physical Investigations

Differences in moments of probability distributions of soil properties measured at multiple scales have been observed by a number of researchers. For example, Sisson and Wierenga (1981) measured steady-state infiltration rates using three infiltrometers of 5-, 25-, and 127-cm inside diameter at a field site near Las Cruces, New Mexico. In this study they found the mean steady-state infiltration rate to increase with the size of the infiltration ring. In a similar study, Parker and Albrecht (1987) measured the saturated hydraulic conductivities on laboratory cores of three different volumes (92, 471, and 1770 ml) taken at two depths in different soil layers along closely, spaced parallel transects. The saturated hydraulic conductivity was noted to increase with

8

increasing sample volume; however, structural disturbance (i.e., increase in sample bulk density) of the samples during coring may be to blame for this behavior. In contrast to these studies, Anderson and Bouma (1973) and Bouma (1983) reported the mean hydraulic conductivity to decrease by a factor of 7 as core length increased by a factor of 3. Although these studies yield different behavior in the sample mean, the sample variance was noted to decrease with increasing sample support in all three cases.

Flint et al. (1994) investigated the behavior of matrix sorptivity (parameter that describes the rate of uptake of water by a porous medium without gravitational effects) as a function of sample support. Sorptivity was calculated from measurements made on core samples of two different sizes (3.2 and 6.1 cm diameter), and from field experiments in boreholes using neutron logs and a field-scale Mariotte system. Measurements were conducted in nonwelded tuff and fractured welded tuff at Yucca Mountain, Nevada. Results of the study found the mean sorptivity for both sizes of core to be virtually identical. Difficulties in comparing the core-scale data to field data were realized due to the presence of fractures in the boreholes that provide an increased, but unknown, surface area for imbibition.

Permeability data for sedimentary and crystalline rocks collected from sixty-seven locations world wide were compiled by Clauser (1992) and Brace (1984). Sample supports range from centimeter-sized core samples to drift ventilation studies on 12 km long adits. The data were found to increase in average permeability by about three orders of magnitude from the laboratory to the borehole scale while at larger scales the permeability was noted to plateau. Similarly, an increase in permeability of up to four orders of magnitude was found between laboratory and bulk permeability values measured on clay beds at a hazardous waste site in Louisiana (Hanor, 1993). The apparent increase in permeability is attributed to the presence of fractures and/or other preferential flow paths that tend to dominate the permeability of otherwise relatively impermeable materials.

In contrast to these studies, Keller et al. (1989) found the bulk conductivity of Warman till (a clayey, low permeability till) to be consistent over a wide range of sample supports. In this study, conductivity estimates were derived from the analysis of the downward propagation of seasonal water table fluctuations, laboratory consolidation and permeameter tests, and slug tests. The difference between these results and those of Hanor (1993) is attributed to the lack of a conductive preferential flow system.

Henriette et al. (1989) performed laboratory experiments to determine whether the effective permeability of sandstone and limestone blocks could be reconstructed from a series of small scale core samples. The study began with the effective permeability being measured on each block (15 x 15 x 50 cm). The blocks were then cut into three intermediate blocks measuring 15 x 15 x 15 cm, and the permeability of each block measured. Finally, each of the intermediate blocks were cut into 100 small plugs which were subsequently tested. The effective permeability of each block was then calculated numerically from the intermediate and plug data. In general, good agreement (within 15% in all but one case) was found between the measured and calculated values. Arithmetic, harmonic, and geometric averages were also used to calculate the effective permeability of the blocks. The best results were found in the case of the arithmetic average. In this experiment, it was calculated that approximately 21% of the original rock material was lost due to cutting and coring of the sample following the initial effective permeability measurements.

Several large field studies have been conducted in which hydraulic conductivity data was collected at multiple sample supports. Of particular importance are the Cape Cod site (Hess et al., 1991), the Twin Lakes site (Killey and Moltyaner, 1988) and the Mobile site (Molz et al., 1990). At the Cape Cod site, characterized by a sand and gravel aquifer, hydraulic conductivity measurements were made via a laboratory permeameter, borehole flow meter, an aquifer test, and tracer test. The mean hydraulic conductivity measured with the flow meter was consistent with the

9

aquifer testing and tracer test results, but was approximately three times larger than the mean for the permeameter tests. The variance associated with the flow meter tests was also noted to be double that associated with the permeameter measurements even though the flow meter interrogated a large aquifer volume. This apparent discrepancy was explained by the fact that the permeameter measurements were oriented normal to aquifer stratification while the flow meter tests were oriented parallel to stratification. At the Twin Lakes site, grain size analysis, borehole dilution tests, and single well response tests were used to estimate the hydraulic conductivity at multiple locations within a fine to medium sand fluvial aquifer. In this test no definitive up-scaling trends were noted in the primary summary statistics of the measured hydraulic conductivity. In contrast to these studies, evidence of scale-dependent hydraulic conductivity were noted at the Mobile site. Molz et al. (1990) measured the hydraulic conductivity of an inter-bedded sand and clay aquifer using large and small scale pump tests and borehole flow meter tests. In this study, the mean hydraulic conductivity was found to remain relatively constant while the sample variance was noted to decrease by more than a factor of four as sample support was increased. Another important finding of each of these field tests was that the geologic media in each case appear to satisfy the most important assumptions of stochastic theories; stationarity of the hydraulic conductivity function.

Numerical Investigations

Probably the first application of numerical techniques to the study of up-scaling behavior was made by Warren and Price (1961). In their study, three-dimensional, statistically uncorrelated permeability fields were simulated from a known distribution with a small variance and the effective permeability calculated for stead and transient flow conditions. The key finding of the study was that a heterogeneous aquifer could be approximated by a homogenous one, using the geometric mean of the permeability distribution. Freeze (1975) building on the work of Warren and Price (1961) showed that the degree of uncertainty associated with hydraulic head predictions increases as the degree of heterogeneity of the hydraulic conductivity increases.

Desbarats (1987) employed a numerical approach to study the up-scaling behavior of a fluvial sand/shale reservoir (binary permeability distribution was assumed). Based on numerical simulations of spatially correlated permeability fields, effective permeability calculations were found to depend on the shale volume fraction, the spatial covariance function, and the dimensionality of the flow system. Numerical simulations were also found to compare fairly well with predictions of the EMT (Dagan, 1979), while comparisons with the stream tube approach (Begg and King, 1985) were found to give accurate results only for low shale fractions.

Gomez-Hernandez and Gorelick (1989) employed a stochastic simulation approach to investigate the influence of spatial variability in permeability and recharge on the estimation of effective aquifer properties. In this study, Monte Carlo realizations were generated of a two-dimensional, unconfined aquifer with groundwater pumping. Nine different cases were studied in which different correlation lengths of the permeability, conditional simulations, and recharge distributions were used. Using power-averaging to estimate the effective permeability, $\omega=-0.4$ was found to best reproduce the modeled head values for the unconditional simulations while $\omega=-0.2$ gave the best results for the conditional simulation case. The implication of this work is that the effective permeability may be calculated only for a particular set of wells, pumping rates, etc.; hence, specification of an effective parameter uniquely defined only by characteristics of the geologic medium may not always be possible. Ababou and Wood (1990) comment on this paper and offer an expression relating sensitivity of the effective permeability to pumping conditions and the correlation length scale.

Numerical studies have also been performed to investigate the effects of shale clasts of variable size, geometry, orientation, and distribution, embedded in a homogenous and isotropic sand matrix on effective permeability calculations (Bachu and Cuthiell, 1990). Simulations were conditioned

10

on data obtained by digitizing cores from a heavy oil reservoir. The effective permeability calculated for steady-state conditions was found to be dependent primarily on the clast fraction and permeability contrast between the clasts and matrix, while the shape, size, geometry and orientation of the shale clasts were found to produce second order effects on the effective permeability. For steady-state flow conditions, the effective permeability was found to follow a spatial power-average model; however, for transient flow, the effective permeability was found to be time and flow dependent, with asymptotic behavior toward the steady-state effective value.

Durlofsky (1992) performed a number of numerical simulations to investigate two basic approaches for assigning coarse-scale grid block permeabilities from highly detailed fine-scale data. The two approaches were sampling, where the permeability of the coarse-scale grid block is simply defined as the fine-scale permeability measured at the grid block center (no averaging performed), and up-scaling, where the coarse scale permeability is calculated from some average (a numerical inverse technique was employed in this study) of the fine-scale data. Two types of up-scaling were considered, global (single effective value assigned to entire flow domain) and local (different values assigned to each grid block). Single phase flow through two-dimensional, spatially correlated permeability fields was simulated. The primary variables evaluated in the study were the correlation length and the variance of the log permeability. For flow conditions driven by smoothly varying boundary conditions, assignment of grid block permeabilities by sampling was found to be more accurate than global up-scaling where the length of a typical grid block is less than the correlation length of the permeability field, regardless of the variance. For flow driven by source terms, more resolution is required hence global up-scaling is preferred to the sampling approach, particularly at high variances. Local up-scaling is shown to be preferable to either sampling or global up-scaling in essentially all cases.

2. APPROACH

The approach adopted in this experimental program is different in two important aspects relative to other up-scaling studies. First, up-scaling of gas permeability is investigated physically using a technique that is non-destructive and consistent regardless of sample support. Second, experiments are performed on a variety of samples that are carefully selected so as to isolate factors believed to influence property scaling and hence allow investigation of their relative contribution to overall up-scaling behavior. By approaching the investigation through controlled, systematic experimentation, data are generated to test current understanding and treatment of up-scaling behavior.

2.1. Physical Experimentation

In this section we describe the methods and approach taken to physically investigate up-scaling behavior of intrinsic permeability. We begin by defining requirements for selecting the experimental system and then introduce a method that meets these criteria. A detailed discussion of the experimental system that has been constructed and how it is used to acquire multi-scale data is then given. We then turn our attention to the approach taken to investigate the influence of various controls (i.e., sampling strategy, geologic characteristics) on up-scaling behavior.

Method Selection

Physical investigation of up-scaling behavior has been limited primarily by the lack of a method for collecting data by consistent means at a variety of sample supports. In general, experimentalists have had to rely on destructive measurement techniques and/or techniques that accomplish the desired measurements in different ways (e.g., comparison of core data, with slug tests and large-scale pump tests). Another limiting factor is the need for relatively large data sets to achieve reliable results. As such, criteria for selecting an experimental method include measurement that is rapid, inexpensive, and non-destructive. In addition, data must be collected in a consistent manner regardless of sample support in order to isolate up-scaling effects. That is, measurements must be made with similar physical boundaries and flow geometry at each scale. Data must also be acquired with a high level of precision that is consistent across sample supports. One instrument, known as the gas permeameter, was found to meet these criteria.

The gas permeameter was originally developed in the petroleum industry (Dykstra and Parsons, 1950; Eijpe and Webber, 1971) for rapid field and laboratory acquisition of gas permeability data. Two basic permeameter designs exist. In one, gas is injected into the test media at a fixed pressure and the resulting steady-state mass flux rate is measured (or steady-flow is established and the resulting pressure measured). Using information on the injection pressure, mass flux rate, and flow geometry (defined by the tip seal through which gas is injected into the test media) the gas permeability is calculated. In such systems, gas is supplied through either a canister of compressed gas (Sharp et al., 1994) or a small hand-operated piston (glass ground syringe) (Davis et al., 1994). The piston-based system has the advantage that it is compact and supplies gas at a low injection pressure which makes it well suited for field investigation of unconsolidated to poorly-consolidated sediments. However, the low injection pressure limits its application to materials with permeabilities above 5×10^{-13} m^2 (0.5 darcys) while the displacement volume of the piston places limits on the scale of measurement achievable by the instrument. Systems using compressed gas are best suited for relatively well consolidated materials while having the capability to test materials with permeabilities as low as 1×10^{-15} m^2 (one millidarcy). The second design is based on a pressure-decay technique (Jones, 1972; 1992). Measurements are made by injecting gas into the sample from a tank of known volume and initial pressure. Based on the pressure decay profile, the gas permeability (corrected for gas-slippage and inertial effects) can be

12

calculated. Advantages of this method include rapid measurement for a wide range of permeabilities; however, sizing of the supply tank to satisfy a range of measurements scales and sample permeabilities would present difficulties.

Over the last ten years the gas permeameter has found wide spread use in the characterization of the spatial distribution of permeability in outcrops as well as rock cores and slabs. A few examples are given here to demonstrate various applications of the gas permeameter as well as the wide range of geologic materials that have been investigated. Gas permeameter studies of the eolian Page Sandstone of northern Arizona identified a distinct correlation between stratigraphic architecture and measured gas permeability (Goggin et al., 1986; Chandler et al., 1989). In this study both depositional and diagenetic controls were noted to influence permeability variations. Similar results were noted for permeameter studies conducted in the fluvial Sierra Ladrones Formation of central New Mexico (Davis et al., 1993). Dreyer et al. (1990) used outcrop gas permeameter measurements to quantify geometrical characteristics of ribbon-like channel sands associated with delta-plain deposits. In other outcrop studies Fuller and Sharp (1992) investigated the influence of surface weathering and varnish on permeability measurements made on the Santana Tuff of Trans-Pecos Texas. They found the gas permeability to decrease by an order of magnitude due to the presence of surface weathering or varnish. Laboratory and outcrop permeameter investigations of the carbonate San Andres Formation in west Texas were performed by Kittridge et al. (1990). In this study they found this carbonate formation to exhibit extreme permeability heterogeneity which is manifest on several discrete scales of correlation. Other studies involving laboratory investigation of core and slab samples include Corbett and Jensen (1992) and Giordano et al. (1985). In general, these studies have been performed using a single tip seal size (approximately 0.31 cm inner seal radius) and hence single sample support.

Method for Acquiring Multi-Scale Data

A gas permeameter test system has been specially designed and constructed at Sandia National Laboratories to support physical investigation of up-scaling behavior. The design is based on steady-state gas flow at a prescribed injection pressure supplied by a compressed gas source. This design was adopted because of the wide permeability range of the instrument (1×10^{-15} to 1×10^{-10} m^2 [1 millidarcy to 100 darcys]) and flexibility in the volumetric gas supply that allows measurements to be performed at a variety of sample supports. A key aspect of this test system is the use of different sized tip seals to acquire gas permeability data at different sample supports.

The gas permeameter test system is comprised of two basic components, the electronic permeameter and the x-y positioning system. Automation of the system is required for efficient data acquisition (this system is capable of making more than 300 measurements in an eight hour period, unattended) and for precise gas permeability measurement (see Section III). The electronic permeameter consists of four mass-flow meters (0-50, 0-500, 0-2000, and 0-20,000 cm^3/min. [at standard conditions]), a pressure transducer (0-100 KPa gauge), a barometer, and temperature sensor that are connected to a regulated source of compressed nitrogen (Figure 2.1a). Operation of the electronic permeameter instruments and solenoids (electronic valves) is controlled by specially adapted PC-based software. The x-y positioning system coupled with a pneumatic piston have likewise been automated for positioning and compressing the permeameter tip seal against the rock surface (Figure 2.1b). Each measurement is made with the tip seal compressed squarely against the sampling surface and at a consistent pressure (compression force is adjusted for the surface area of each tip seal); thus, considerably limiting measurement error. Because measurements of this nature are not possible by hand, especially with the larger tip seals (Tidwell et al., 1993), our program opted for the automated laboratory based system rather than one of the common portable field based systems.

A series of specially designed tip seals, the diameter of which defines the scale of measurement, are used to establish a known boundary condition on the rock surface. By increasing the size of

13

a).

Differential Pressure Transducer 0-15 psi

Barometer

Micrometering Valve

Valve

N2

Solenoid — Mass Flow Meter 0-20,000 sccm

Solenoid — Mass Flow Meter 0-2000 sccm

Solenoid — Mass Flow Meter 0-500 sccm

Solenoid — Mass Flow Meter 0-50 sccm

Temperature Sensor

Tip Seal

Pressure Relief Valve

b).

POSITIONING ARM

AIR CYLINDER

TIP SEAL

ROCK SAMPLE

c).

Pressure Port

Gas Inlet

Tip Seal Housing

Spring

Plunger Stop

Plunger

Silicone Seal

Figure 2.1. Automated Gas Permeameter Test System; a) schematic of electronic gas permeameter, b) schematic of positioning system, and c) schematic of tip seal.

14

the tip seal, the permeameter interrogates larger volumes of rock. Tip seal sizes which are in current use have inner radii (r_i) of 0.15, 0.31, 0.63, 1.27, and 2.54 cm, and an outer radii (r_o) measuring twice the inner. One large tip seal, 7.62 cm inner radius, is also used for making a single "effective permeability" measurement that fully integrates over the entire sampling domain. Two basic tip seal designs are used. For the larger tip seals (i.e., 0.63 cm radius and larger), a soft, durable silicone rubber is used to establish the seal between the injection nozzle and the rock surface while an internal spring-driven plunger maintains a consistent inner seal diameter under compression (Figure 2.1c). For the 0.31 cm radius and smaller tip seals, norprene® tubing forms the tip seal while a barbed brass tubing mount, which secures the tip seal to the injection nozzle, maintains a consistent inner-seal diameter.

For measurements in a semi-infinite half-space (outcrop or large block measurements), the boundary of the resulting gas-flow field can be approximated as a hemisphere with effective radius r_{eff}. Based on numerical experimentation Goggin et al. (1988) concluded that r_{eff}, defined as a surface bounding 95% of the mass flux (Figure 2.2), is approximately four times r_i. Similar studies have indicated an r_{eff} of 2.5 times r_i; however, bounding only 90% of the mass flux (Corbett and Jensen, 1992). Suboor (1994) performed a series of laboratory experiments to physically investigate r_{eff}. Using a core of Berea sandstone, a transect of measurements were collected from the centerline to the edge using two different tip seals. Measurements were repeated with each tip seal, but with the edge of the core covered with modeling clay. Comparison of the data indicate that r_{eff} is a function of tip seal geometry. For a wide tip seal (r_i:r_o of 4.5) r_{eff} was found to be 5.2 times r_i while r_{eff} for a smaller seal (r_i:r_o of 2) was 2.8 times r_i. Prediction of r_{eff} is further complicated if the permeability field is characterized by strong anisotropy (Young, 1989). Given such uncertainty concerning the size of r_{eff} in theory, r_{eff} is determined empirically in our investigations (as described in Section III).
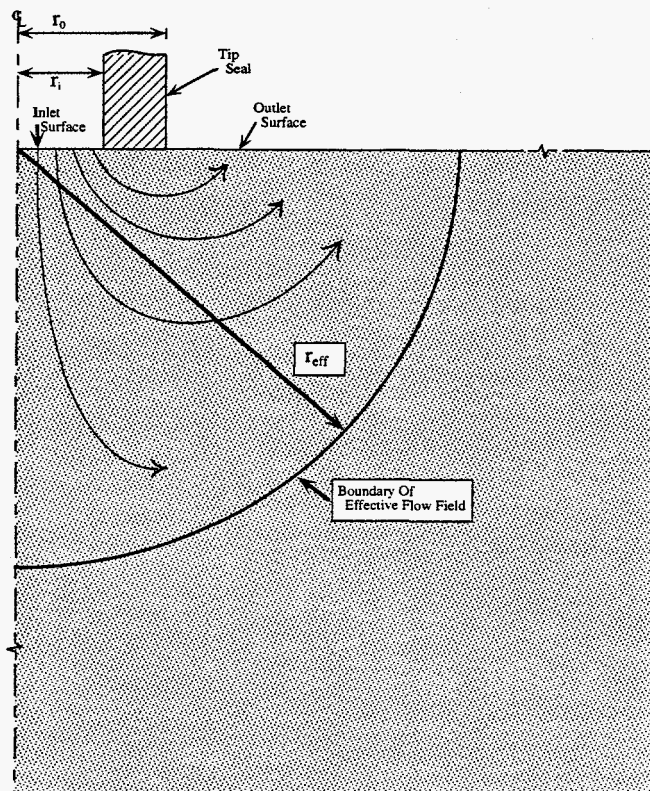
Figure 2.2. Schematic of the flow geometry in a semi-infinite medium.

Given a hemispherical flow-field the volume of rock interrogated by the permeameter V, and hence the scale of the measurement is,

$$V = 0.66 \cdot \pi \cdot (r_{eff})^3 \qquad (2.1)$$

The five tip seals noted above provide a range in sample support from tenths to hundreds or thousands (depending on r_{eff}) of cubic centimeters. That is, a three to four order of magnitude range in sample support. By including the largest tip seal (7.62 cm inner radius), this increases the range to over seven orders of magnitude.

Gas permeability is calculated directly from information on seal geometry, flow rate, and injection pressure. These calculations are accomplished by means of a modified form of Darcy's Law as developed by Goggin et al. (1988).

$$k = \frac{Q_1 P_1 \mu}{0.5 r_i G_o \left(P_1^2 - P_o^2 \right)} \qquad (2.2)$$

where k is gas permeability, Q_1 is gas-flow rate, P_o is atmospheric pressure, P_1 is gas injection pressure, μ is gas viscosity, and G_o is a geometric factor. In this model, complexities associated with the flow-field geometry are summarized by a single, empirically derived, dimensionless quantity, G_o, which is a function of tip seal size.

A number of experimental controls have been employed to monitor the performance of the gas permeameter test system. Two simple investigations are performed prior to sampling any new rock face. First, measurements are made on a series of standards (metal porous plates with permeabilities spanning the range of the permeameter) to evaluate the stability of the electronic equipment. Second, a series of repeated measurements are made with each tip seal to quantify the measurement error for that sample. Prior to the collection of each data set, the permeameter is leak tested by compressing the tip seal on a plate of roughened glass and measuring the permeability (which should be zero). Additionally, each of the electronic instruments are zeroed and the room temperature and humidity recorded. Results of these tests along with the up-scaling data generated by this program are maintained in a scientific notebook in electronic and hard-copy form.

The calculated gas permeability may be adversely influenced by gas slippage effects (Klinkenberg, 1941), high velocity (inertial) effects, and/or head loss in the tip seal. As such, appropriate corrections to the collected data may be required. Treatment of gas slippage is accomplished by taking a limited number of measurements (for each rock) in which the sampling location is maintained while the gas pressure is varied. Using this information the gas slippage coefficient can be calculated and used to correct the measured gas permeability data. However, experimental difficulties, which have yet to be resolved, have precluded quantification of such effects; hence, the data presented here have not been corrected for gas slippage. The potential for high velocity effects to influence measurements made by the gas permeameter has been evaluated for each tip seal using a suite of natural and man-made materials that fully span the permeability range of the instrument. In all cases, particularly the high permeability samples, the mass flux rate was found to be a linear function of injection pressure, hence high velocity effects are not of concern with this permeameter. In contrast, head loss was found to be a problem for the smaller tip seals at large mass flux rates. To correct for this effect, an empirical head loss factor is subtracted from the measured injection pressure. The head loss factor was determined by measuring unrestricted gas flow from each tip seal to determine the pressure drop in the connecting hose and tip seal as a function of the flow rate.

Another important detail of the experimental method concerns the acquisition and preparation of samples for investigation. Large boulders of rock, capable of yielding blocks measuring 0.6-1.3 m on a side, are preferred. Shaping of boulders into blocks is necessary to provide a fresh (free of weathering rinds, etc.), flat surface for making measurements. Blocks are preferred over slabs because blocks provide a sampling domain that is thick relative to the depth of penetration of the permeameter measurement. Also, the three-dimensionality of the block allows samples with anisotropic heterogeneity structure to be interrogated in three orthogonal orientations (samples are cut along the inferred principal permeability axes). Rock samples are cut using a diamond-impregnated wire line saw. Fresh water is used to lubricate and cool the wire line during cutting as well as to pressure wash the sawn surfaces (to remove cuttings from open rock pores).

Up-scaling studies on a rock sample are initiated by aligning (with respect to marked origin) and leveling the sample under the x-y positioning table. The table is then lowered into position and leveled. Measurements are made on a square grid in which the nodes are spaced according to the inferred correlation length of the sample (2 to 3 measurements per correlation length where possible). Care is taken to center the grid a sufficient distance from the edges of the block (~10 cm or 4 times r_i of the largest tip seal) to avoid violation of Equation 2.2, which assumes an infinite medium. This same sampling grid is then used for all but the one large-scale (7.62 cm) tip seal. After measurements are completed for each tip seal, the rock is moved, flipped to another face, and re-positioned. The same grid is once again employed to conduct sampling on the new face (maintaining a constant sampling domain size). In general, this sampling strategy yields between 500 and 1000 measurements per block face per tip seal and complete coverage of the sampling domain. As such, the measured distribution functions and related moments are robust given the large sample population, while the sample semi-variograms have sufficient resolution to define the underlying spatial structure.

An integral part of the up-scaling studies described here is a detailed qualitative and quantitative description of the rock samples that are investigated. Qualitative aspects of interest include a description of the depositional environment and the relationship of that sample to the environment, diagenetic history, and general rock characteristics (i.e., color, type of fabric, mineralogy, cementation, grain size, shape, orientation, nature of pores). Efforts are also made to quantify those aspects of the sample which may influence the spatial permeability pattern (e.g., the size and geometry of cross-bedding, thickness of laminar beds, size and shape of permeable grains dispersed in a tight matrix). In general, these relationships can be quantified by simple point counting methods. Where such structural features can be visually discerned, optical imaging techniques, coupled with computer-aided image analysis, are used to facilitate quantification of their size and shape (see Section III).

Approach to Physical Experimentation

As pointed out above, other researchers have physically measured effective properties at multiple scales and made comparisons; however, these studies have limited data collection to a single block of rock, outcrop, or agricultural field. This lack of careful, systematic experimentation makes it very difficult, if not impossible, to accurately interpret available up-scaling data, to identify and quantify key controls on up-scaling behavior, and to thoroughly test current up-scaling theory. For this reason, we approach the investigation of up-scaling behavior through systematic physical experimentation. This involves performing a suite of investigations in which controls influencing up-scaling behavior are systematically isolated (to the extent practical), experiments are performed, and results compared.

There are a number of controls that will potentially influence up-scaling behavior; however, in this study we focus on only the geologic characteristics of the porous medium. Geologic controls are isolated, to the extent practical, through careful selection of samples for investigation. In particular, the spatial structure (e.g., bedded, welded), statistical characteristics (e.g.,

unimodal/bimodal, high/low variance), and the depositional/diagenetic history of the rock are used to guide sample selection. With these controls in mind, blocks of volcanic tuff were selected for investigation each exhibiting varying degrees of welding, and bedding, as well as the extent and size of pumice/lithics/lithophysae inclusions.

2.2. Theoretical Approach

Analysis of acquired up-scaling data focuses on identifying trends that are diagnostic of up-scaling behavior followed by the interpretation these trends in light of applicable theory. Data analysis is initiated by summarizing the acquired data using standard univariate and multivariate statistics. Trends relating these statistical measures with changes in sample support are then sought. Interpretation of the measured behavior is pursued through comparison with appropriate theoretical up-scaling models. Where poor comparisons are encountered, alternative measures which may be used to quantify up-scaling behavior are explored.

The first step in analysis of the gas permeameter data involves the calculation of the basic univariate and multivariate statistics. This process begins with the generation of gray-scale plots of the gas permeability data for each tip seal and rock face investigated. The plots are reviewed to identify gross structural features and artifacts induced by the measurement system or sampling scheme (should such occur). The distribution of each data set is then investigated by means of a normal probability plot. The data are further summarized according to its basic univariate statistics. Geostatistics are then employed to investigate the spatial structure of the permeability fields. Sample semi-variograms are constructed in an array of search directions in efforts to identify the principal permeability axes. Models are then fit to the sample semi-variograms oriented in these directions.

The second step in the analysis is aimed at identifying trends diagnostic of up-scaling behavior. In particular, we are interested in how the distribution function, semi-variogram, sample mean, sample variance, or other data descriptors behave with respect to increasing sample support. In general, the theoretical models reviewed in Section I focus on the behavior of the mean and in some instances the covariance function (or semi-variogram). As such, we begin by investigating these first two moments. However, for the sake of completeness, the behavior of other basic data descriptors are consistently tracked.

18

3. DISCUSSION

In this section we review recent results generated by the up-scaling studies program. We begin by investigating the precision of the gas permeameter test system with respect to the needs of the up-scaling experimentation. These results are followed by a review and analysis of multi-scale gas permeability data collected from a number of volcanic tuff and sandstone samples.

3.1. Precision of the Automated Gas Permeameter Test System

Investigation of up-scaling behavior requires all measurements, regardless of the time, position, or support to be made in a consistent manner. That is, the acquired data must not be significantly influenced by artifacts of the measurement technique that may mask the up-scaling behavior of interest. As discussed in Section II, particular effort is taken to make all measurements in a consistent manner. As such, we need only to demonstrate the capability of the gas permeameter to acquire precise data at each sample support. This is accomplished through simple hypothesis testing. We begin by investigating the precision of the distributional characteristics of the measured data by means of the Kolmogorov-Smirnov test. One-way analysis of variance is then employed to investigate the contribution of measurement error to the measured sample variance.

As the distribution function is a key diagnostic feature of up-scaling behavior, we utilize the non-parametric (i.e., independent of any distributional assumptions) Kolmogorov-Smirnov test to investigate the precision related to its measurement. Four replicate sets of 54 measurements were made on a block of volcanic tuff (in which the permeability varied by over three-orders of magnitude and the spatial correlation was very weak [i.e., measurements were effectively independent]) using each of the five tip seals. The measured distribution functions were then analyzed by means of a Kolmogorov-Smirnov test to determine whether differences in the four replicate distribution functions (per tip seal size) were statistically significant. Results are given in Table 3.1 where D_{max} is the maximum absolute difference between any of the four measured distribution functions and f-critical is the critical value for a sample size of 54 and significance level of 0.05. As can be seen, D_{max} is always considerably less than f-critical, hence the null hypothesis that the each of the four measured distribution functions are from the same distribution cannot be rejected. As such, the gas permeameter is seen to yield precise measurement of the distribution function, regardless of sample support.

Table 3.1: Kolmogorov-Smirnov test results for comparison of replicate (four) log permeability data sets (each consisting of 54 measurements) for each of the five sample supports.

Tip Size, r_i (cm)	D_{max}	f-critical (5%)
0.15	0.019	0.18
0.31	0.043	0.18
0.62	0.055	0.18
1.27	0.056	0.18
2.54	0.056	0.18

One-way analysis of variance (ANOVA) provides a convenient means of evaluating the contribution of measurement error to the measured variance of the sample. In our program, such tests are performed prior to the investigation of each new rock sample. In Table 3.2, ANOVA results are given for a block of volcanic tuff that is representative of findings on other samples. For each tip-seal, four replicate groups of nine independent measurements are collected for analysis

(i.e., a suite of nine measurements at different locations was made then this same suite of measurements was repeated three more times). Each measurement is spaced so as to exceed the correlation length of the sample to assure statistical independence. As shown below, the ratio of mean square error between groups (a measure of the variance due to rock property heterogeneity) to the mean square error within groups (a measure of the variance resulting from instrument error), is large, as indicated by the F-value. Because the F-value is much larger than the f-statistic, estimated at a significance level of 5%, the null hypothesis that the means of the 9 groups of permeability measurements are equal is rejected. Thus, variance of the data is not significantly influenced by measurement error of the permeameter, but rather is related to the variability inherent to the tuff sample. In fact, instrument error is very small in absolute terms, less than 0.1% of the mean permeability, and consistent across tip seals (within an order of magnitude).

Table 3.2: Results of one-way analysis of variance performed to quantify the influence of measurement error on permeability data acquired with the automated gas-permeameter test system. In this test, the degrees of freedom between groups is 8, while the degrees of freedom within groups is 27.

Tip Size, r_i (cm)	Mean Square Between Groups	Mean Square Within Groups	F-value	f-statistic (5%)
0.15	21.55	1.37×10^{-2}	1.56×10^3	2.31
0.31	16.06	2.60×10^{-3}	6.16×10^3	2.31
0.62	17.67	1.11×10^{-3}	1.58×10^4	2.31
1.27	17.68	1.41×10^{-3}	1.24×10^4	2.31
2.54	9.72	2.10×10^{-3}	4.62×10^3	2.31

3.2. Results of Up-Scaling Studies

The up-scaling behavior of saturated matrix permeability has been investigated on a number of rock samples each exhibiting differing physical characteristics (Tidwell, 1994a; 1994b). Here, we will focus on the results from three different samples; two volcanic tuffs from Yucca Mountain, and a bedded eolian sandstone. The tuff samples were selected for investigation because they exhibit very different physical attributes, which are nevertheless characteristic of those encountered in many of the tuff units at Yucca Mountain. The sandstone sample is analyzed because of its very different characteristics with respect to that of the tuff samples (i.e., bedded structure with very low permeability variation) and because the sandstone is in a broad sense an analog to the bedded air fall units at Yucca Mountain (from which we are currently unable to excavate meter scale samples for investigation).

Analysis of Up-Scaling Behavior

Tiva Cliff Sample

The first sample that will be discussed is a volcanic tuff collected from Yucca Mountain that is associated with the Tiva Canyon Tuff of the Paintbrush Group, Upper Cliff (called Tiva Cliff) microstratigraphic unit (Scott and Bonk, 1984) (this unit has recently been referred to as the crystal rich non-lithophysal zone of the Tiva Canyon Tuff in the Paintbrush Group [D.C. Buesch, USGS, written communication, 1994]). The Tiva Cliff sample (1.3 by 1.3 by 0.6 m block) is a welded tuff that has undergone vapor phase alteration. The sample exhibits a clastic fabric; lithic and pumice fragments bound by a fine-grain groundmass. The lithics and pumice are subround to

angular. In contrast to the lithics, the pumice fragments are distinctly flattened resulting in a "pancake" appearance.

To date, gas permeability measurements have only been made on a single face of the Tiva Cliff sample. Measurements were collected from the face cut normal to the direction of pumice flattening. Data were acquired from a 45.7 by 45.7 cm area centered on the block. Two grids of differing resolutions were used to collect the data. For the 0.15 and 0.31 cm tip seals, measurements were collected on a square grid (54 by 54) with 0.85 cm centers. For the 0.63, 1.27 and 2.54 cm tip seals a square grid (36 by 36) with 1.27 cm centers was used. A single measurement centered on the block face was also accomplished using the 7.62 cm tip seal. It should be noted that some overlap between neighboring measurements is expected for all tip seals (see Equation 2.1).

Gray-scale plots of the log (natural) transformed gas permeability fields measured on the Tiva Cliff sample for the 0.15, 0.31, 1.27, and 2.54 cm tip seals (sample support) are shown in Figure 3.1. The 0.63 cm field was omitted to facilitate presentation. The most notable feature of the permeability fields is the distinct smoothing that accompanies increasing sample support. These data (log permeabilities) are summarized, by sample support, via their cumulative frequency distribution and shown in Figure 3.2. Each of the five distributions are unimodal and non-Gaussian; however, each distribution appears to be characterized by two distinct populations, a low- and high-permeability population associated with the groundmass and pumice fractions of the rock respectively. We further summarize the log permeability data by calculating the moments of the measured distributions. Univariate statistics for each of the five tip seals can be found in Table 3.3. Several notable trends are evident. Except for the 0.15 cm tip seal, the sample mean, variance, and maximum value consistently decrease with increasing sample support while the sample minimum value increases. In contrast the sample median and skewness are noted to remain relatively constant. The single effective permeability measurement made with the 7.62 cm tip was -30.29, which suggests a slight deviation from the inversely related sample mean/sample support relationship noted above.

Multivariate analysis of the Tiva Cliff data has also been performed. Spatial continuity of the log permeability measurements was investigated by means of the sample semi-variogram (Isaaks and Srivastava, 1989; Journel and Huijbregts, 1978). At each sample support, semi-variograms were calculated for a series of different search directions, from which it was determined that the log permeability field in the plane of measurement is isotropic. For this reason, the sample semi-variograms presented (Figure 3.3) and discussed in this section were calculated using an omni-directional search.

Each of the five sample semi-variograms display a sill with a finite range and magnitude that corresponds closely to the sample variance. Such behavior is common among geologic media and is routinely fit with a spherical semi-variogram model. Accordingly, each of the sample semi-variograms were fit with a spherical model and are shown in Figure 3.3 (the associated modeling parameters are given in Table 3.4). As with the univariate statistics, definite trends are apparent in the results of the semi-variogram analysis. In particular, the sill (except for the 0.15 cm tip) and nugget were found to decrease with increasing sample support while the range (which defines the correlation length of the media) was found to increase.

Also of interest is whether visibly observable characteristics of the rock fabric (heterogeneity) can be related to the geostatistical models (i.e., semi-variograms) developed for the Tiva Cliff sample. To evaluate such relationships, an independent measure of the size and shape of the heterogeneity structure of the sample is needed. In this sample, the primary heterogeneity is represented by the high-porosity pumice grains that give rise to contrast in the measured gas permeability field. To aid in measuring the size of the pumice grains, a high resolution image of the rock face was acquired using a digital, charged-coupled device (CCD) camera. Analysis of the

21
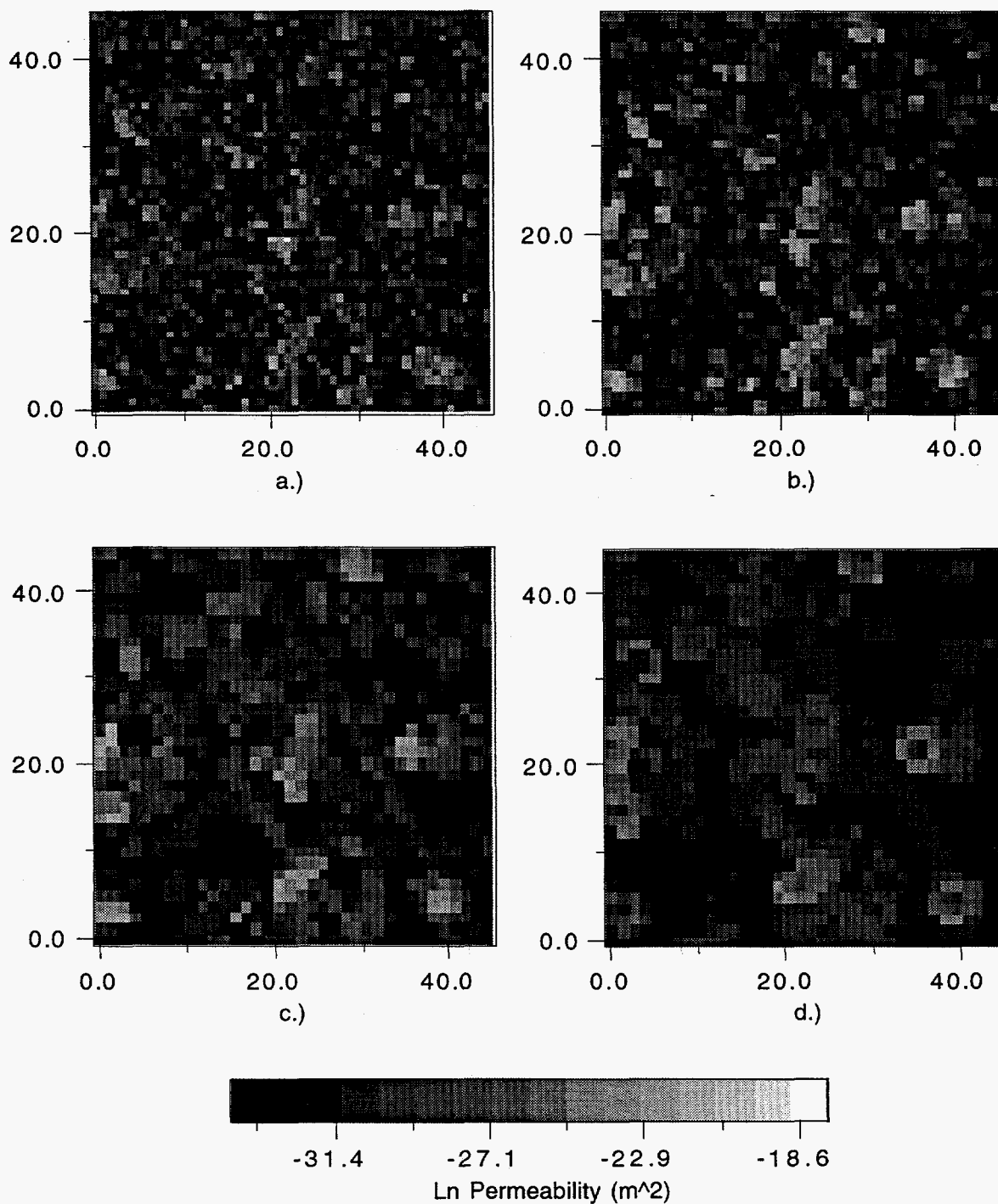
Figure 3.1. Gray-scale gas permeability field for the Tiva Cliff sample as measured with the a). 0.31, b). 0.62, c). 1.27, and d). 2.54 cm tip seals. Data are reported in terms of the natural log of the gas permeability in units of m².
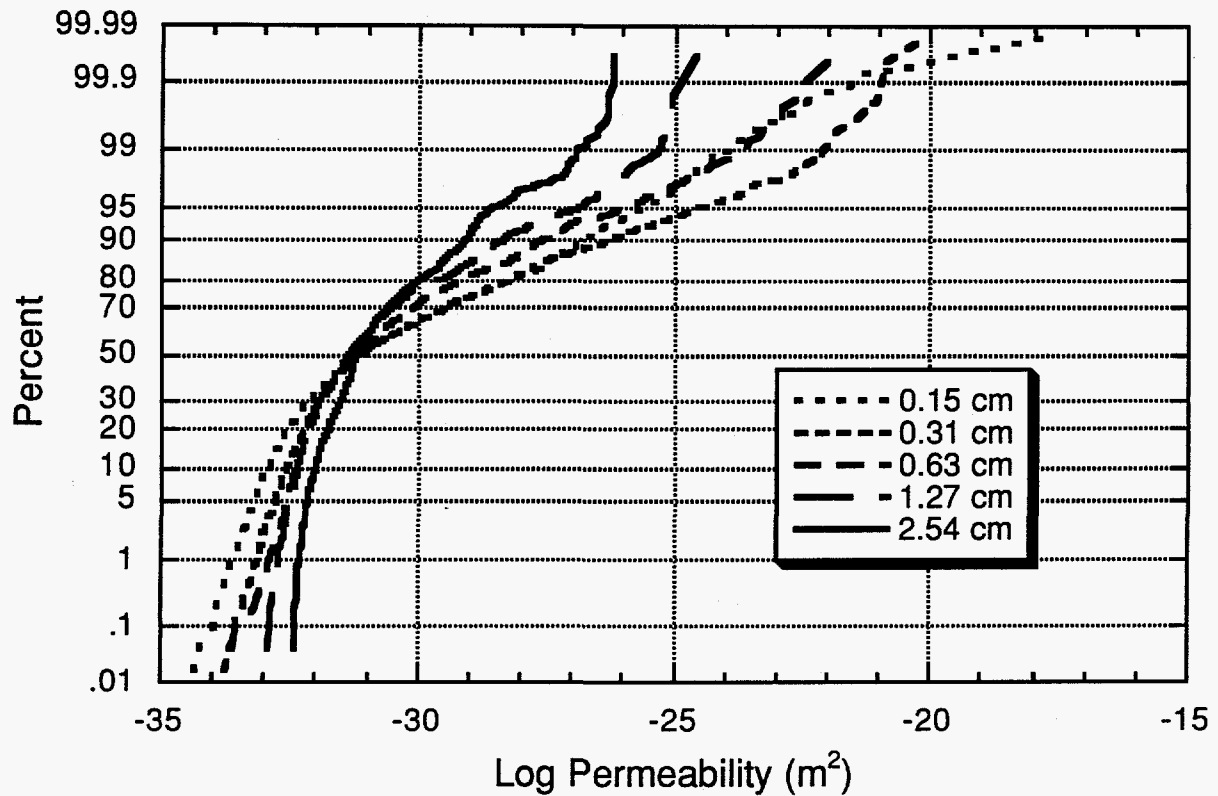
Figure 3.2. Comparison of the log permeability distribution functions measured with different size tip seals on the Tiva Cliff sample.

Table 3.3: Univariate summary statistics for the log (natural) permeability (m²) measured at five different sample supports on the Tiva Cliff sample.

Tip Seal	0.15 cm	0.31 cm	0.63 cm	1.27 cm	2.54 cm
Mean	-30.40	-30.13	-30.50	-30.77	-30.80
Median	-31.15	-31.05	-31.19	-31.32	-31.15
Standard Deviation	2.41	2.60	2.06	1.69	1.18
Variance	5.83	6.74	4.23	2.85	1.40
Kurtosis	0.34	1.21	1.90	1.54	1.94
Skewness	0.95	1.32	1.47	1.41	1.39
Range	16.52	13.66	11.69	8.35	6.25
Minimum	-34.34	-33.76	-33.60	-32.92	-32.41
Maximum	-17.82	-20.10	-21.92	-24.57	-26.15
Count	2916	2916	1296	1296	1296
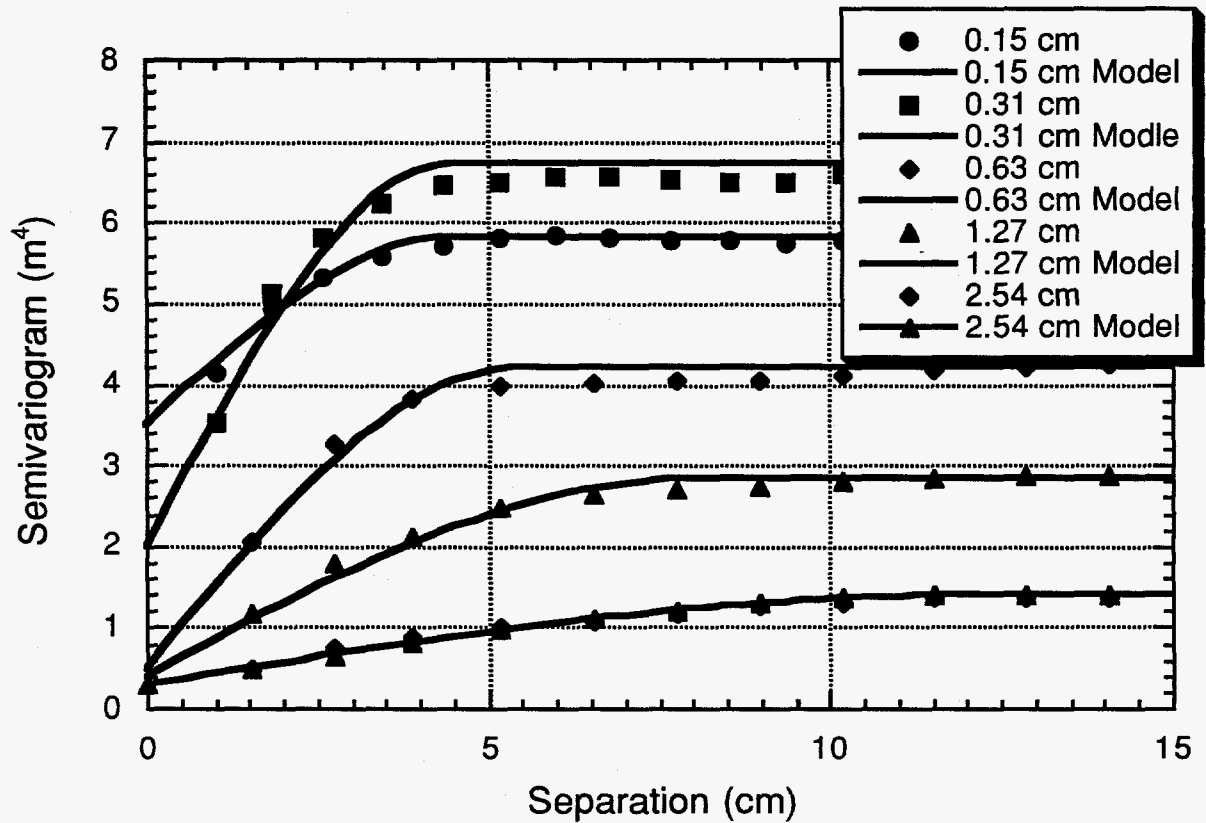
Figure 3.3. Comparison of the log permeability sample semi-variograms measured with different sized tip seals on the Tiva Cliff sample. The sample semi-variograms were generated using an omni-directional search. A spherical semi-variogram model has been fit to each data set (model parameter values are given in Table 3.4).

image yielded the size and shape of each pumice grain. The frequency distribution of pumice grain size (length of the major grain axis) is given in Figure 3.4. In this figure, frequency is noted to decrease exponentially with grain size, with very few grains larger than 3.5 cm.

Tiva Cap Sample

The second volcanic tuff investigated is also from Yucca Mountain and is associated with the Tiva Canyon Tuff of the Paintbrush Group, Caprock (called Tiva Cap) microstratigraphic unit (Scott and Bonk, 1984) (this unit has recently been referred to as the crystal rich, vitric zone of the Tiva Canyon Tuff in the Paintbrush Group [D.C. Buesch, USGS, written communication, 1994]). The Tiva Cap sample (1.2 by 0.6 by 0.4 m block) is a poorly welded tuff that exhibits an isotropic, aphanitic fabric with very sparse subround pumice fragments. Measurements were made on two faces of the block. On face 1, data were collected from an area, centered on the block measuring 94 cm by 25 cm. A 37 by 10 grid on 2.54 cm centers was used for all five tip seals. On face 2, data were acquired from a 101 by 46 cm area using a 40 by 18 grid on 2.54 cm centers. A measurement with the 7.62 cm tip seal was performed only on face 2 because face 1 was too narrow to achieve accurate results.

Gray-scale plots of the log (natural) transformed gas permeability fields for the 0.15, 0.31, 1.27, and 2.54 cm tip seals are shown in Figure 3.5 and 3.6. Again, the 0.63 cm field was omitted to facilitate presentation. For both faces, general features of the permeability field are preserved across the different sample supports; however, these features are subject to significant smoothing as the support increases. The composite (i.e., the two faces combined) cumulative frequency distributions are shown in Figure 3.7. Each of the five distributions are unimodal and non-Gaussian; however, the distributions do not exhibit the strong positive tail noted with the Tiva Cliff sample. In fact, the data approach Gaussian behavior as the sample support is increased. Univariate statistics for each of the five tip seals can be found in Table 3.5. Again, the sample mean, variance, and maximum value consistently decrease with increasing sample support while the sample median remains relatively consistent. In contrast to the Tiva Cliff sample the skewness is seen to decrease with increasing support while the minimum value is erratic. The single effective permeability measurement made with the 7.62 cm tip was -32.7, which is consistent with the aforementioned trend in the mean.

Multivariate analysis of the Tiva Cap data has also been performed. At each sample support, semi-variograms were calculated for a series of different search directions, from which it was determined that the log permeability field in the face 2 plane of measurement is isotropic. However, a notable geometric anisotropy (i.e., difference in the range of correlation in different search directions) oriented normal to face 2 was detected. The range was found to vary by a factor of 1.6 between these two directions. For this reason, sample semi-variograms were constructed using an omni-direction search in the face 2 plane (Figure 3.8) and separately along a search direction oriented normal to face 2 (Figure 3.9). Each of the sample semi-variograms were fit with a spherical model and are shown in Figure 3.8 and 3.9 (the associated modeling parameters are given in Table 3.6 and 3.7). In general, the spherical model fit the data well except in the semi-variogram for face 2 at separations of 5 and 7.5 cm. At these separations it was noted that few data pairs were available for calculating the semi-variogram (due to the rectangular shape of the sampling grid). Hence the noted descepancy is a result of the computaion of the semi-variogram and not an indicator of nested structure. As with the Tiva Cliff sample, the sill decreases with increasing sample support while the range increases. The nugget was found to decrease with increasing support in the semi-variograms oriented normal to face 2 while exactly the opposite was noted for the omni-directional semi-variogram in the plane of face 2. There were no visibly observable characteristics in the rock fabric of the Tiva Cap sample which could be correlated with the measured geostatistical models.

Table 3.4: Spherical model parameters fit to the sample semi-variograms measured at five different sample supports on the Tiva Cliff sample.

Tip Seal	0.15 cm	0.31 cm	0.63 cm	1.27 cm	2.54 cm
Sill (m^4)	5.83	6.74	4.23	2.85	1.40
Range (cm)	4.0	4.5	5.5	8.0	12.0
Modeled Variance(m^4)	2.33	4.75	3.73	2.44	1.10
Nugget (m^4)	3.5	2.0	0.5	0.4	0.3
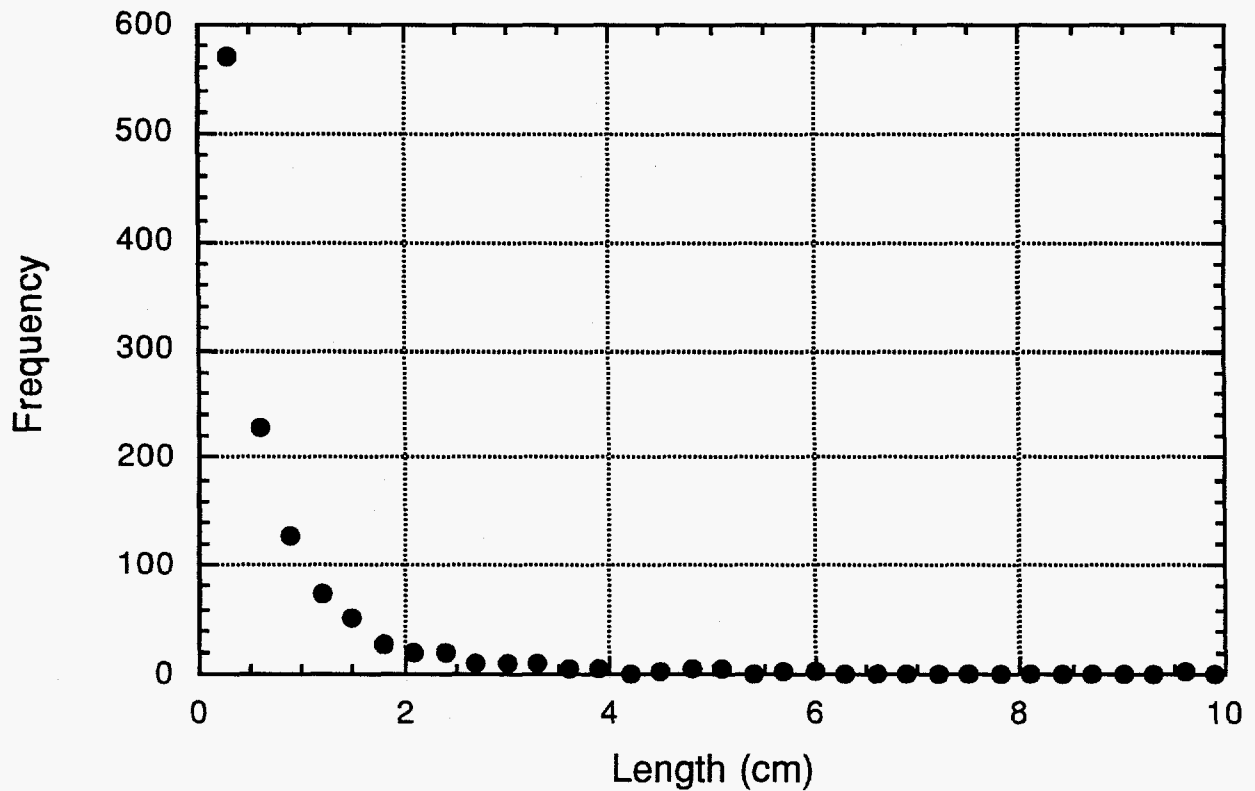
Figure 3.4. Frequency distribution of pumice grain size (length of major axis) for the Tiva Cliff sample. Measurements were acquired using a high resolution optical imaging system.

Figure 3.5. Gray-scale gas permeability field for the Tiva Cap sample, face 1 as measured with the a). 0.15, b). 0.31, c). 1.27, and d). 2.54 cm tip seals. Data are reported in terms of the natural log of the gas permeability in units of m².

27

Figure 3.6. Gray-scale gas permeability field for the Tiva Cap sample, face 2 as measured with the a). 0.15, b). 0.31, c). 1.27, and d). 2.54 cm tip seals. Data are reported in terms of the natural log of the gas permeability in units of m².

28
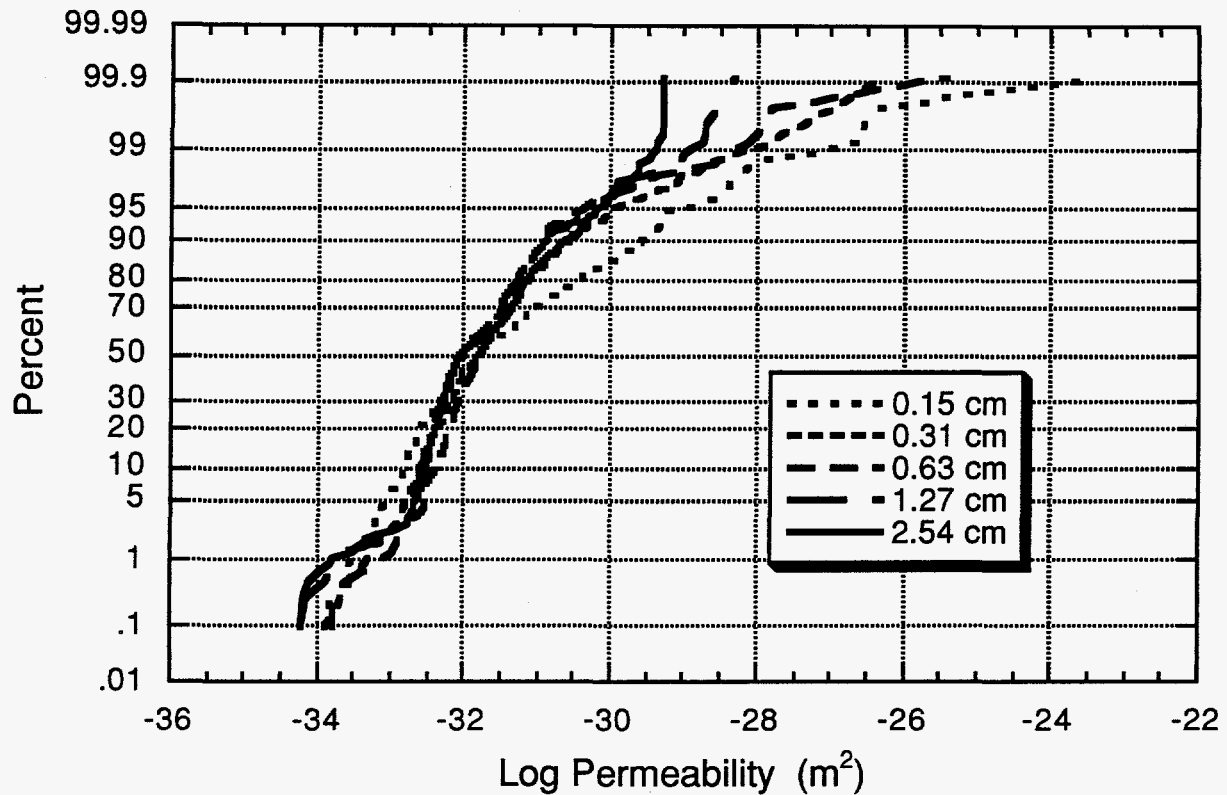
Figure 3.7. Comparison of the log permeability distribution functions measured with different size tip seals on the Tiva Cap sample.

Table 3.5: Univariate summary statistics for the log (natural) permeability (m²) measured at five different sample supports on the Tiva Cap sample.

Tip Seal	0.15 cm	0.31 cm	0.63 cm	1.27 cm	2.54 cm
Mean	-31.78	-32.00	-32.05	-32.25	-32.16
Median	-32.06	-32.09	-32.07	-32.27	-32.27
Standard Deviation	1.39	1.10	1.03	1.10	1.09
Variance	1.94	1.20	1.07	1.22	1.19
Kurtosis	2.75	4.02	4.48	1.65	0.36
Skewness	1.26	1.02	0.53	0.18	0.12
Range	11.17	10.40	10.22	7.62	6.57
Minimum	-34.73	-35.00	-35.61	-35.79	-35.33
Maximum	-23.56	-24.60	-25.39	-28.17	-28.76
Count	1090	1090.	1090	1090	1090
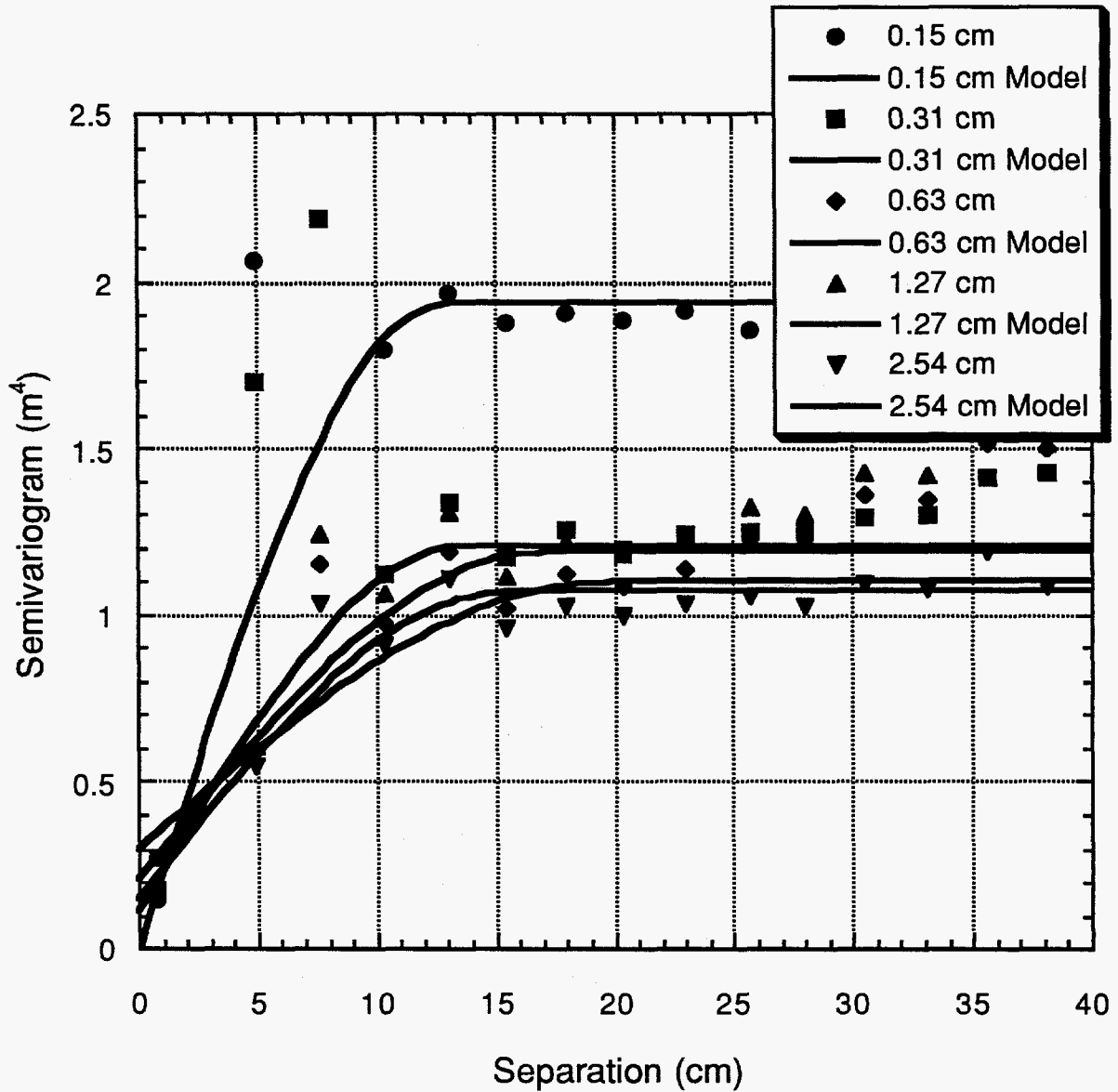
Figure 3.8. Comparison of the log permeability sample semi-variograms measured with different size tip seals on the Tiva Cap sample. The sample semi-variograms were generated using an omni-directional search in the face 2 plane. A spherical semi-variogram model has been fit to each data set (model parameter values are given in Table 3.6).
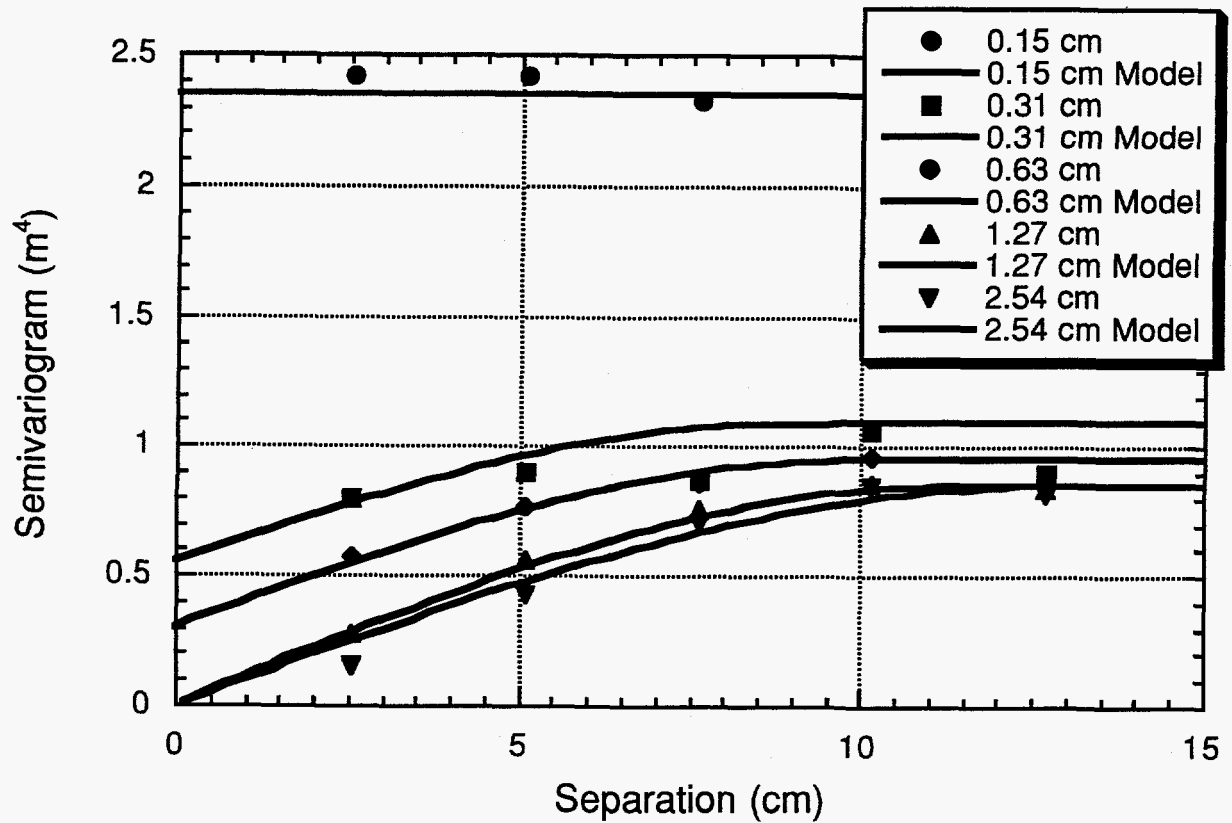
Figure 3.9. Comparison of the log permeability sample semi-variograms measured with different size tip seals on the Tiva Cap sample. The sample semi-variograms were generated using a directional search oriented normal to face 2. A spherical semi-variogram model has been fit to each data set (model parameter values are given in Table 3.7).

Table 3.6: Spherical model parameters fit to the sample semi-variograms measured at five different sample supports on the Tiva Cap sample, face 1.

Tip Seal	0.15 cm	0.31 cm	0.63 cm	1.27 cm	2.54 cm
Sill(m^4)	2.35	1.09	0.95	0.85	0.85
Range (cm)	-	9.0	10.0	11.5	13.0
Modeled Variance(m^4)	0.0	0.54	0.65	0.85	0.85
Nugget(m^4)	2.35	0.55	0.3	0.0	0.0

Table 3.7: Spherical model parameters fit to the sample semi-variograms measured at five different sample supports on the Tiva Cap sample, face 2.

Tip Seal	0.15 cm	0.31 cm	0.63 cm	1.27 cm	2.54 cm
Sill(m^4)	1.88	1.21	1.11	1.19	1.02
Range (cm)	13.0	13.8	15.5	17.0	19.7
Modeled Variance(m^4)	1.88	1.10	0.92	0.98	0.78
Nugget(m^4)	0.0	0.11	0.19	0.21	0.24

Berea Sample

A small block (0.3 by 0.3 by 0.3 m) of Berea Sandstone, acquired from Cleveland Quarries in Amherst, Ohio, was also subjected to up-scaling studies. The Berea Sandstone is fluvial in origin and exhibits a massive or homogeneous texture; however, close inspection reveals faint cross-bedding. Measurements were made on two faces of the block. In each case, data were collected within a 20 by 20 cm area using a 24 by 24 grid with 0.846 cm centers. At this resolution, data were acquired using the 0.15, 0.31, 0.63 and 1.27 cm tip seals. Given the small size of the sample only four measurements were made with the 2.54 cm tip seal and no measurements were made with the 7.62 cm tip.

Gray-scale plots of the log (natural) transformed gas permeability fields for the 0.15, 0.31, 0.63, and 1.27 cm tip seals are shown in Figure 3.10 and 3.11. Distinct bedding is evident in each of the permeability fields, which again tend to become smoother with increasing support. The composite (i.e., the two faces combined) cumulative frequency distributions are shown in Figure 3.12. Each of the four distributions are unimodal. The 0.15 cm data appear the be log-normally distributed; however, as the sample support increases the distribution tends to stray from this behavior. Univariate statistics for each of the five tip seals can be found in Table 3.8. It is noted that the sample variance and the maximum value consistently decrease with increasing sample support while the skewness and minimum value increase. The mean and median both are seen to remain constant with changing support.

Multivariate analysis of the Berea data reveals a strong geometric anisotropy. Semi-variograms directed normal to bedding show a range of correlation of approximately 1.9 cm (Figure 3.13) while the range of correlation parallel to bedding is beyond the length of the sample (as shown by the linear nature of the semi-variogram, Figure 3.14). Each of the sample variograms oriented normal to bedding were fit with spherical variogram models (the associated modeling parameters
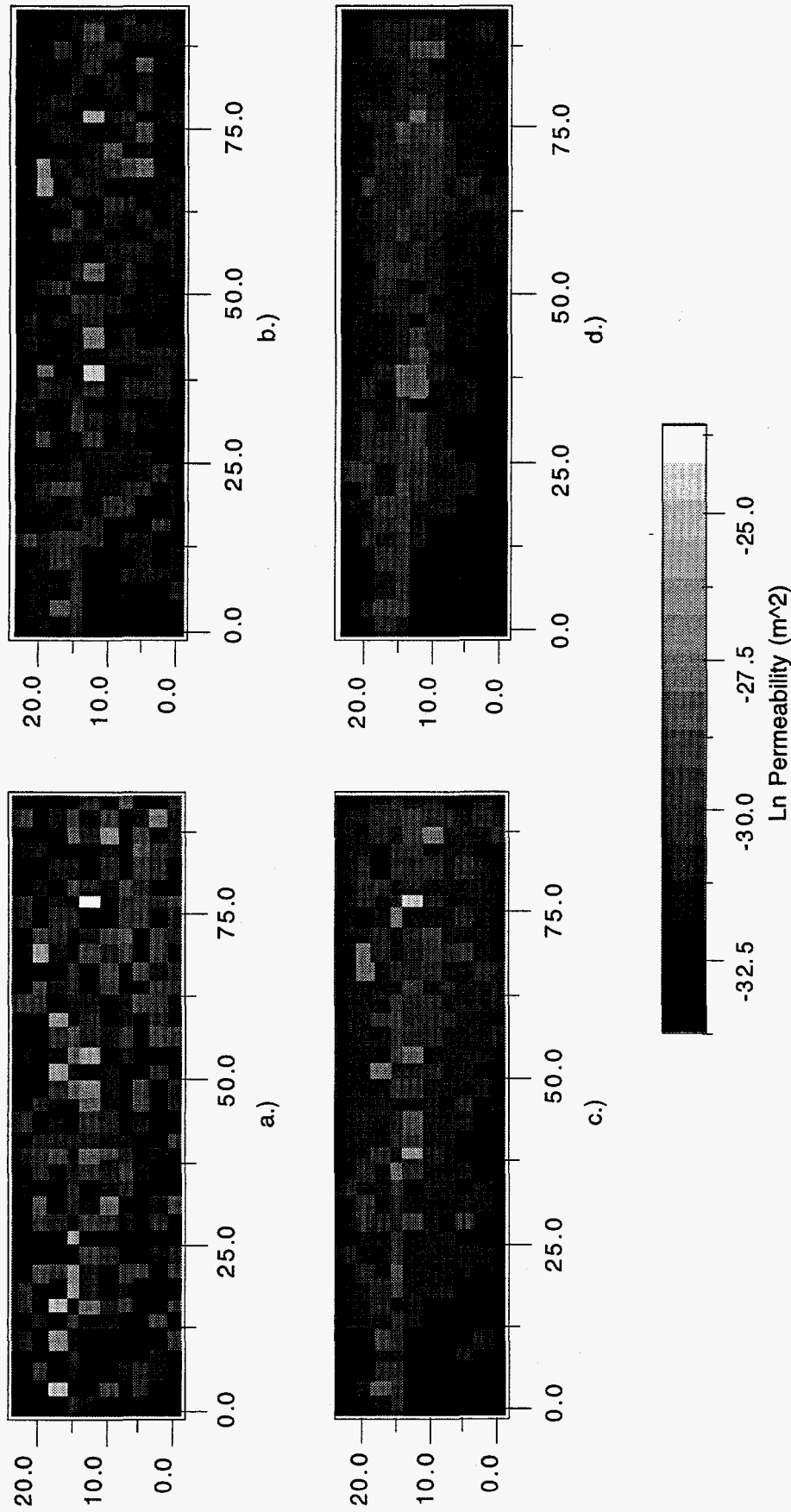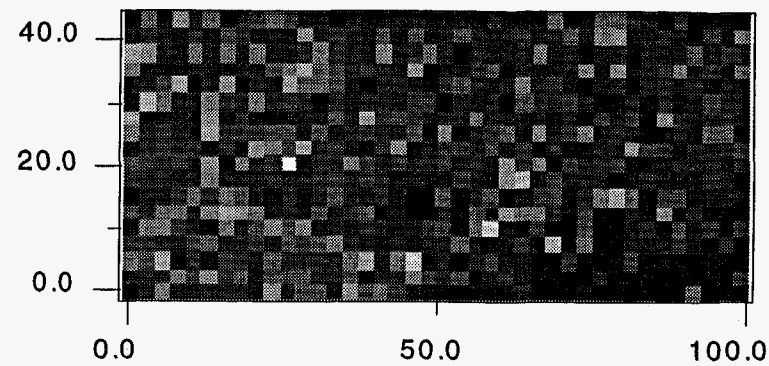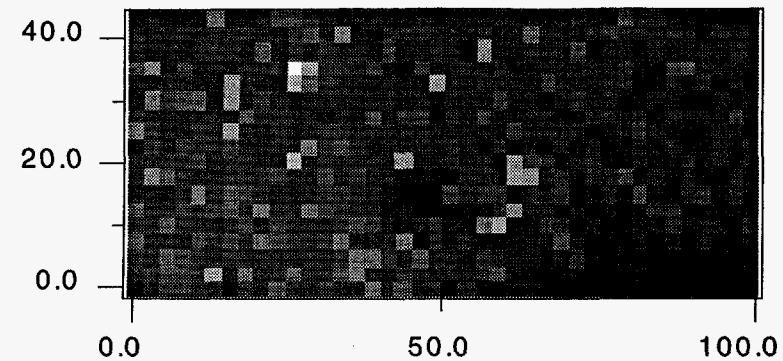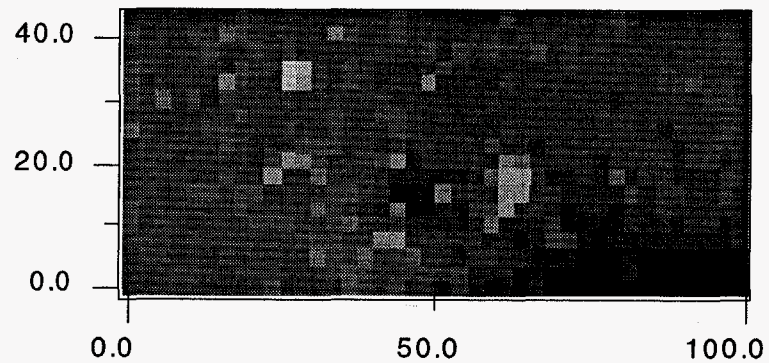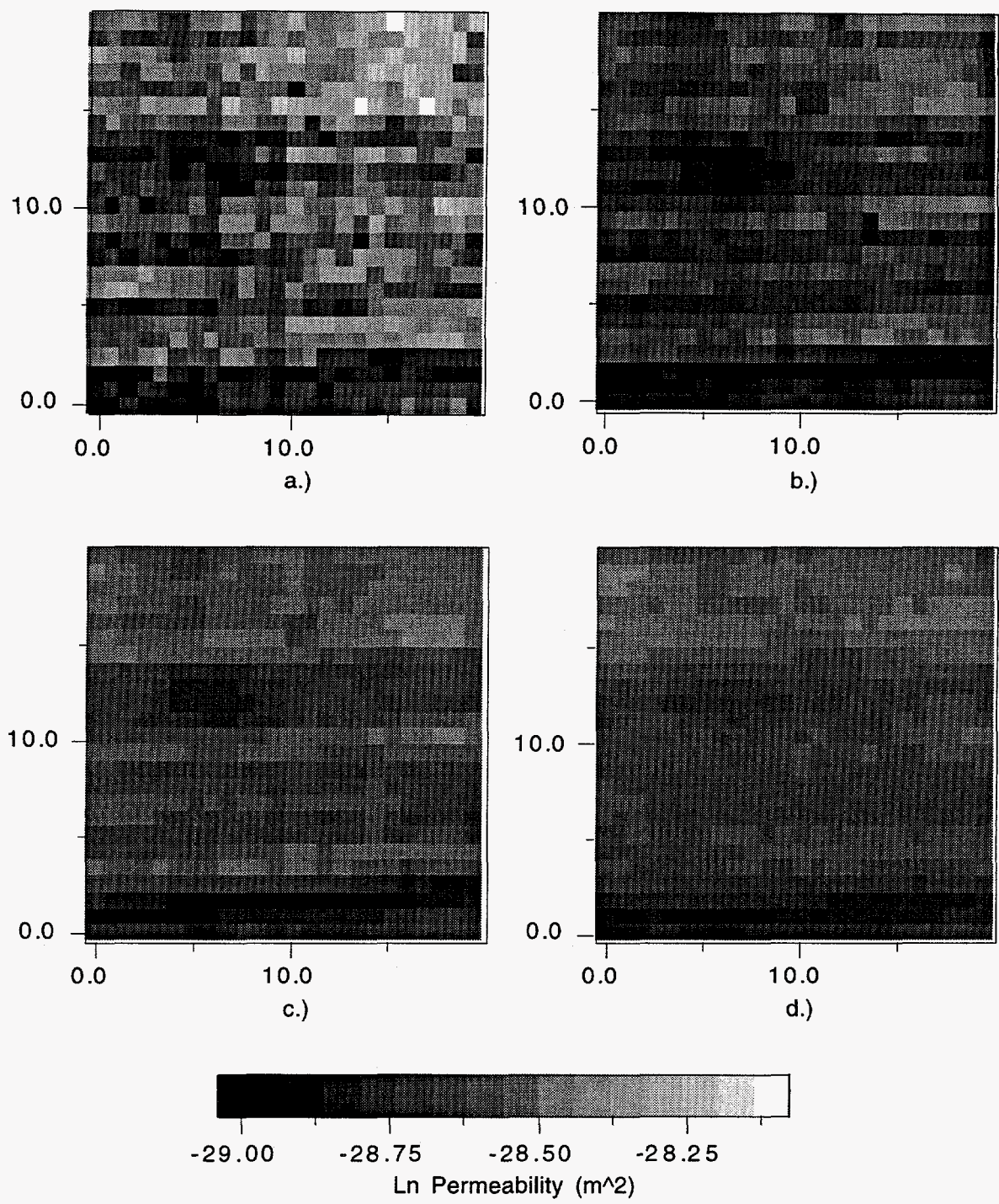
Figure 3.10. Gray-scale gas permeability field for the Berea sample, face 1 as measured with the a). 0.15, b). 0.31, c). 0.63, and d). 1.27 cm tip seals. Data are reported in terms of the natural log of the gas permeability in units of m².
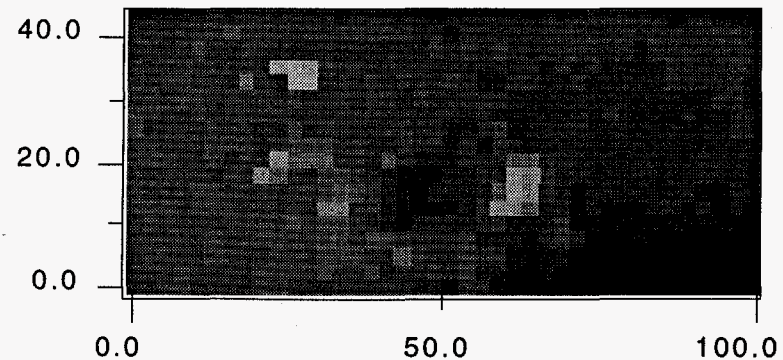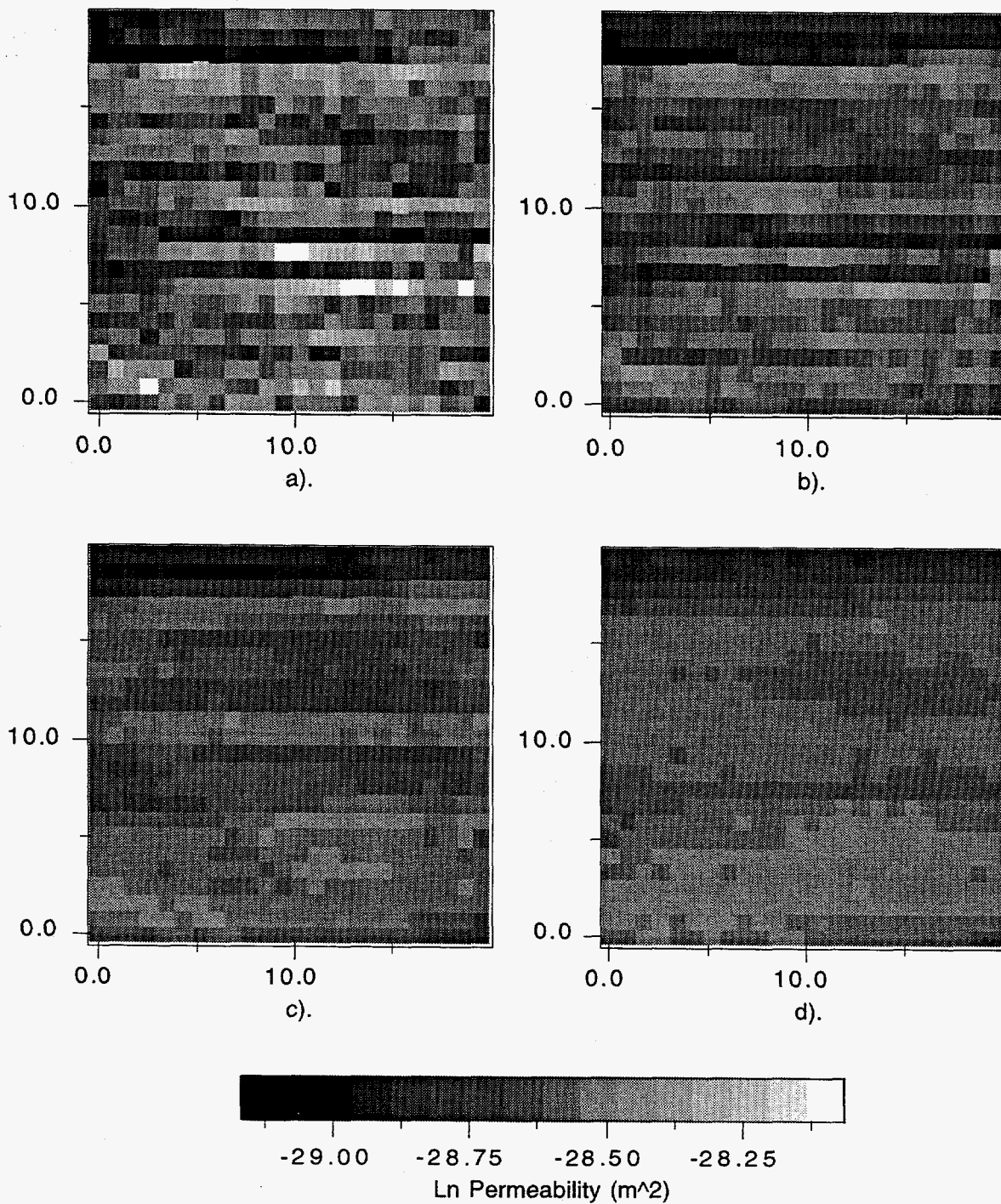
Figure 3.11. Gray-scale gas permeability field for the Berea sample, face 2 as measured with the a). 0.15, b). 0.31, c). 0.63, and d). 1.27 cm tip seals. Data are reported in terms of the natural log of the gas permeability in units of m².

34
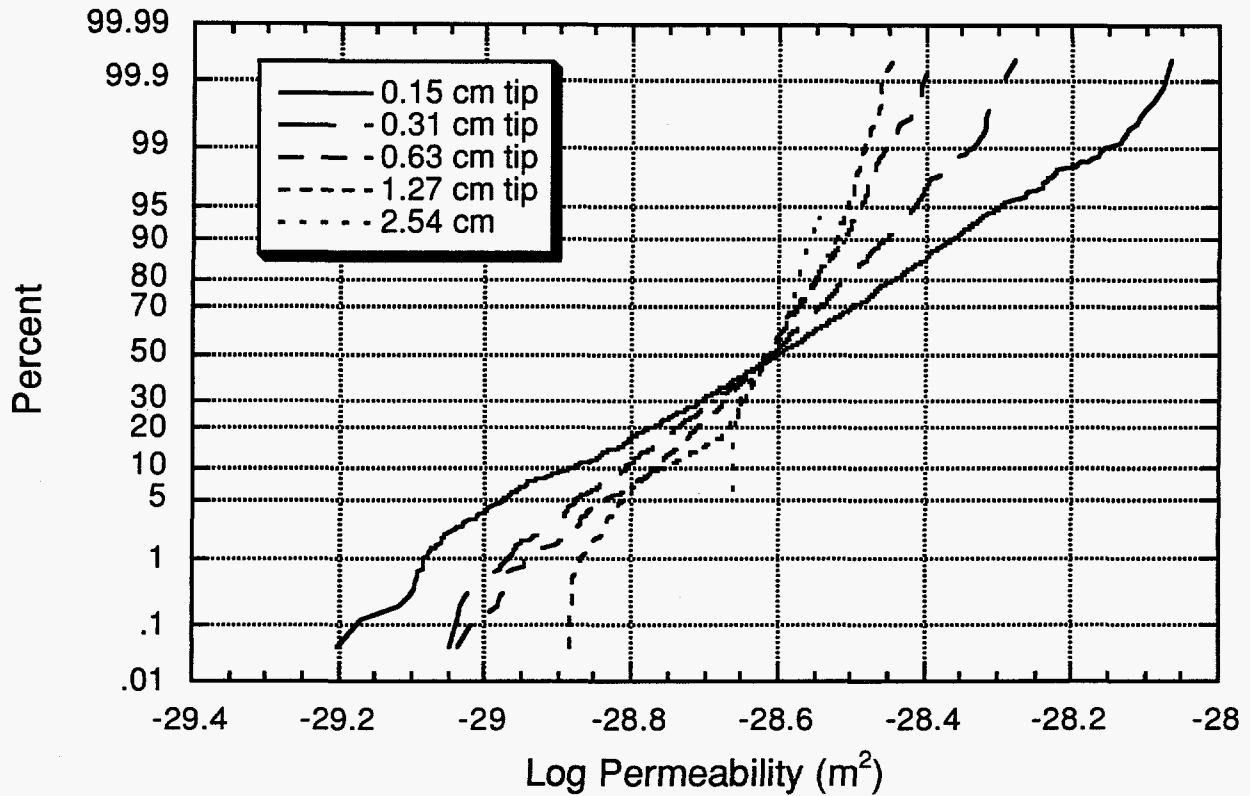
Figure 3.12. Comparison of the log permeability distribution functions measured with different size tip seals on the Berea sample.

Table 3.8: Univariate summary statistics for the log (natural) permeability (m²) measured at five different sample supports on the Berea sample.

| Tip Seal	0.15 cm	0.31 cm	0.63 cm	1.27 cm	2.54 cm
Mean	-28.61	-28.62	-28.63	-28.62	-28.61
Median	-28.60	-28.61	-28.62	-28.61	
Standard Deviation	0.20	0.14	0.10	0.09	
Variance	0.04	0.02	0.01	0.01	
Kurtosis	-0.12	-0.09	0.78	0.66	
Skewness	-0.20	-0.38	-0.80	-0.93	
Range	1.14	0.77	0.64	0.44	
Minimum	-29.20	-29.05	-29.04	-28.88	
Maximum	-28.06	-28.28	-28.39	-28.45	
Count	1152	1152	1152	1152	8
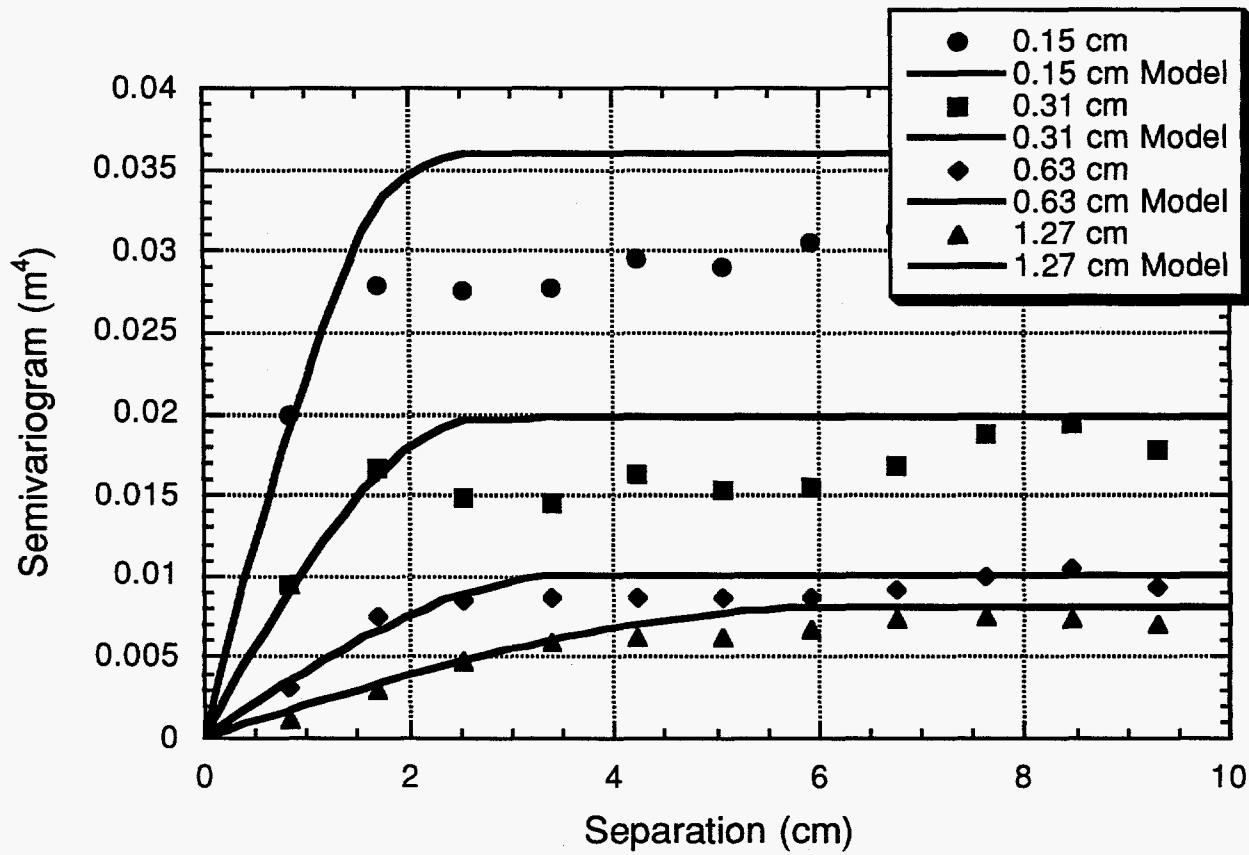
Figure 3.13. Comparison of the log permeability sample semi-variograms measured with different size tip seals on the Berea sample. The sample semi-variograms were generated using a search direction oriented normal to bedding. A spherical semi-variogram model has been fit to each data set (model parameter values are given in Table 3.9).
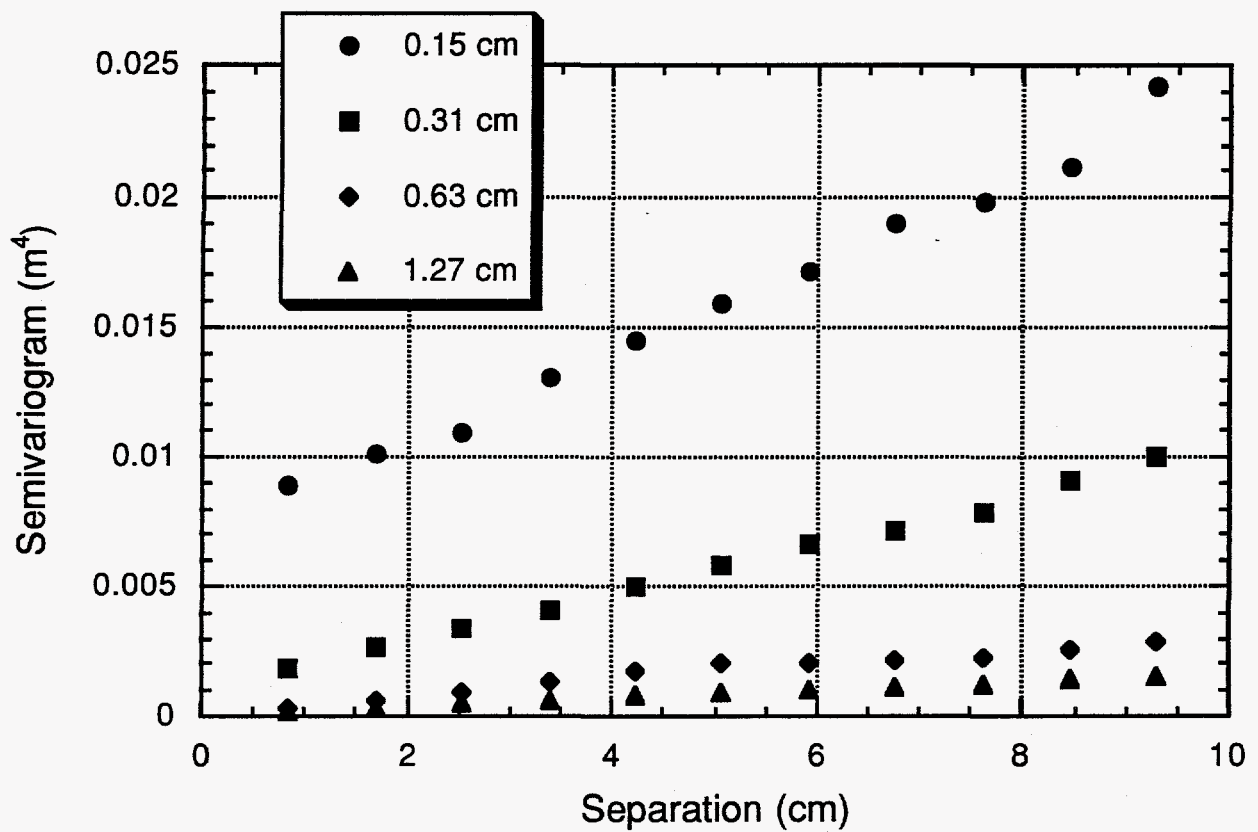
Figure 3.14. Comparison of the log permeability sample semi-variograms measured with different size tip seals on the Berea sample. The sample semi-variograms were generated using a directional search oriented parallel to bedding.

are given in Table 3.9) while no attempt was made to model the sample semi-variograms oriented parallel to bedding. Again, it is noted that the sill decreases with increasing sample support while the range increases. In all cases the nugget is very small or non-existent. It is also interesting to note that the average bedding thickness is between 1.27 and 2.54 cm, which corresponds well with the measured range of correlation.

Table 3.9: Spherical model parameters fit to the sample semi-variograms measured at four different sample supports on the Berea sample.

Tip Seal	0.15 cm	0.31 cm	0.63 cm	1.27 cm
Sill(m^4)	0.036	0.02	0.01	0.008
Range (cm)	2.4	2.7	3.6	6.1
Modeled Variance(m^4)	0.036	0.02	0.01	0.008
Nugget(m^4)	0.0	0.0	0.0	0.0

Interpretation of Measured Up-Scaling Behavior

The key result drawn from the analysis of these samples is the evidence of distinct trends that relate sample support to various statistical measures. At this time, we wish to determine whether these measured trends can be explained using current conceptual models of up-scaling behavior.

Up-scaling behavior of the sample variance and distribution range (difference in the maximum and minimum values) can be explained in a purely qualitative sense. As noted previously, the sample variance consistently decreases with increasing sample support. For a fixed domain size, the sample variance must decrease because larger sample volumes average (or smooth) over more heterogeneity than do smaller volumes. For this same reason, the range of the distribution (as was seen above) will also decrease with increasing sample support. Favorable qualitative comparisons can also be drawn between observable characteristics of the rock fabric and the geostatistical models describing the spatial continuity of the gas permeability. For the case of the Tiva Cliff and the Berea samples, quantifiable structural characteristics of the sample can be correlated with behavior of the range of correlation. In the Tiva Cliff sample the correlation length (3.4 cm, see discussion below) and the upper extent of the pumice size frequency distribution (~3.5 cm as shown in Figure 3.4) are seen to closely coincide, while the thickness of individual beds in the Berea Sandstone (~1.27 to 2.54 cm) is found to closely correspond to the measured range of correlation (~1.9 cm, see discussion below). At this time, explanation of the behavior of the modeled nugget is difficult but is believed to be influenced both by measurement error and the selection of sampling grids.

To extend our analysis, a quantitative evaluation of the data is performed by comparing the measured up-scaling behavior with that predicated by a simple analytical model. We begin by analyzing the sample semi-variograms to determine the correlation length and effective radius of measurement for each tip seal used (i.e., sample support). This information, along with the measured univariate statistics will form the basis of our analysis.

It is well established that the range of the sample semi-variogram will increase in proportion to the increasing size of the sample support,

$$\lambda_V = \lambda_o + L \qquad (3.1)$$

38

where λ_V is the range of the sample semi-variogram measured at a given support, λ_o is the range of the point support semi-variogram (i.e., where the random variable is associated with a mathematical point rather than a sample volume), and L is some measure of the size of the sample support (Clark, 1977; Journel and Huijbregts, 1978; Clark, 1979). For the case of the hemispherical flow field associated with the gas permeameter, L is simply equal to two times the effective radius of the measurement r_{eff}. This relationship is quite sensible considering that measurements with increasing support will have to be that much further apart (i.e., $2*r_{eff}$)before they become independent. From our tests, λ_V is known from each of the sample semi-variograms (Table 3.4, 3.6, 3.7, and 3.9); however, explicit measures of λ_o and r_{eff} are lacking. Nevertheless, estimates of λ_o and r_{eff} are made based on the measured incremental increase in λ_V and the assumption that r_{eff} increases as a relatively consistent function of tip seal size. Using this approach λ_o and r_{eff} are estimated for each rock sample and reported in Tables 3.10 - 3.12.

It should be noted that the measured r_{eff} is much smaller than $4* r_i$ as predicted by Goggin et al. (1988). What this means is that although the gas flow field may extend up to or beyond $4* r_i$ the measurement is most sensitive to the porous material directly under the seal. As such, the measured r_{eff} reflects the effective averaging volume and not the extent of the gas flow field.

Table 3.10: The range and predicted effective measurement radii r_{eff} for the point support and each of the five tip seals used on the Tiva Cliff sample.

Tip Seal	Point	0.15 cm	0.31 cm	0.63 cm	1.27 cm	2.54 cm
Range (cm)	3.4	4.0	4.5	5.5	8.0	12.0
r_{eff} (cm)	~0.0	0.31	0.56	1.06	2.31	4.31

Table 3.11: The range and predicted effective measurement radii r_{eff} for the point support and each of the five tip seals used on the Tiva Cap sample.

Tip Seal	Point	0.15 cm	0.31 cm	0.63 cm	1.27 cm	2.54 cm
Range (cm) in plane	12.5	13.0	13.8	15.5	17.0	19.7
Range (cm) normal	7.7	-	9.0	10.0	11.5	13.0
r_{eff} (cm)	~0.0	0.25	0.65	1.45	2.20	3.60

Table 3.12: The range and predicted effective measurement radii r_{eff} for the point support and each of the five tip seals used on the Berea sample.

Tip Seal	Point	0.15 cm	0.31 cm	0.63 cm	1.27 cm
Range (cm) parallel to bedding	>10	>10	>10	>10	>10
Range (cm) normal to bedding	1.92	2.4	2.7	3.6	6.1
r_{eff} (cm)	~0.0	0.24	0.39	0.84	2.09

Quantitative analysis of the measured up-scaling behavior is pursued through the use of the analytic model proposed by Dimitrakopoulos and Desbarats (1993). This model was selected because it provides a convenient means of up-scaling both the sample mean and variance. As discussed in Section I.B, the sample mean and variance are predicted to scale according to,

$$E[\ln(k_V)] = k_g + (\omega/2)\gamma_{avg}(V,V) \tag{3.2}$$

$$Var[\ln(k_V)] = \sigma_y^2 - \gamma_{avg}(V,V) \tag{3.3}$$

respectively. From the measurements made on the various rock samples, $E[\ln(k_V)]$, $Var[\ln(k_V)]$, k_g, and σ_y^2 are known while $\gamma_{avg}(V,V)$ (known as the dispersion variance in the geostatistical literature) is estimated from tables in Journel and Huijbregts (1978). For each sample, the ensemble mean $E[\ln(k_V)]$ has been calculated using an ω of 1 (arithmetic average), 0 (geometric average), and -1 (harmonic average) and plotted with the measured sample mean. The ensemble variance $Var[\ln(k_V)]$ has also been calculated and plotted with the measured variance. In each case, the statistical measures are plotted verses dimensionless scale which is taken to be the ratio of the sample support ($2 \cdot r_{eff}$) to the sample correlation length (λ_o) (Tables 3.10-3.12).

For the Tiva Cliff sample, the measured and modeled up-scaling behavior of the mean and variance are plotted in Figures 3.15 and 3.16, respectively. The 0.15 cm data was excluded from the analysis because of the noted inconsistencies in the mean and variance with respect to the other tip seal data (see Table 3.3; at this time it is uncertain whether this discrepancy is due to experimental error or a particular feature of the sample). In Figure 3.15 the sample mean is seen to be bound by the geometric and harmonic average. More specifically, the mean is seen to best follow a power average of $\omega = -0.3$. In Figure 3.16, the measured variance is seen to be modeled quite well by equation 3.3.

Somewhat different behavior is noted for the Tiva Cap sample. In this case, the sample mean is noted to follow quite closely to the harmonic average (Figure 3.17). Also, a significant discrepancy between the measured and modeled variance is evident (Figure 3.18). The measured variance decreases quickly and then flattens out; whereas, the modeled variance predicts a gradual decrease, underestimating that which was measured.

The Berea sample is found to behave much like the Tiva Cliff sample. In general, the sample mean follows a geometric average (Figure 3.19). The scatter in the data is due to measurement error which is not difficult to accept considering the very small absolute difference in permeability measured by the five tip seals. The measured and modeled variance are seen to behave in a similar manner (Figure 3.20). Again, a notable relative difference between the measured and modeled data exist; however, in absolute terms the difference is very small.

Conclusions

Based on the qualitative and quantitative analysis presented above some important conclusions can be drawn. First, the rock samples tested up-scale qualitatively as our conceptual models predict. That is, the variance and distribution range decrease with increasing scale while the range of correlation increases. We have also seen that in two cases the range of correlation can be related to quantifiable geologic information (i.e., bedding thickness and pumice size). Also of importance is that up-scaling of the sample mean is bound by the arithmetic and geometric average (this would likely not be the case for up-scaling of the composite fracture-matrix permeability). In contrast, quantitative prediction of up-scaling behavior is still a difficult task. We see that these three samples with very different physical characteristics scale quantitatively in very different ways. In

40

Figure 3.15. Comparison of up-scaling behavior for the sample mean as measured on the Tiva Cliff sample and that predicted using the model of Dimitrakopoulos and Desbarats (1993). Up-scaling of the mean according to an ω of 1 (arithmetic average), 0 (geometric average), and -1 (harmonic average) are shown for comparison. Dimensionless scale is taken as the ratio between the sample support ($2 \cdot r_{eff}$) and the sample correlation length (λ_o).

Figure 3.16. Comparison of up-scaling behavior for the sample variance as measured on the Tiva Cliff sample and that predicted using the model of Dimitrakopoulos and Desbarats (1993). Dimensionless scale is taken as the ratio between the sample support ($2 \cdot r_{eff}$) and the sample correlation length (λ_o).
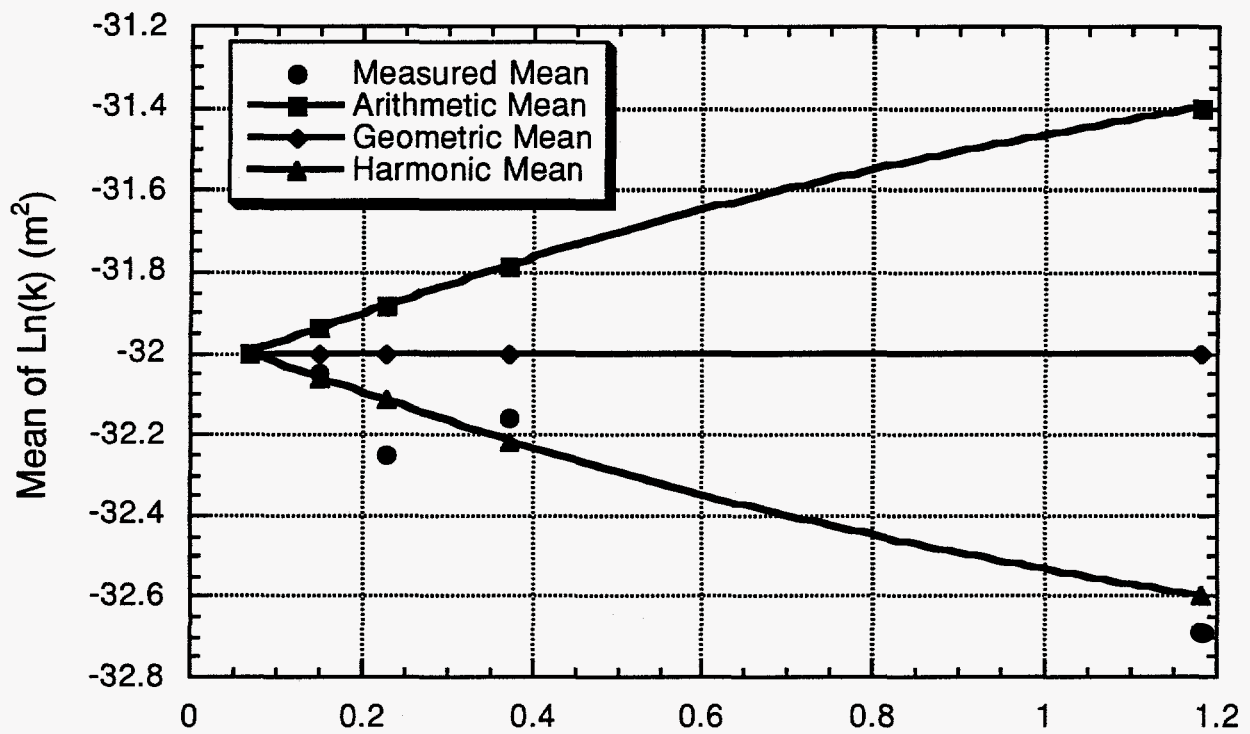
Figure 3.17. Comparison of up-scaling behavior for the sample mean as measured on the Tiva Cap sample and that predicted using the model of Dimitrakopoulos and Desbarats (1993). Up-scaling of the mean according to an ω of 1 (arithmetic average), 0 (geometric average), and -1 (harmonic average) are shown for comparison.
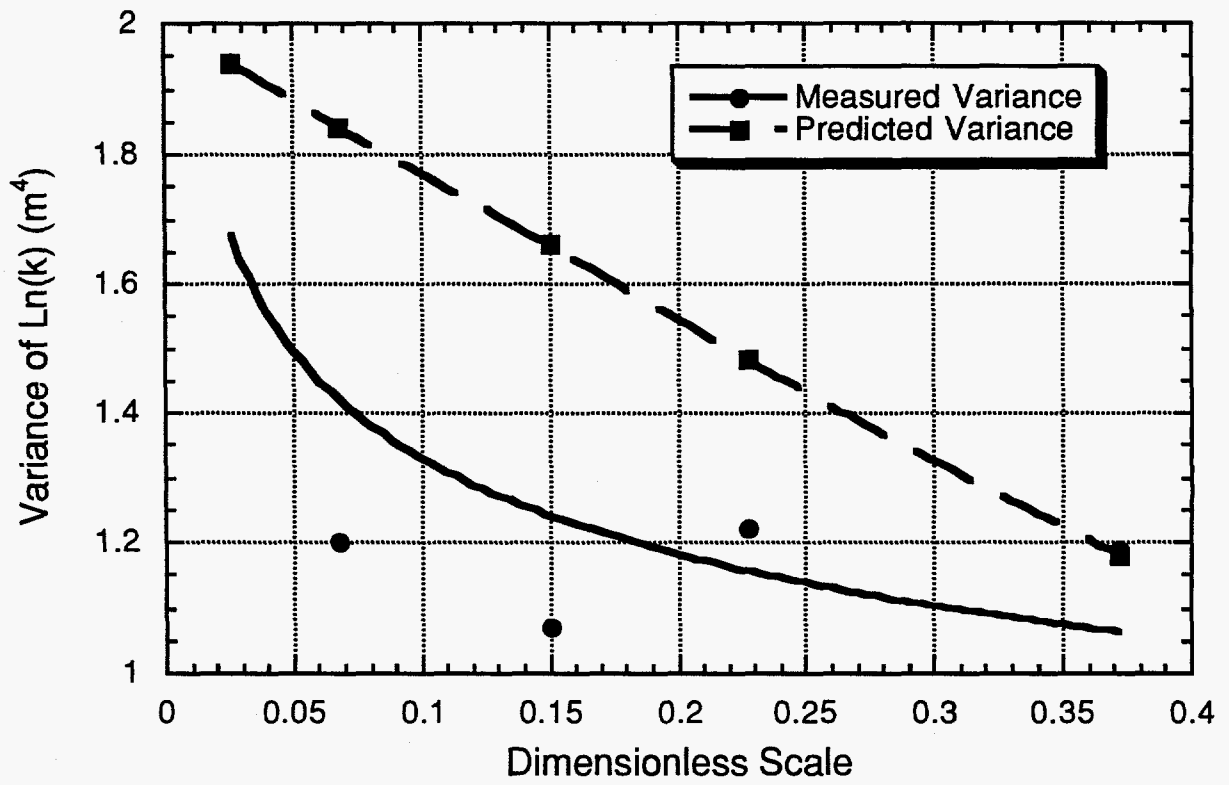
Figure 3.18. Comparison of up-scaling behavior for the sample variance as measured on the Tiva Cap sample and that predicted using the model of Dimitrakopoulos and Desbarats (1993).
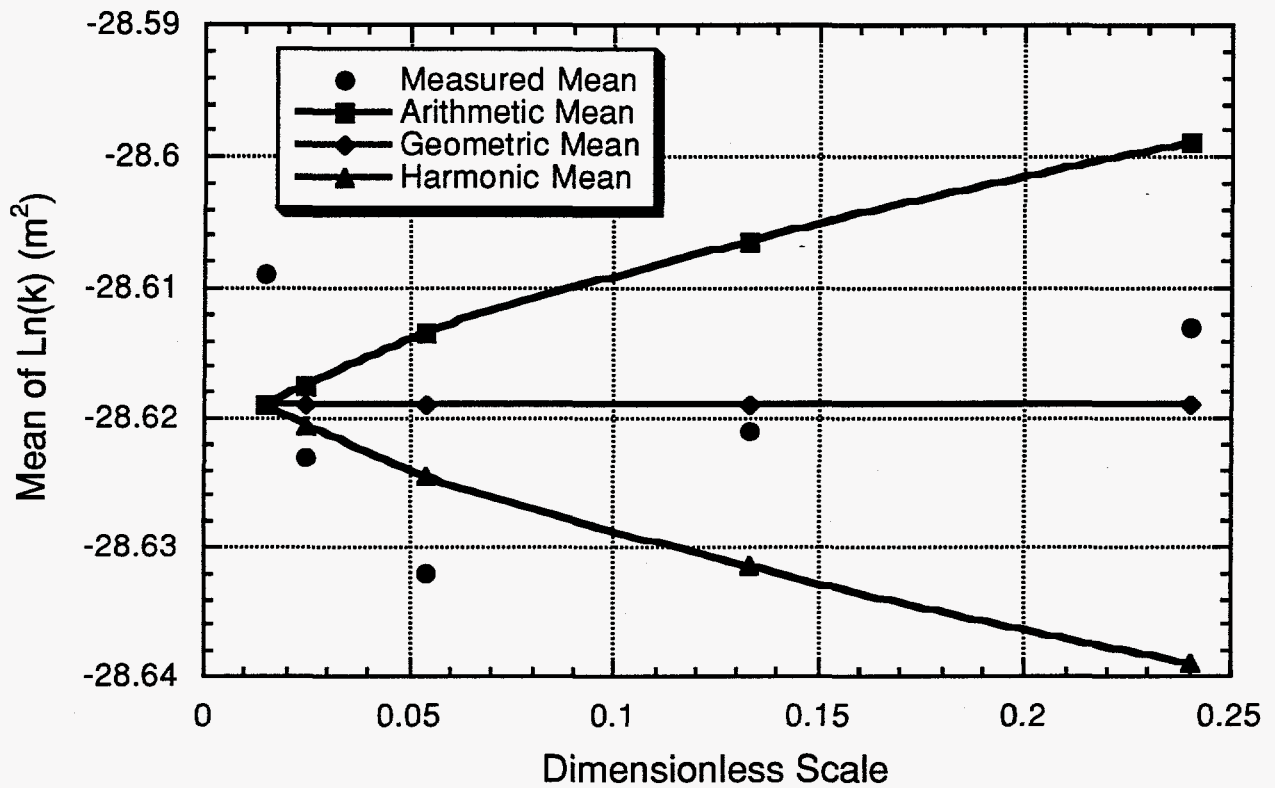
Figure 3.19. Comparison of up-scaling behavior for the sample mean as measured on the Berea sample and that predicted using the model of Dimitrakopoulos and Desbarats (1993). Up-scaling of the mean according to an ω of 1 (arithmetic average), 0 (geometric average), and -1 (harmonic average) are shown for comparison.
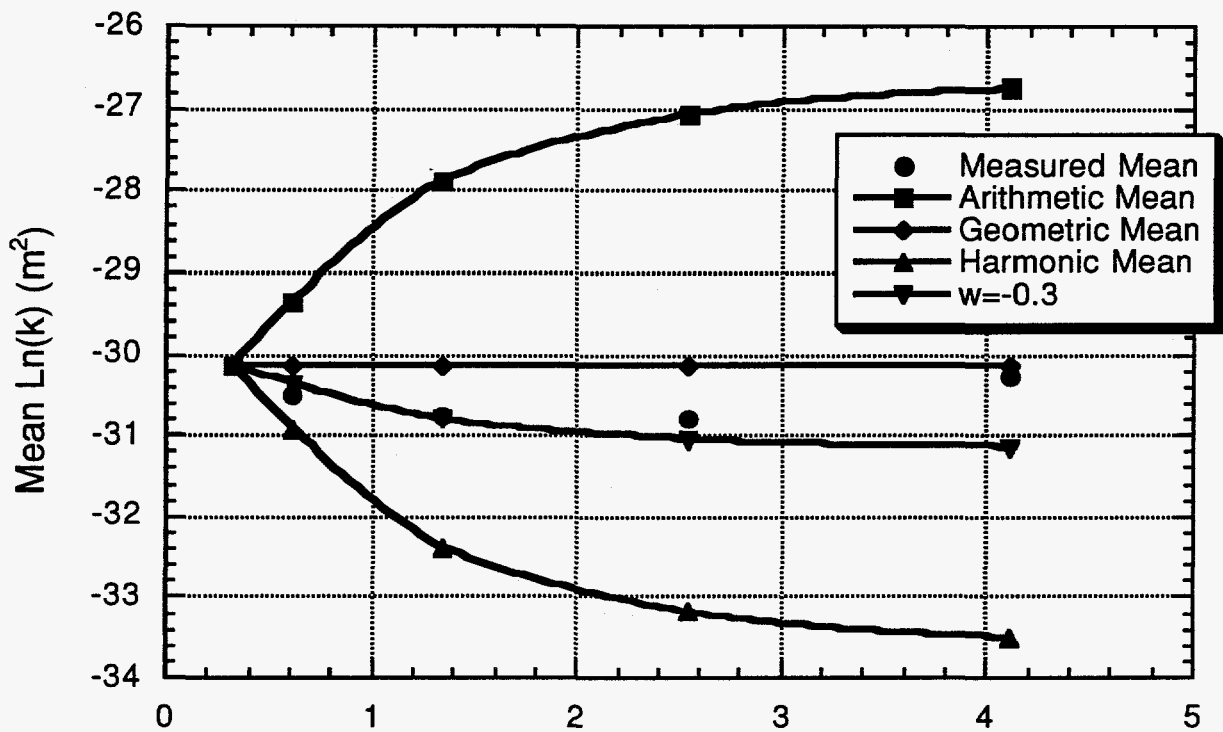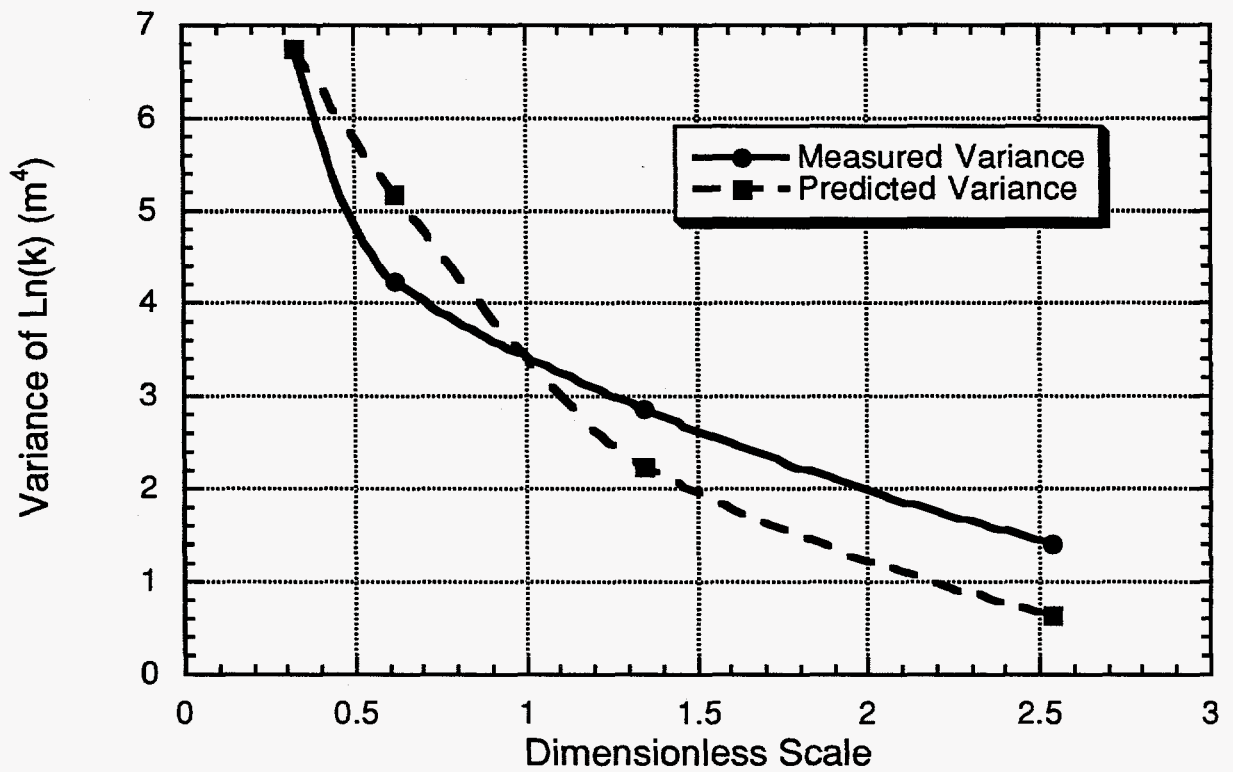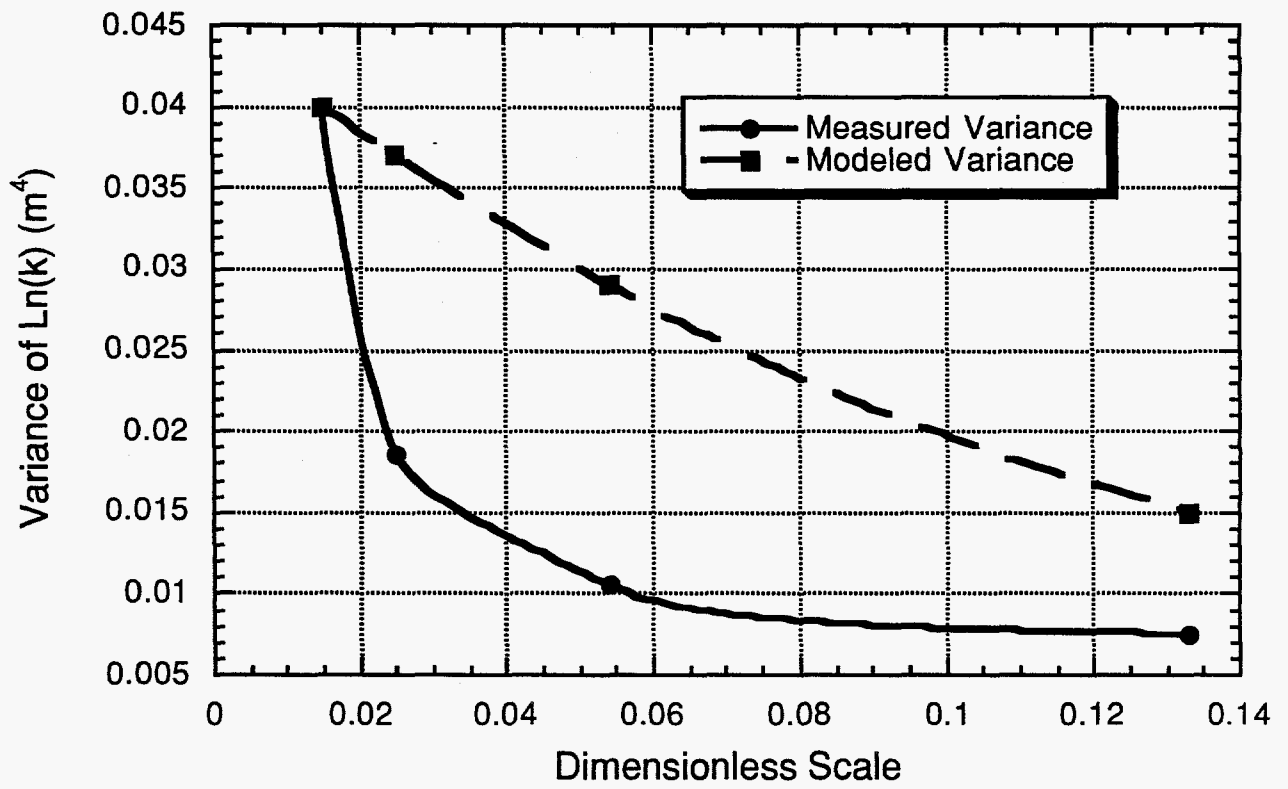
Figure 3.20. Comparison of up-scaling behavior for the sample variance as measured on the Berea sample and that predicted using the model of Dimitrakopoulos and Desbarats (1993).

particular, the mean and variance of the Tiva Cliff sample are seen to change more radically with scale than either the Tiva Cap or Berea sample. All three samples are also seen to up-scale according to different spatial averages (ω=-0.3 for the Tiva Cliff sample; ω=-1.0 for the Tiva Cap sample; and ω=0.0 for the Berea sample). These noted differences undoubtedly arise from the physical characteristics of the porous medium (i.e., structure and intensity of the heterogeneity) and characteristics of the measurement.

An alternative means of analyzing the data is to simply model the empirically derived relationships. As such, the mean and variance have been plotted verses dimensionless scale (Figures 3.21 and 3.22, respectively). In this case we have used the raw permeability data to facilitate modeling (i.e., not the log transformed data as before). The most striking feature of these plots is the degree to which the mean and variance change as a function of support. For the Tiva Cliff sample the mean changes by over two orders of magnitude while the variance decreases six orders of magnitude over a relatively small change in sample support. However, the fact that both the mean and variance for all three samples follow a power law functional relation is encouraging. That is, the power law may provide a convenient means of modeling up-scaling, which requires the determination of a single parameter, the power coefficient. Although the mean and variance are seen to scale according to different powers (i.e., -1.73 and -5.1 for the Tiva Cliff sample), these powers are expected to be related in a quantifiable manner. This does not suggest that these measured scaling models should be used to scale matrix permeability for Yucca Mountain, but that additional work should be done to explore the possibility of using the power law as a means of scaling constitutive properties. In particular, the next step needs to be the establishment of a theoretical basis for the noted power law scaling behavior.

47
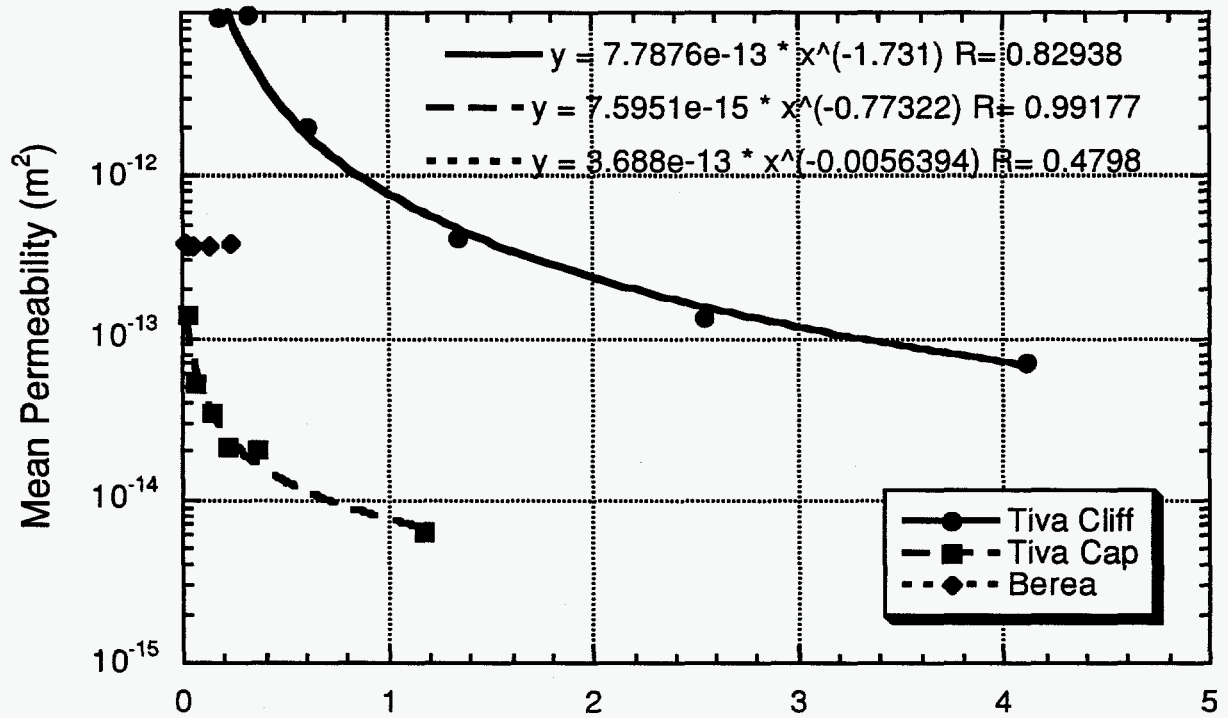
Figure 3.21. Comparison of the up-scaling behavior of the sample mean for each of the three rock samples tested. A power law functional relation has been fit to the empirical data.
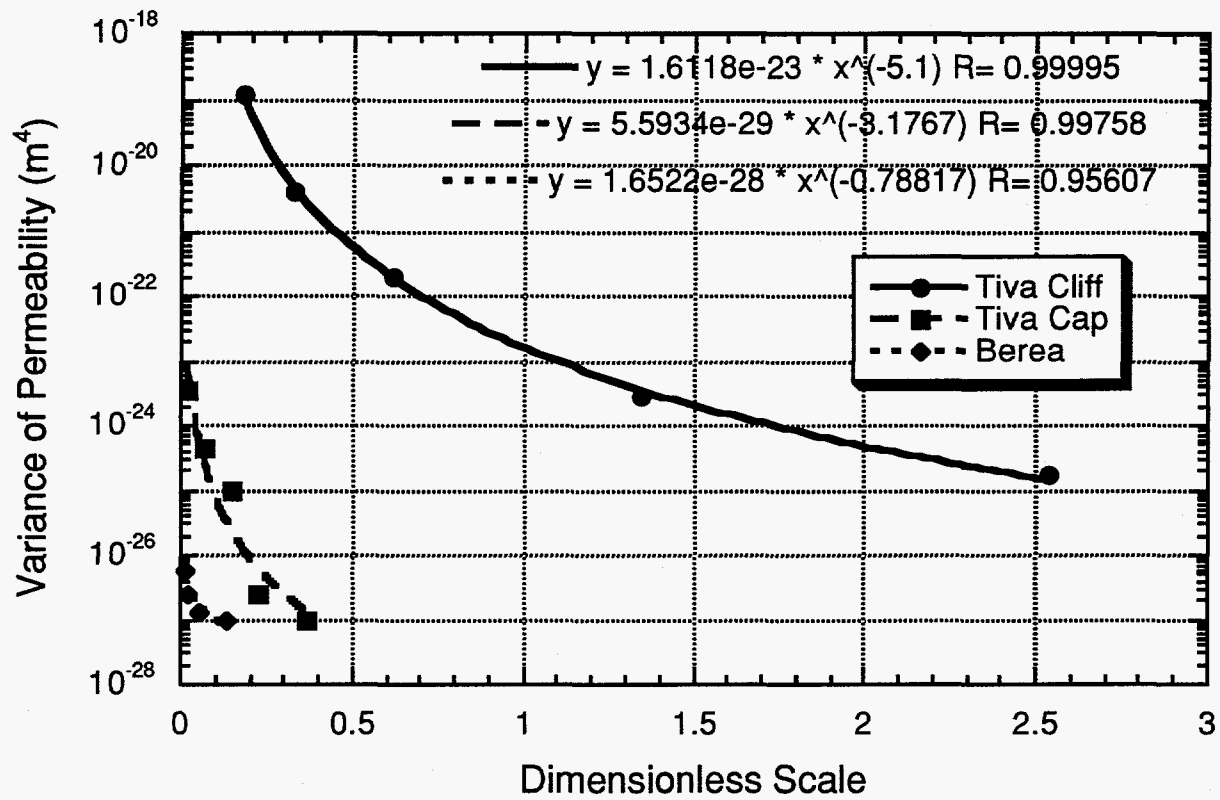
Figure 3.22. Comparison of the up-scaling behavior of the sample variance for each of the three rock samples tested. A power law functional relation has been fit to the empirical data.

4. UP-SCALING OF MATRIX SORPTIVITY: SCOPING STUDIES

As unsaturated flow is of primary interest at Yucca Mountain, models for scaling relative permeability and pressure-saturation relations will be required in support of various PA exercises. For this reason, scoping studies have been performed to identify an experimental method for measuring the up-scaling behavior of critical unsaturated flow parameters. In general, we would like to approach the investigation of unsaturated flow property up-scaling in much that same manner as was taken for saturated permeability. That is, in a controlled systematic fashion. This requires the measurement technique(s) to be simple, fast, inexpensive, and consistent regardless of the sample support. Based on a review of the literature, matrix sorptivity was identified as a good candidate. Matrix sorptivity, which is a constitutive property quantifying the capillarity of a porous medium, is measured by simply monitoring the imbibition of water into a slab or block of rock as a function of time. Matrix sorptivity was selected for investigation because it meets the experimental criteria stated above, we had the equipment necessary to make the measurements on hand, and most importantly the matrix sorptivity can be related both to the relative permeability and pressure-saturation functions of the porous medium.

The primary objectives of this effort are: 1) determine whether suitable measurements of matrix sorptivity can be made at a variety of different spatial scales, and 2) determine whether the resulting data are useful in predicting the up-scaling behavior of the relative permeability and pressure-saturation functions of the rock slabs tested. We begin by introducing the experimental method used to measure imbibition into heterogeneous tuff slabs at a variety of spatial scales. We then describe how the acquired data are used to calculate matrix sorptivity. Finally, we present the results of the scoping experiments performed and our recommendations relative to the viability of this approach.

4.1. Physical Experiment

Matrix sorptivity up-scaling experiments were performed in a simple fracture-matrix system oriented normal to the fracture plane. The test system consisted of two air-dried rock slabs (Topopah Spring Tuff from Busted Butte, Nevada Test Site), each measuring roughly 50 by 15 by 2.5 cm thick. The slabs were mated along the 50 cm (sawn) edge to form a single 0.1 mm slot fracture. The test system was wrapped in mylar to minimize evaporation; however, a 1 cm gap was maintained between the tuff slabs and mylar to allow unrestricted movement of air from the slabs. A constant flux boundary condition was applied at the top of the vertically oriented fracture (5 ml/min.) and a constant suction boundary (10 cm water) was applied at the bottom of the fracture with a hanging water column (Figure 4.1).

At the onset of infiltration, water moved rapidly through the fracture and began to drip from the bottom of the hanging column. Water did not fully span the width of the fracture but instead fingered within the 2.5 cm fracture thickness. As time progressed, fluid moved from the fracture into the matrix (initially at near zero saturation) until the wetting fronts neared the outside edges of the tuff slabs, at which time the experiment was stopped. During this period, x-ray imaging was performed using a 60 kV potential and exposure time of 3 minutes (Tidwell and Glass, 1994). Two-dimensional x-ray images, integrated over the thickness of the slab, were acquired at 5, 15, 30, 60, 120 and 180 minutes. Potassium iodide (KI) was dissolved in the water (10% by weight) to enhance the x-ray adsorption contrast between air and water. Following the experiment, the slabs were rinsed for several weeks to remove all KI, oven dried, vacuum saturated with fresh KI solution, and finally re-imaged to yield the fully saturated field (necessary in quantifying matrix saturation and porosity).

50
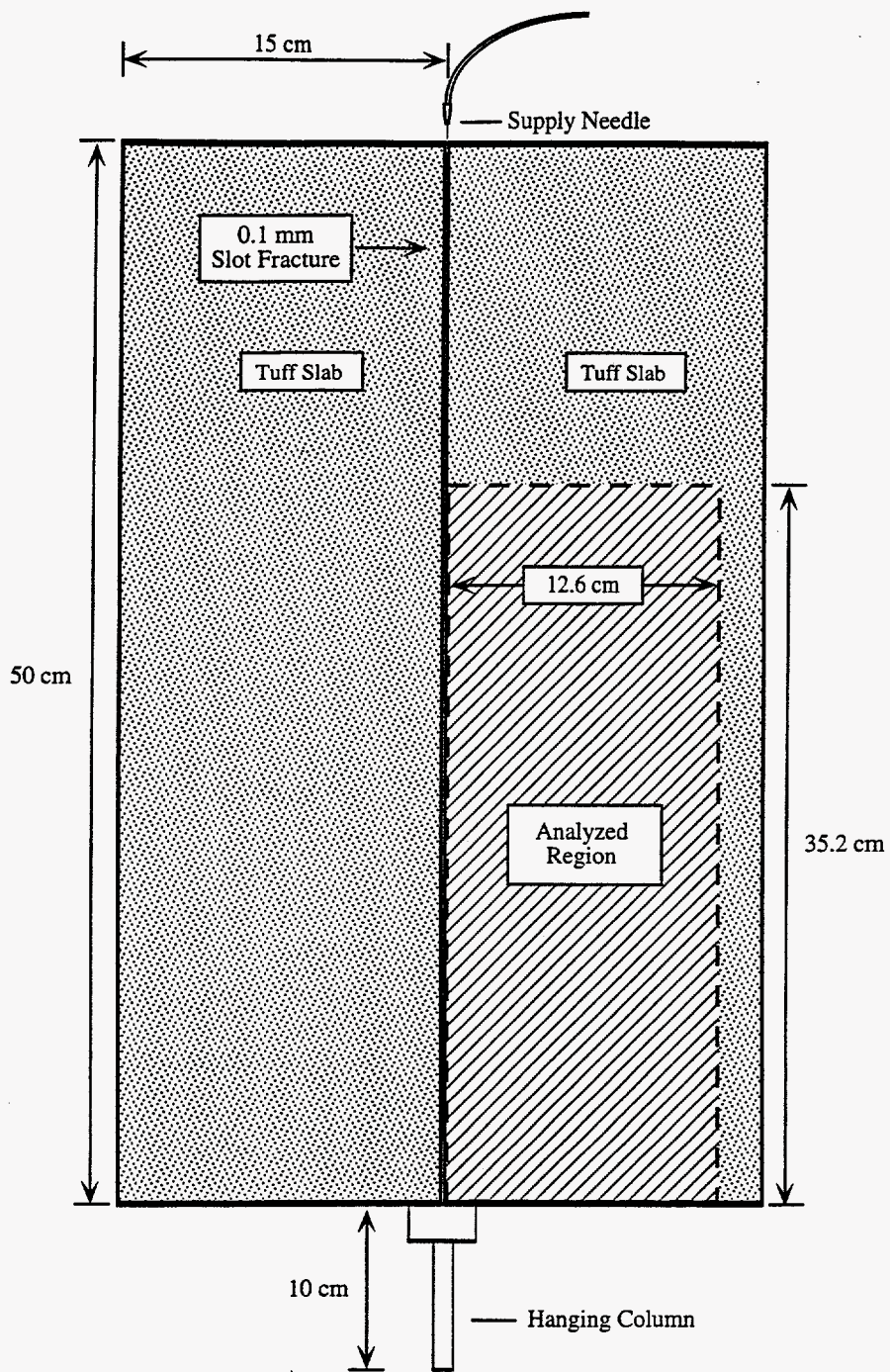
Figure 4.1. Schematic of the Fracture-matrix experiment. The boxed region delineated the area analyzed.

Using a digital camera, the x-ray images recorded on film were digitized into arrays of 1024 by 1024 pixels (0.44 mm by 0.44 mm) each with a dynamic gray-scale range of 4096 levels. A subsection of the experiment, 800 pixels tall and 288 pixels wide (352 mm tall, 126.7 mm wide), was chosen for analysis (Figure 4.1). Saturation fields as a function of time were then calculated for this region from the digitized images using the method of Tidwell and Glass (1994). The porosity field was also determined. This involves subtracting the log (natural) transformed background (dry) image from the log (natural) transformed vacuum saturated image, normalizing the difference image by its mean intensity, then multiplying by the average porosity for the slab (determined independently gravimetricly to be 0.20 ±0.005). Figure 4.2 presents the saturation fields at 5, 15, 60, and 180 minutes along with the porosity field.

4.2. Matrix Sorptivity

Richards equation for one-dimensional, capillary-dominated flow may be written in the non-linear diffusion form:

$$\frac{\partial \theta}{\partial t} = \frac{\partial}{\partial x}\left(D(\theta)\frac{\partial \theta}{\partial x} \right) \tag{4.1}$$

subject to the boundary and initial conditions:

$$\begin{aligned}
\theta(x, t=0) &= \theta_i \\
\theta(x=0, t>0) &= \theta_o \\
\theta(x \to \infty, t \geq 0) &= \theta_i
\end{aligned} \tag{4.2}$$

where θ is the liquid saturation, and $D(\theta)$ is the water diffusivity of the medium. Equation (4.1) with (4.2) admit a similarity transform to the non-linear ordinary differential equation:

$$\frac{\eta}{2}\frac{\partial \theta}{\partial \eta} = \frac{\partial}{\partial \eta}\left(D(\theta)\frac{\partial \theta}{\partial \eta} \right) \tag{4.3}$$

with boundary conditions:

$$\begin{aligned}
\theta(\eta = 0) &= \theta_o \\
\theta(\eta \to \infty) &= \theta_i
\end{aligned} \tag{4.4}$$

where η is the similarity variable given by $x/t^{1/2}$. Although Equation 4.3 is non-linear, its solution, subject to the boundary conditions given in (4.4), is dependent only on η regardless of the functional form of $D(\theta)$. If the analysis and assumptions given above adequately model system behavior and the hydraulic properties of the medium are homogeneous, any given saturation level (θ) must propagate through the medium with a $t^{1/2}$ dependence. Similarly, the total volume of water imbibed per cross-sectional area of medium I (or fracture) must be linearly related to $t^{1/2}$. The constant of proportionality relating I and $t^{1/2}$ is called the sorptivity (Philip, 1955), denoted by S:

$$I(t) = S(\theta_o, \theta_i)t^{1/2} \tag{4.5}$$

The sorptivity, which embodies capillarity and has dimensions of $[L/T^{1/2}]$, is dependent on the supply saturation θ_o, and the initial saturation of the medium θ_i. Given the relative ease of measuring the sorptivity, it has found common use in solutions to unsaturated flow problems and estimation of other more difficult to measure hydraulic properties (Zimmerman et al., 1993).

Figure 4.2: Observed saturation fields for the right hand block at a) 5 minutes, b) 30 minutes, c) 60 minutes, and d) 180 minutes at low resolution (50 by 18 grid). The 180 minute image at full resolution (800 by 288 points) is shown for comparison in e).
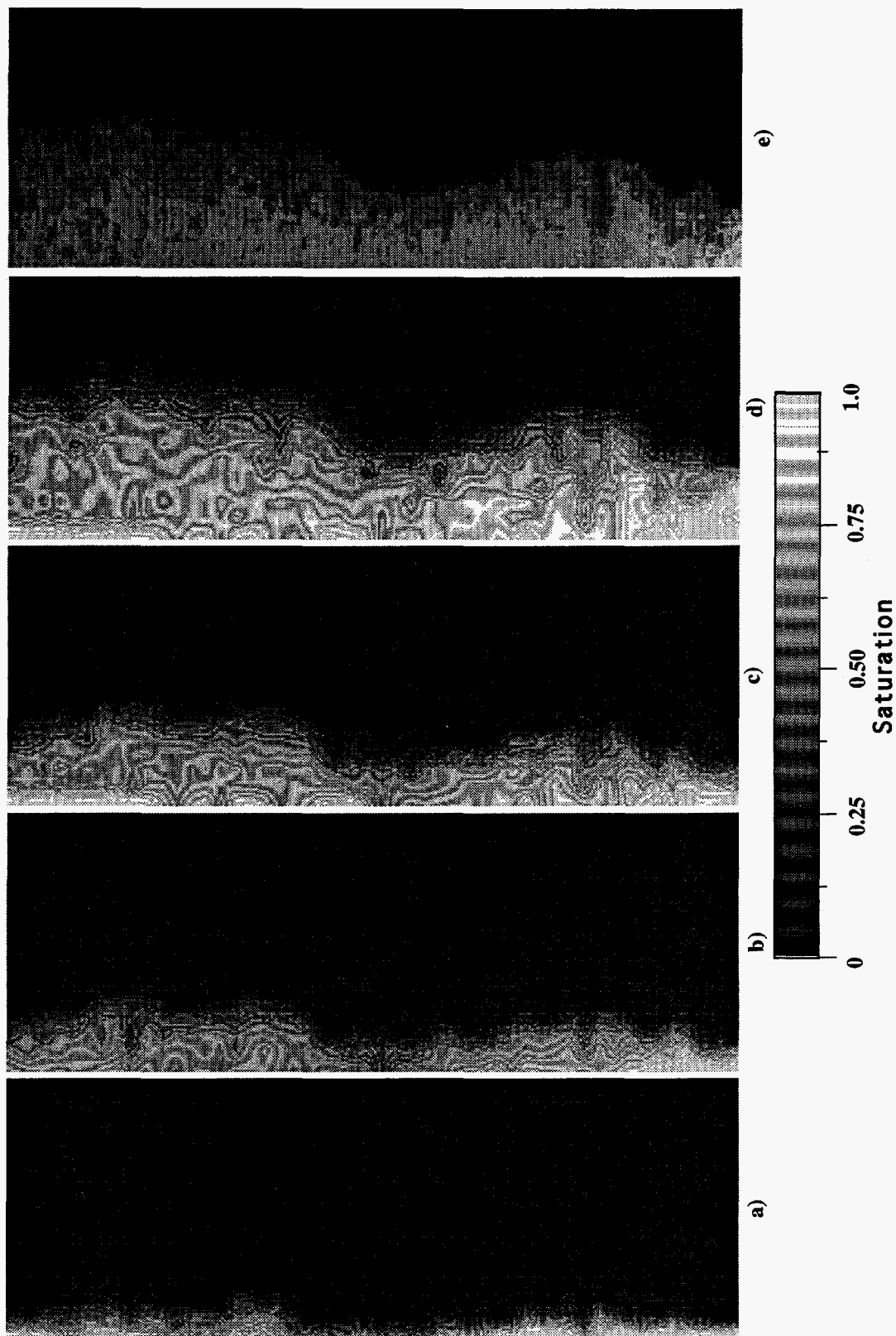
53

In applying this conceptual model, I(t) was calculated from the measured saturation and porosity images (Figure 4.2) at t = 5, 15, 30, 60, 120, and 180 minutes. These calculations were made at four different resolutions corresponding to fracture lengths of 0.44, 7.0, 28.2, and 112.6 mm (i.e., calculations integrated over 1, 16, 64, and 256 rows of saturation data, respectively). In each case, I(t) was calculated at 0.44 mm intervals along the fracture (a moving average was used in the latter three cases). Sorptivity was then calculated at each resolution according to Equation 4.5 via simple linear regression. In this way, S is a measure of matrix imbibition integrated over the thickness of the slab and corresponding fracture length. Results are plotted versus fracture position in Figure 4.3. The effective sorptivity at the scale of the analyzed region (352 mm fracture length) was calculated to be 0.058 mm/min$^{1/2}$.

4.3. Discussion

In this section we analyze the acquired sorptivity data. We begin by first evaluating the suitability of using Equation 4.5 to model matrix imbibition measured in the scoping experiments. Once verified, we turn our attention to analysis of the measured matrix sorptivity up-scaling behavior.

Evaluation of the Matrix Sorptivity Model

The appropriateness of using Equation 4.5 to model matrix imbibition from our flowing fracture can be evaluated by investigating the linearity of the I vs. $t^{1/2}$ relationship as quantified by the correlation coefficient r. For the 800 measurements of S made on the tuff slab at the 0.44 mm resolution, r ranged from 0.958 to 0.999 with mean of 0.995 and standard deviation 0.005. As measurement resolution decreased (i.e., fracture length increased) these statistics were noted to consistently improve. Based on these data, it is evident that I and $t^{1/2}$ exhibit a strong linear relationship.

Linearity of the I vs. $t^{1/2}$ relation would be jeopardized in any system for which Richards equation is an inappropriate governing equation or when any of the assumptions upon which the similarity transform of Richards equation is based are violated. That is, the medium is assumed homogeneous, and matrix imbibition is 1-D and capillary dominated (with negligible gravitational forces). In addition, a uniform initial condition is assumed with prescribed uniform saturation along one boundary while the other boundary must be at sufficient distance to be unaffected by the imbibing wetting front. Of these conditions, two were not met by this experiment: the fracture was not uniformly saturated and the matrix was heterogeneous.

Non-uniform saturation in the fracture had its greatest influence on matrix imbibition at early times in the experiment. At early times there was a component of matrix flow transverse (from the finger edges toward the slab faces) to the wetting front. This behavior is evidenced in our data by the intercept of the I vs. $t^{1/2}$ relationship that is generally different than zero (mean of -0.08 mm and standard deviation of 0.05 mm). However, in our experiment the slab is thin, hence transverse flow is limited and linear imbibition is quickly attained.

The tuff slabs used in this experiment are characterized by thin pumice inclusions (visible in Figure 4.2e) dispersed within a dense matrix. The pumice inclusions are oriented normal to the fracture but rarely span the full thickness of the tuff slab (~one every 20 cm). As these pumice inclusions are very porous, they form the primary heterogeneity relative to matrix imbibition. The intensity of this matrix heterogeneity is demonstrated by constant-head permeameter measurements made on 10 core samples trimmed from the tuff slabs. These tests produced conductivity measurements ranging from 3.6 E-8 to 2.3 E-4 cm/sec (Glass et al., 1994). Matrix heterogeneity is expected to influence imbibition in one of two ways. First, heterogeneity dispersed along the path of the wetting front may induce variations in the imbibition rate and thus non-linearity in the I vs.
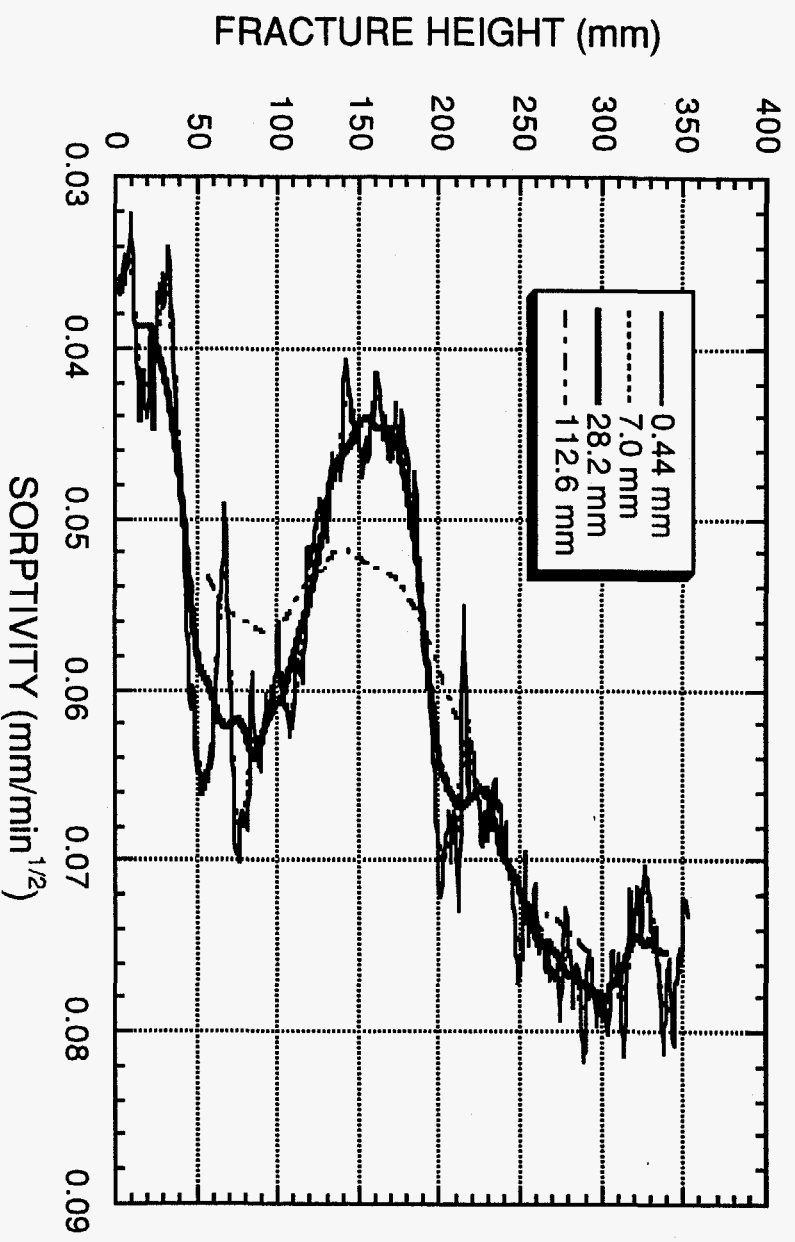
54

Figure 4.3. Sorptivity as measured along the height of the fracture. Traces are presented for four different measurement resolutions corresponding to fracture lengths of 0.44, 7.0, 28.2, and 112.6 mm.

$t^{1/2}$ relationship. The strong linearity of the data presented above argues against such behavior. Second, matrix heterogeneity transverse to flow may promote violation of simple 1-D imbibition. Where strong spatial variation in hydraulic properties occurs, transverse diffusion (within the plane of the tuff slab) of the wetting front will be promoted. If this indeed occurs, then linearity and hence r will decrease where S changes quickly (e.g., in the vicinity of fracture heights 45, 130, and 190 mm). However, inspection of Figure 4.4 suggests that this is not the case.

Results of Matrix Sorptivity Up-Scaling Studies

We begin our analysis of the up-scaling of matrix sorptivity by inspecting the behavior of the sorptivity traces given in Figure 4.3. It is evident that smoothing of the traces occur as the sample support increases; however, the degree of smoothing is relatively minor. This behavior is reflected in the summary statistics as well (Table 4.1). Here, only a small decrease in the mean and variance occurs with increasing sample support. The sample semi-variograms have also been constructed for each sample support (Figure 4.5). The search direction in each case is oriented parallel with the fracture. The semi-variograms exhibit a strong hole effect due to the periodicity of the sorptivity trace (Figure 4.3). Also, the range of correlation is seen to increase in proportion to the increase in fracture length over which the sorptivity was measured (see Equation 3.1). The range increases from approximately 60 mm (0.44 mm), to 65 mm (7.0 mm), 74 mm (28.2 mm), and beyond the resolution of the semi-variogram (112.6 mm). In general, matrix sorptivity was noted to change very little with increasing sample support.

Table 4.1: Comparison of summary statistics for sorptivity data (mm min$^{-1/2}$) collected at different sample supports.

Fracture Length (mm)	0.44	7.0	28.2	112.6
Mean	0.061	0.061	0.061	0.060
Median	0.063	0.0631	0.062	0.056
Standard Deviation	0.0135	0.0132	0.0120	0.0082
Variance	0.000182	0.000174	0.000144	0.00006
Kurtosis	-1.16	-1.18	-1.19	-1.15
Skewness	-0.33	-0.33	-0.23	0.68
Range	0.0495	0.0443	0.0395	0.0239
Minimum	0.0322	0.0347	0.0387	0.0517
Maximum	0.0817	0.079	0.0782	0.0756
Count	800	784	737	546

Conclusions

In conclusion, we see that matrix sorptivity up-scales in a qualitatively similar manner to the matrix permeability but at a much reduced rate. This is likely due to sorptivity being given to much less spatial variability than the permeability (due to differences in the physics governing these constitutive parameters). For the tuff sample investigated, the saturated matrix hydraulic conductivity varied by five orders of magnitude while the sorptivity varies by a factor of only 2.5. For this reason, it would be very difficult to use sorptivity with its low variability to predict up-scaling behavior of highly variable properties like relative permeability and pressure saturation relations. However, the low variability of the sorptivity and its ease of measurement suggest that it may represent an important tool for modeling matrix flow. That is, consideration should be given

56

to modeling matrix flow directly using sorptivity rather than the hydraulic conductivity. However, such applications are limited by the assumptions governing the sorptivity, as discussed above.
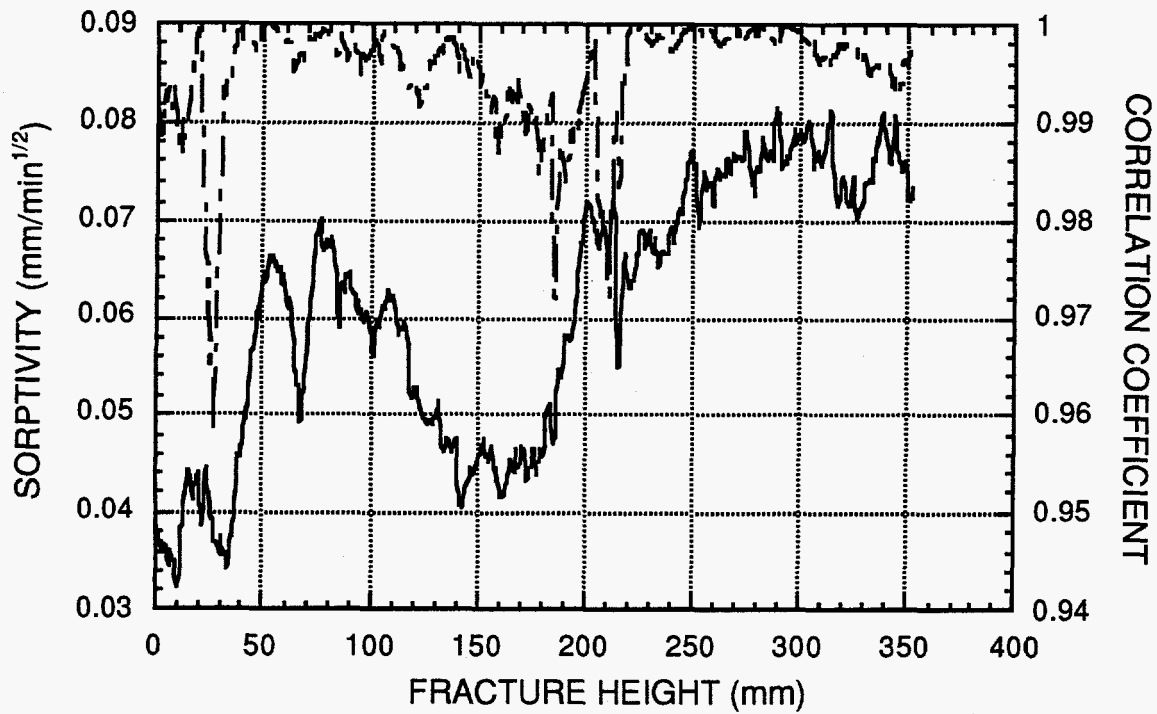

Figure 4.4. Sorptivity (measured at a resolution of 0.44 mm) and associated correlation coefficient vs. fracture height. The sold line traces the sorptivity profile, while the broken line traces the correlation coefficient.
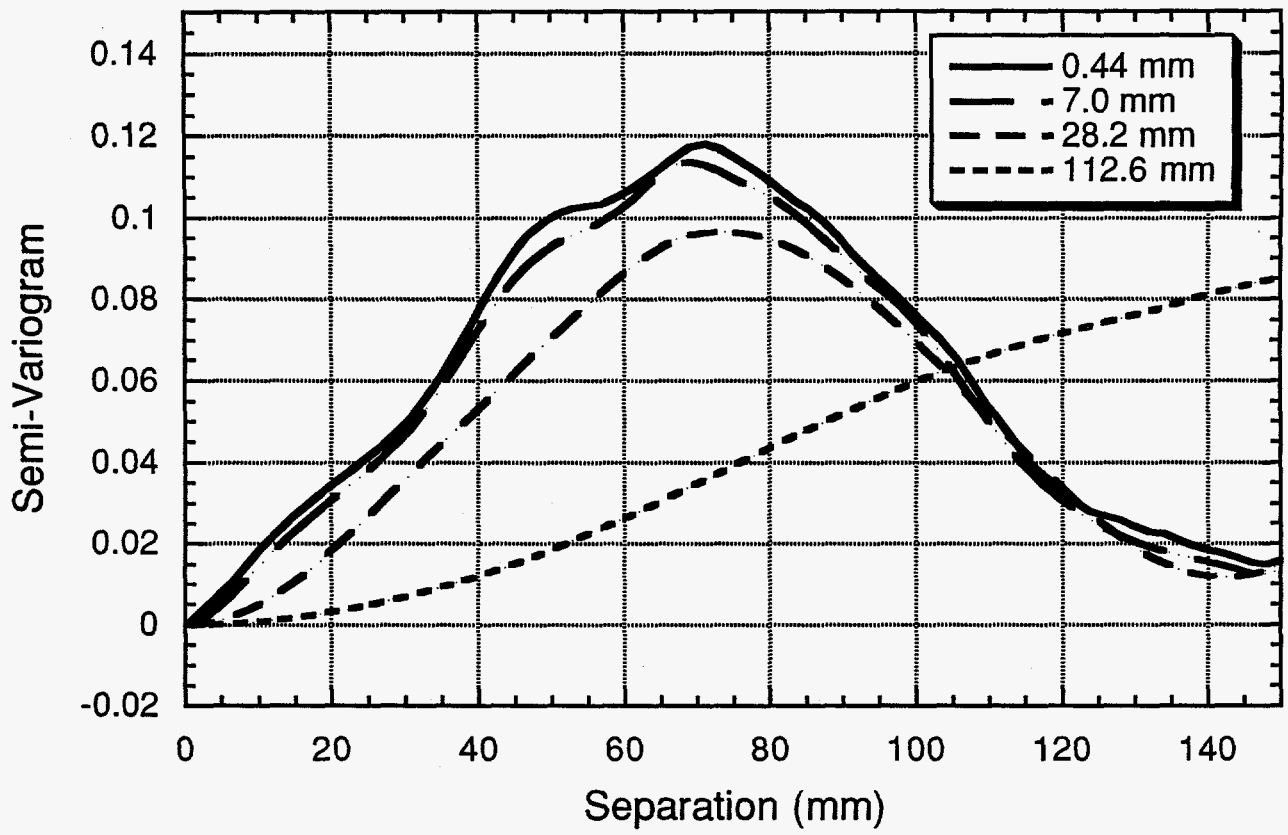
Figure 4.5. Sample semi-variograms measured at each of the four different sample supports.

5. CONCLUSIONS

Because many constitutive rock properties must be measured at one scale but applied at another, scaling behavior is an issue facing the Yucca Mountain site characterization and PA programs. The scaling behavior of gas permeability has been investigated on three rock samples; two blocks of volcanic tuff from Yucca Mountain (Upper Cliff and Caprock microstratigraphic units of the Tiva Canyon Member of the Paintbrush Tuff) and a block of Berea Sandstone. Results of these scaling studies consistently showed the sample mean and variance to decrease as a function of increasing sample support. Conversely, the measured correlation length scale was noted to scale in proportion to the dimension (i.e., diameter) of the sample support. Although each sample exhibited similar up-scaling trends, the rate at which the mean and variance changed as a function of sample support was very different. This difference in up-scaling behavior can be largely attributed to differences in the basic attributes of the samples; specifically, differences in the intensity and basic structure of the permeability fields. Scoping studies aimed at investigating scaling behavior of the unsaturated parameter, sorptivity yielded similar results to that of intrinsic permeability. Of primary interest was whether sorptivity could be used as a surrogate for the more difficult to measure relative permeability and pressure-saturation relation; however, results suggest that such use would meet with little success.

Of significance is the fact that each sample up-scaled qualitatively as our conceptual models predict. In particular, up-scaling behavior was bound by an arithmetic and harmonic averaging process. Unfortunately, results also indicate that statistical moments up-scaled according to arithmetic and harmonic averaging processes may differ by orders of magnitude. Also, noted was the lack of tools with which to quantitatively up-scale permeability between these bounds. However, both the mean and variance for all three samples were found to up-scale according to a power law functional relation. This encouraging result suggests that with additional work, such a functional relation may form the basis for a convenient model by which to up-scale permeability.

Incorporation of up-scaling behavior into PA calculations will require additional work on behalf of YMP participants and other researchers. Specifically, efforts need to continue toward enhancing fundamental understanding of the up-scaling process. Results given in this report indicate the methodology developed here provides a good vehicle for pursuing such understanding and hence should be continued at some level. Concurrently, investigations need to be initiated to investigate up-scaling of fractures and fracture network properties. These studies, in part, can be accomplished by analyzing existing data acquired from pump tests, single-well packer tests, and core plug testing carried out by YMP. Analysis of this multi-scale data integrated with numerical experimentation should provide valuable insight into the up-scaling of fracture network intrinsic permeability. In addition to aiding in the understanding of up-scaling processes, studies of intrinsic permeability scaling (matrix and fracture network) will help lay a foundation from which to investigate more difficult to measure unsaturated properties. In this way, experience and understanding gained from the aforementioned studies will be invaluable in developing a strategy for addressing other properties of interest to YMP.

59

6. REFERENCES

R. Ababou, and E.F. Wood, "Comment on 'Effective Groundwater Model Parameter Values: Influence of Spatial Variability of Hydraulic Conductivity, Leakance, and Recharge,' by J.J. Gomez-Hernandez and S.M. Gorelick, " Water Resources Research, 26(8), pp. 1843-1846 (1990).

R. Ababou, D. McLaughlin, L.W. Gelhar, and A.F.B. Tompson, "Numerical Simulation of Three-Dimensional Saturated Flow in Randomly Heterogeneous Porous Media," Transport in Porous Media, 4(6), pp. 549-565 (1989).

J.L. Anderson, and J. Bouma, "Relationships Between Saturated Hydraulic Conductivity and Morphometric Data of an Argillic Horizon," Soil Society of America Journal, 37(3), pp. 408-413 (1973).

T.B. Anderson, and R. Jackson, "A Fluid Mechanical Description of Fluidized Beds," Industrial and Engineering Chemistry Fundamentals, 6(4), pp. 527-539 (1967).

S. Bachu, and D. Cuthiell, "Effects of Core-Scale Heterogeneity on Steady State and Transient Fluid Flow in Porous Media: Numerical Analysis," Water Resources Research, 26(5), pp. 863-874 (1990).

A.A. Bakr, L.W. Gelhar, A.L. Gutjahr, and J.R. MacMillan, "Stochastic Analysis of Spatial Variability in Subsurface Flows, 1, Comparison of One- and Three-Dimensional Flows," Water Resources Research, 14(2), pp. 263-272 (1978).

C.C. Barton, and E. Larsen, "Fractal Geometry of Two-Dimensional Fracture Networks at Yucca Mountain, Southwestern Nevada," paper presented at the International Symposium on Fundamentals of Rock Joints, Swedish National Group of the International Society of Rock Mechanics, Bjorkliden, Sweden, 15-20 September, Centek Publ., Lulea, Sweden, pp. 77-84 (1985).

P. Baveye, and G. Sposito, "The Operational Significance of the Continuum Hypothesis in the Theory of Water Movement Through Soils and Aquifers," Water Resources Research, 20(5), pp. 521-530 (1984).

J. Bear, and Y. Bachmat, Introduction to Modeling of Transport Phenomena in Porous Media, Kluwer Academic Publishers, Boston, p. 553 (1990).

J. Bear, Dynamics of Fluids in Porous Media, Elsevier Science, New York, p. 764 (1972).

S.H. Begg, and P.R. King, "Modeling the Effects of Shales on Reservoir Performance: Calculation of Effective Vertical Permeability, " SPE 13529 presented at the 1985 SPE Reservoir Simulation Symposium, Dallas, February 10-13, 1985, ed. L.C. Young, pp. 331-344 (1985).

S.H. Begg, D.M. Chang, and H.H. Haldorsen, " A Simple Statistical Method for Calculating the Effective Vertical Permeability of a Reservoir Containing Discontinuous Shales," SPE 14271 presented at the 1985 SPE Reservoir Simulation Symposium, Dallas, September 22-25, 1985 (1985).

J. Bouma, "Use of Soil Survey Data to Select Measurement Techniques for Hydraulic Conductivity," Agricultural Water Management, 6(2-3), pp. 177-190 (1983).

W.F. Brace, "Permeability of Crystalline Rocks: New In Situ Measurements," Journal of Geophysical Research, 89(B6), pp. 4327-4330 (1984).

P.A. Burrough, "Multiscale Sources of Spatial Variation in Soil. I.: The Application of Fractal Concepts to Nested Levels of Soil Variation," Journal of Soil Science, 34(3), pp. 577-597 (1983).

W.T. Cardwell, Jr., and R.L. Parsons, "Average Permeabilities of Heterogeneous Oil Sands," Transactions American Institute of Mining, Metallurgical and Petroleum Engineering, 160, pp. 34-42 (1945).

M.A. Chandler, G. Kocurek, D.J. Goggin, and L.W. Lake, "Effects of Stratigraphic Heterogeneity on Permeability in Eolian Sandstone Sequence, Page Sandstone, Northern Arizona," American Association of Petroleum Geologists Bulletin, 73(5), pp. 658-668 (1989).

I. Clark, "Regularization of a Semi-Variogram," Computers and Geosciences, 3, pp. 341-346 (1977).

I. Clark, Practical Geostatistics, Elsevier Applied Science Publishers, New York (1979).

C. Clauser, "Permeability of Crystalline Rocks," Eos Transactions American Geophysical Union, 73(21), pp. 233, 237-238, May 26 (1992).

P.W.M. Corbett, and J.L. Jensen, "Variation of Reservoir Statistics According to Sample Spacing and Measurement Type for Some Intervals in the Lower Brent Group," The Log Analyst, 33(1), pp. 22-41 (1992).

J.H. Cushman, "On Unifying the Concepts of Scale, Instrumentation, and Stochastics in the Development of Multiphase Transport Theory," Water Resources Research, 20(11), pp. 1668-1676 (1984).

J.H. Cushman, "On Measurement, Scale, and Scaling," Water Resources Research, 22(2), pp. 129-134 (1986).

J.H. Cushman, "An Introduction to Hierarchical Porous Media," Chapter 1, in Dynamics of Fluids in Hierarchical Porous Media, ed. by J.H. Cushman, Academic Press, New York, pp. 1-6 (1990).

G. Dagan, "Models of Groundwater Flow in Statistically Homogeneous Porous Formations," Water Resources Research, 15(1), pp. 47-63 (1979).

G. Dagan, "Analysis of Flow Through Heterogeneous Random Aquifers by the Method of Embedding Matrix 1. Steady Flow," Water Resources Research, 17(1), pp. 107-121 (1981).

G. Dagan, "Analysis of Flow through Heterogeneous Random Aquifers 2. Unsteady Flow in Confined Formations," Water Resources Research, 18(5), pp. 1571-1585 (1982).

G. Dagan, "Statistical Theory of Groundwater Flow and Transport : Pore to Laboratory, Laboratory to Formation, and Formation to Regional Scale," Water Resources Research, 22(9), pp. 120S-134S (1986).

G. Dagan, Flow and Transport in Porous Formations, Springer-Verlag, New York, NY, (1989).

J.M. Davis, R.C. Lohmann, F.M. Phillips, J.L. Wilson, and D.W. Love, "Architecture of the Sierra Ladrones Formation, Central New Mexico: Depositional Controls on the Permeability Correlation Structure," Geological Society of America Bulletin, 105(8), pp. 998-1007 (1993).

J.M. Davis, J.L. Wilson, and F.M. Phillips, "A Portable Air-Minipermeameter for Rapid In-Situ Field Measurements," Ground Water, 32(2), pp. 258-266 (1994).

A.J. Desbarats, "Numerical Estimation of Effective Permeability in Sand-Shale Formations," Water Resources Research, 23(2), pp. 273-286 (1987).

A.J. Desbarats, "Support Effects and the Spatial Averaging of Transport Properties," Mathematical Geology, 21(3), pp. 383-389 (1989).

A.J. Desbarats, "Spatial Averaging of Hydraulic Conductivity in Three-Dimensional Heterogeneous Porous Media," Mathematical Geology, 24(3), pp. 249-267 (1992).

A.J. Desbarats, and S. Bachu, "Geostatistical Analysis of Aquifer Heterogeneity from the Core Scale to the Basin Scale: A Case Study," Water Resources Research, 30(3), pp. 673-684 (1994).

C.V. Deutsch, "Calculating Effective Absolute Permeability in Sandstone/Shale Sequences," SPE Formation Evaluation, 4(3), pp. 343-348 (1989).

R. Dimitrakopoulos, and A.J. Desbarats, "Geostatistical Modeling of Gridblock Permeabilities for 3D Reservoir Simulators," SPE Reservoir Engineering, 8(1), pp. 13-18 (1993).

T. Dreyer, A. Scheie, and O. Walderhaug, "Minipermeameter-Based Study of Permeability Trends in Channel Sand Bodies," AAPG Bulletin, 74(4), pp. 359-374 (1990).

J-P. Duquerroix, P. Lemouzy, B. Noetinger, and R.K. Romeu, "Influence of the Permeability Anisotropy Ratio on Large-Scale Properties of Heterogeneous Reservoirs," in Reservoir Engineering Proceedings, October 3-6, 1993, Houston, TX, SPE 26612 (1993).

L.J. Durlofsky, "Representation of Grid Block Permeability in Coarse Scale Models of Randomly Heterogeneous Porous Media," Water Resources Research, 28(7), pp. 1791-1800 (1992).

B.B. Dykaar and P.K. Kitanidis, "Determination of the Effective Hydraulic Conductivity for Heterogeneous Porous Media Using a Numerical Spectral Approach 1. Method," Water Resources Research, 28(4), pp. 1155-1166 (1992a).

B.B. Dykaar and P.K. Kitanidis, "Determination of the Effective Hydraulic Conductivity for Heterogeneous Porous Media Using a Numerical Spectral Approach 2. Results," Water Resources Research, 28(4), pp. 1167-1178 (1992b).

H. Dykstra and R.L. Parsons, "The Prediction of Oil Recovery by Water Flood," Secondary Recovery of Oil in the United States, 2nd ed., American Petroleum Institute, New York, pp. 160-174 (1950).

R. Eijpe, and K.J. Webber, "Mini-Permeameters for Consolidated Rock and Unconsolidated Sand," American Association of Petroleum Geologists Bulletin, 55(2), pp. 307-309 (1971).

H.I. Ene, "Application of the Homogenization Method to Transport in Porous Media," Chapter VIII, in Dynamics of Fluids in Hierarchical Porous Media, ed. by J.H. Cushman, Academic Press, New York, pp. 225-241 (1990).

A.L. Flint, L.E. Flint, and K.A. Richards, "Evaluation of Measurement Scale Using Imbibition Experiments in Volcanic Tuffs," Soil Science Society of America Journal, 58, pp. 94-102 (1994).

R.A. Freeze, "A Stochastic-Conceptual Analysis of One-Dimensional Groundwater Flow in Nonuniform Homogeneous Media," Water Resources Research, 11(5), pp. 724-741 (1975).

C.M. Fuller and J.M. Sharp, Jr., "Permeability and Fracture Patterns in Extensive Volcanic Rocks: Implication from the Welded Santana Tuff, Trans-Pecos Texas," Geological Society of America Bulletin, 104, pp. 1485-1496 (1992).

L.W. Gelhar, and C.L. Axness, "Three-Dimensional Stochastic Analysis of Macrodispersion in Aquifers," Water Resources Research, 19(1), pp. 161-180 (1983).

L.W. Gelhar, "Stochastic Subsurface Hydrology from Theory to Applications," Water Resources Research, 22(9), pp. 135S-145S (1986).

L.W. Gelhar, Stochastic Subsurface Hydrology, Prentice-Hall, Englewood Cliffs, New Jersey, p. 390 (1993).

R.M. Giordano, S.J. Salter, and K.K. Mohanty, "The Effects of Permeability Variations on Flow in Porous Media," SPE 14365, presented at the 60th Annual Technical Conference, September 22-25, 1985, Las Vegas (1985).

Glass, R.J., V.C. Tidwell, A.L. Flint, W. Peplinski, and Y. Castro, Fracture-matrix interaction in Topopah Spring Tuff: Experiment and numerical analysis, Proceedings of the Fifth Annual International High Level Radioactive Waste Management Conference, May 22-26,1994, Las Vegas, NV, 4, pp. 1905-1914 (1994).

D.J. Goggin, M.A. Chandler, G.A. Kocurek, and L.W. Lake, "Patterns of Permeability in Eolian Deposits: Page Sandstone (Jurassic), Northeastern Arizona," Society of Petroleum Engineers Formation Evaluation, 3, pp. 297-306 (1986).

D.J. Goggin, R.L. Thrasher, and L.W. Lake, "A Theoretical and Experimental Analysis of Minipermeameter Response Including Gas Slippage and High Velocity Flow Effects," In Situ, 12(1-2), pp. 79-116 (1988).

J.J. Gomez-Hernandez, and S.M. Gorelick, "Effective Groundwater Model Parameter Values: Influence of Spatial Variability of Hydraulic Conductivity, Leakance, and Recharge," Water Resources Research, 25(3), pp. 405-419 (1989).

A.L. Gutjahr, L.W. Gelhar, A.A. Bakr, and J.R. Macmillan, "Stochastic Analysis of Spatial Variability in Subsurface Flows, 2, Evaluation and Application," Water Resources Research, 14(5), pp. 953-960 (1978).

H.H. Haldorsen, "Simulator Parameter Assignment and the Problem of Scale in Reservoir Engineering," in Reservoir Characterization, ed. by L.W. Lake and H.B. Carroll, Jr., pp. 293-340 (1986).

H.H. Haldorsen and L.W. Lake, "A New Approach to Shale Management in Field-Scale Models," Society of Petroleum Engineers Journal, 24(4), pp. 447-457 (1984).

J.S. Hanor, "Effective Hydraulic Conductivity of Fractured Clay Beds at a Hazardous Waste Landfill, Louisiana Gulf Coast," Water Resources Research, 29(11), pp. 3691-3698 (1993).

63

M. Hassanizadeh, and W.G. Gray, "General Conservation Equations for Multi-phase Systems, 1, Averaging Procedure," Advances in Water Resources, 2(3), pp. 131-144 (1979).

A. Henriette, C.G. Jacquin, and P.M. Adler, "The Effective Permeability of Heterogeneous Porous Media," PCH PhysicoChemical Hydrodynamics, 11(1), pp. 63-80 (1989).

K.M. Hess, S.H. Wolf, M.A. Celia, and S.P. Garabedian, "Macrodispersion and Spatial Variability of Hydraulic Conductivity in a Sand and Gravel Aquifer, Cape Cod, Massachusetts," EPA/600/M-91/005, Environmental Research Brief, Environmental Protection Agency, Ada, OK (1991).

T.A. Hewett, "Fractal Distributions of Reservoir Heterogeneity and their Influence on Fluid Transport," SPE 15386, in 61st Annual Technical Conference and Exhibition of the Society of Petroleum Engineers, New Orleans, Louisiana, October 5-8, 1986, Society of Petroleum Engineers, Richardson, TX (1986).

E.L. Hinrichsen, A. Aharony, J. Feder, A. Hansen, T. Jossang, and H.H. Hardy," A Fast Algorithm for Estimating Large-Scale Permeabilities of Correlated Anisotropic Media," Transport in Porous Media, 12(1), pp. 55-72 (1993).

P. Indelman and B. Abramovich, "A Higher-Order Approximation to Effective Conductivity in Media of Anisotropic Random Structure," Water Resources Research, 30(6), pp. 1857-1864 (1994).

P. Indelman, and G. Dagan, "Upscaling of Permeability of Anisotropic Heterogeneous Formations 1. The General Framework," Water Resources Research, 29(4), pp. 917-923 (1993).

E.H. Isaaks, and R.M. Srivastava, An Introduction to Applied Geostatistics, Oxford University Press, New York, p. 561 (1989).

J.L. Jensen, "Use of the Geometric Average for Effective Permeability Estimation," Mathematical Geology, 23(6), pp. 833-840 (1991).

S.C. Jones, "A Rapid Accurate Unsteady-State Klinkenberg Permeameter," Society of Petroleum Engineers Journal, 12(5), pp. 385-397 (1972).

S.C. Jones, "The Profile Permeameter -- A New, Fast, Accurate Minipermeameter," SPE 24757, in Formation Evaluation and Reservoir Geology Proceedings, Proceedings of the 67th Annual SPE Conference and Exhibition, October 4-7, 1992, Washington, D.C., pp. 973-983 (1992).

G.A. Journel, and C.J. Huijbregts, Mining Geostatistics, Academic Press, New York, p. 600 (1978).

G.A. Journel, C.V. Deutsch , and A.J. Desbarats, "Power Averaging for Block Effective Permeability," SPE 15128, in Proceeding of the 56th Annual California Regional Meeting of the Society of Petroleum Engineers, Oakland, April 2-3, 1986, pp. 329-334 (1986).

E. Kasap and L.W. Lake, "Calculating the Effective Permeability Tensor of a Gridblock," SPE Formation Evaluation, 5(2), pp. 192-200 (1990).

A.J. Katz, and A.H. Thompson, "Fractal Sandstone Pores: Implications for Conductivity and Pore Formation," Physical Review Letters, 54(12), pp. 1325-1328 (1985).

C.K. Keller, G. van der Kamp, and J.A. Cherry, "A Multiscale Study of the Permeability of a Thick Clayey Till," Water Resources Research, 25(11), pp. 2299-2317 (1989).

R.W.D. Killey, and G.L. Moltyaner, "Twin Lake Tracer Tests: Setting, Methodology, and Hydraulic Conductivity Distribution," Water Resources Research, 24(10), pp. 1585-1612 (1988).

P.R. King, "The Use of Renormalization for Calculating Effective Permeability," Transport in Porous Media, 4(1), pp. 37-58 (1989).

P.K. Kitanidis, "Effective Hydraulic Conductivity for Gradually Varying Flow," Water Resources Research, 26(6), pp. 1197-1208 (1990).

M.G. Kittridge, L.W. Lake, F.J. Lucia, and G.E. Fogg, "Outcrop/Subsurface Comparisons of Heterogeneity in the San Andres Formation," SPE Formation Evaluation, 5(3), pp. 233-240 (1990).

L.J. Klinkenberg, "The Permeability of Porous Media to Liquids and Gases," API Drilling and Production Practice, pp. 200-213 (1941).

C.A. Kossack, J.O. Aasen, and S.T. Opdal, "Scaling Up Heterogeneities with Pseudofunctions," SPE Formation Evaluation, 5(3), pp. 226-232 (1990).

T.J. Lasseter, J.R. Waggoner, and L.W. Lake, "Reservoir Heterogeneities and their Influence on Ultimate Recovery," in Reservoir Characterization, ed. by L.W. Lake and H.B. Carroll, Jr., pp. 545-560 (1986).

G. Le Loc'h, "An Efficient Strategy for Combining the Permeabilities. Practical Application on a Simulated Reservoir," Third International Geostatistics Conference, Avingon, September 5-9, 1988, ed. by M. Armstrong, Kluwer Academic Press, Dordrecht, Netherlands, 2, pp. 557-568 (1989).

G. Matheron, Elements Pour Une Theorie des Mileux Poreux, Masson et Cie, Paris (1967).

S.A. McKenna and C.A. Rautman, Scaling of Properties for Yucca Mountain: Literature Review and Numerical Experiments on Saturated Hydraulic Conductivity, SAND95-2338, Sandia National Laboratories, Albuquerque, NM (1996).

C.C. Mei, and J.L. Auriault, "Mechanics of Heterogeneous Porous Media with Several Spatial Scales," Proceedings of the Royal Society of London, Series A, A426(1871), pp. 391-423 (1989).

S. Mohanty and M.M. Sharma, "A Recursive Method for Estimating Single and Multiphase Permeabilities," Proceeding of the 65th Annual Technical Conference and Exhibition of the Society of Petroleum Engineers, New Orleans, September 23-26, 1990, Society of Petroleum Engineers, Richardson, TX, pp. 9-18 (1990).

F.J. Molz, O. Guven, J.G. Melville and C. Cardone, "Hydraulic Conductivity Measurement at Different Scales and Contaminant Transport Modeling," Chapter III, in Dynamics of Fluids in Hierarchical Porous Media, ed. by J.H. Cushman, Academic Press, New York, pp. 37-59 (1990).

S. P. Neuman, "Universal Scaling of Hydraulic Conductivities and Dispersivities in Geologic Media," Water Resources Research, 26(8), pp. 1749-1758 (1990).

S. P. Neuman, "Generalized Scaling of Permeabilities: Validation and Effect of Support Scale," Geophysical Research Letters, 21(5), pp. 349-353 (1994).

H. Parker, "The Volume Variance Relationship: A Useful Tool for Mine Planning," in Geostatistics, ed. by P. Mousset-Jones, pp. 61-91, McGraw Hill, New York (1979).

J.C. Parker, and K.A. Albrecht, "Sample Volume Effects on Solute Transport Predictions," Water Resources Research, 23(12), pp. 2293-2301 (1987).

J.R. Philip, Numerical solution of equations of the diffusion type with diffusivity concentration-dependent, Journal of the Chemical Society, Faraday Transactions, 51, 885-892, 1955.

A.R. Piggott, and D. Elsworth, "Analytical Models for Flow Through Obstructed Domains," Journal of Geophysical Research, 97(B2), pp. 2085-2093 (1992).

C.A. Rautman and T.H. Robey, "Recent Developments in Stochastic Modeling and Upscaling of Hydrologic Properties in Tuff," in Proceedings of the Fourth Annual International High Level Radioactive Waste Management Conference, April 26-30, 1994, Las Vegas, Nevada, pp. 1437-1445 (1993).

Y. Rubin, and J.J. Gomez-Hernandez, "A Stochastic Approach to the Problem of Upscaling of Conductivity in Disordered Media: Theory and Unconditional Numerical Simulations," Water Resources Research, 26(4), pp. 691-701 (1990).

B. Sapoval, M. Rosso, and J.F. Gouyet, "The Fractal Nature of a Diffusion Front and the Relation to Percolation," Journal of Physics Letters, 46(4), pp. L149-L156 (1985).

R.B. Scott, and J. Bonk, "Preliminary Geologic Map of Yucca Mountain, Nye County, Nevada, with Geologic Sections," U.S. Geological Survey Open-File Report 84-494 (1984).

J.M. Sharp, Jr., L. Fu, P. Cortez, and E. Wheeler, "An Electronic Minipermeameter for Use in the Field and Laboratory," Ground Water, 32(1), pp. 41-46 (1994).

J.B. Sisson, and P.J. Wierenga, "Spatial Variability of Steady-State Infiltration Rates as Stochastic Processes," Soil Science Society of America Journal, 45, pp. 699-704 (1981).

M.A. Suboor, The Operating Characteristics of Minipermeameter and its Ability to Investigate the Small Scale Permeability Heterogeneity, M.S. Thesis, New Mexico Institute of Mining and Technology, Socorro, NM, p. 115 (1994).

V.C. Tidwell, "Scaling Behavior of Gas Permeability Measurements in Volcanic Tuffs," in Proceedings of the Fifth Annual International High-Level Radioactive Waste Management Conference, May 22-26, 1994, Las Vegas, Nevada, 4, pp. 2500-2509 (1994a).

V.C. Tidwell, "Laboratory Investigation of Constitutive Property Scaling Behavior," SPE 28456, Proceedings of the 1994 SPE Annual Technical Conference and Exhibition, New Orleans, September 25-28, pp. 947-957 (1994b).

V.C. Tidwell and R.J. Glass, "X-ray and visible light transmission for laboratory measurement of two-dimensional saturation fields in thin-slab systems," Water Resources Research, 30(11), pp. 2873-2882, 1994.

V.C. Tidwell, J.D. VonDoemming, and K. Martinez, "Scale Dependence of Effective Media Properties," Proceeding of the 1993 Annual International High Level Radioactive Waste Management Conference, Las Vegas, Nevada, April 26-30, 1, pp. 1059-1065 (1993).

A.F.B. Tompson, and W.G. Gray, "A Second-Order Approach for the Modeling of Dispersive Transport in Porous Media 1. Theoretical Development," Water Resources Research, 22(5), pp. 591-599 (1986).

J.E. Warren, and H.S. Price, "Flow in Heterogeneous Porous Media," Society of Petroleum Engineering Journal, 1, pp. 153-169 (1961).

S.W. Wheatcraft, and S.W. Tyler, "An Explanation of Scale-Dependent Dispersivity in Heterogeneous Aquifers Using Concepts of Fractal Geometry," Water Resources Research, 24(4), pp. 566-578 (1988).

S. Whitaker, "Diffusion and Dispersion in Porous Media," AIChE Journal, 13(3), pp. 420-427 (1967).

M.L. Wilson, J.H. Gauthier, R.W. Barnard, G.E. Barr, H.A. Dockery, E. Dunn, R.R. Eaton, D.C. Guerin, N. Lu, M.J. Martinez, R. Nilson, C.A. Rautman, T.H. Robey, B. Ross, E.E. Ryder, A.R. Schenker, S.A. Shannon, L.H. Skinner, W.G. Halsey, J.D. Gansemer, L.C. Lewis, A.D. Lamont, I.R. Triay, A. Meijer, and D.E. Morris, Total-System Performance Assessment for Yucca Mountain - SNL Second Iteration (TSPA 1993), Volume 1, SAND93-2675, Sandia National Laboratories, Albuquerque, NM (1994).

G.R. Young, Determining Permeability Anisotropy from a Core Plug Using a Minipermeameter, M.S. Thesis, University of Texas, Austin, TX, p. 118 (1989).

R.W. Zimmerman, G.S. Bodvarsson, A.L. Flint, and L.E. Flint, "An inverse procedure for estimating the unsaturated hydraulic conductivities of volcanic tuffs", Proceedings of the Fourth Annual International High Level Radioactive Waste Management Conference, April 26-30, 1993, Las Vegas, NV, 1, pp. 1052-1058 (1993).

YUCCA MOUNTAIN SITE CHARACTERIZATION PROJECT
UC814 - DISTRIBUTION LIST
SAND95-1888

1   D. A. Dreyfus (RW-1)
Director
OCRWM
US Department of Energy
1000 Independence Avenue SW
Washington, DC 20585

1   L. H. Barrett (RW-2)
Acting Deputy Director
OCRWM
US Department of Energy
1000 Independence Avenue SW
Washington, DC 20585

1   S. Rousso (RW-40)
Office of Storage and Transportation
OCRWM
US Department of Energy
1000 Independence Avenue SW
Washington, DC 20585

1   R. A. Milner (RW-30)
Office of Program Management
   and Integration
OCRWM
US Department of Energy
1000 Independence Avenue SW
Washington, DC 20585

1   D. R. Elle, Director
Environmental Protection Division
DOE Nevada Field Office
US Department of Energy
P.O. Box 98518
Las Vegas, NV 89193-8518

1   T. Wood (RW-14)
Contract Management Division
OCRWM
US Department of Energy
1000 Independence Avenue SW
Washington, DC 20585

4   Victoria F. Reich, Librarian
Nuclear Waste Technical Review Board
1100 Wilson Blvd., Suite 910
Arlington, VA 22209

1   Wesley Barnes, Project Manager
Yucca Mountain Site Characterization
   Office
US Department of Energy
P.O. Box 98608--MS 523
Las Vegas, NV 89193-8608

1   Director, Public Affairs Office
c/o Technical Information Resource Center
DOE Nevada Operations Office
US Department of Energy
P.O. Box 98518
Las Vegas, NV 89193-8518

8   Technical Information Officer
DOE Nevada Operations Office
US Department of Energy
P.O. Box 98518
Las Vegas, NV 89193-8518

1   J. R. Dyer, Deputy Project Manager
Yucca Mountain Site Characterization Office
US Department of Energy
P.O. Box 98608 -- MS 523
Las Vegas, NV 89193-88608

1   M. C. Brady
Laboratory Lead for YMP
M&O/Sandia National Laboratories
1261 Town Center Drive
Bldg. 4, Room 421A
Las Vegas, NV 89134

1   J. A. Canepa
Laboratory Lead for YMP
EES-13, Mail Stop J521
M&O/Los Alamos National Laboratory
P.O. Box 1663
Los Alamos, NM 87545

1   Repository Licensing & Quality
   Assurance
Project Directorate
Division of Waste Management, MS T7J-9
US NRC
Washington, DC 20555

1   Senior Project Manager for Yucca
   Mountain
Repository Project Branch
Division of Waste Management, MS T7J-9
US NRC
Washington, DC 20555

1   NRC Document Control Desk
Division of Waste Management, MS T7J-9
US NRC
Washington, DC 20555

1	Chad Glenn NRC Site Representative 301 E Stewart Avenue, Room 203 Las Vegas, NV 89101		1	B. T. Brady Records Specialist US Geological Survey MS 421 P.O. Box 25046 Denver, CO 80225

1   Chad Glenn
NRC Site Representative
301 E Stewart Avenue, Room 203
Las Vegas, NV 89101

1   Center for Nuclear Waste
Regulatory Analyses
Southwest Research Institute
6220 Culebra Road
Drawer 28510
San Antonio, TX 78284

2   W. L. Clarke
Laboratory Lead for YMP
M&O/ Lawrence Livermore Nat'l Lab
P.O. Box 808 (L-51)
Livermore, CA 94550

1   Robert W. Craig
Acting Technical Project Officer/YMP
US Geological Survey
101 Convention Center Drive, Suite P-110
Las Vegas, NV 89109

1   J. S. Stuckless, Chief
Geologic Studies Program
MS 425
Yucca Mountain Project Branch
US Geological Survey
P.O. Box 25046
Denver, CO 80225

1   L. D. Foust
Technical Project Officer for YMP
TRW Environmental Safety Systems
101 Convention Center Drive
Suite P-110
Las Vegas, NV 89109

1   A. L. Flint
U. S. Geological Survey
MS 721
P. O. Box 327
Mercury, NV 89023

1   Robert L. Strickler
Vice President & General Manager
TRW Environmental Safety Systems, Inc.
2650 Park Tower Dr.
Vienna, VA 22180

1   Jim Krulik, Geology Manager
US Bureau of Reclamation
Code D-8322
P.O. Box 25007
Denver, CO 80225-0007

1   B. T. Brady
Records Specialist
US Geological Survey
MS 421
P.O. Box 25046
Denver, CO 80225

1   M. D. Voegele
Deputy of Technical Operations
M&O/SAIC
101 Convention Center Drive
Suite P-110
Las Vegas, NV 89109

2   A. T. Tamura
Science and Technology Division
OSTI
US Department of Energy
P.O. Box 62
Oak Ridge, TN 37831

1   P. J. Weeden, Acting Director
Nuclear Radiation Assessment Div.
US EPA
Environmental Monitoring Sys. Lab
P.O. Box 93478
Las Vegas, NV 89193-3478

1   John Fordham, Deputy Director
Water Resources Center
Desert Research Institute
P.O. Box 60220
Reno, NV 89506

1   The Honorable Jim Regan
Chairman
Churchill County Board of
  Commissioners
10 W. Williams Avenue
Fallon, NV 89406

1   R. R. Loux
Executive Director
Agency for Nuclear Projects
State of Nevada
Evergreen Center, Suite 252
1802 N. Carson Street
Carson City, NV 89710

1   Brad R. Mettam
Inyo County Yucca Mountain
  Repository Assessment Office
P. O. Drawer L
Independence, CA 93526

1   Vernon E. Poe
Office of Nuclear Projects
Mineral County
P.O. Box 1600
Hawthorne, NV 89415

1	Les W. Bradshaw Program Manager Nye County Nuclear Waste Repository Project Office P.O. Box 1767 Tonopah, NV 89049
1	Florindo Mariani White Pine County Coordinator P. O. Box 135 Ely, NV 89301
1	Tammy Manzini Lander County Yucca Mountain Information Officer P.O. Box 10 Austin, NV 89310
1	Jason Pitts Lincoln County Nuclear Waste Program Manager P. O. Box 158 Pioche, NV 89043
1	Dennis Bechtel, Coordinator Nuclear Waste Division Clark County Dept. of Comprehensive Planning P.O. Box 55171 Las Vegas, NV 89155-1751
1	Juanita D. Hoffman Nuclear Waste Repository Oversight Program Esmeralda County P.O. Box 490 Goldfield, NV 89013
1	Sandy Green Yucca Mountain Information Office Eureka County P.O. Box 714 Eureka, NV 89316
1	Economic Development Dept. City of Las Vegas 400 E. Stewart Avenue Las Vegas, NV 89101
1	Community Planning & Development City of North Las Vegas P.O. Box 4086 North Las Vegas, NV 89030
2	Librarian YMP Research & Study Center 101 Convention Center Drive, Suite P-110 Las Vegas, NV 89109

1	Library Acquisitions Argonne National Laboratory Building 203, Room CE-111 9700 S. Cass Avenue Argonne, IL 60439
1	Glenn Van Roekel Manager, City of Caliente P.O. Box 158 Caliente, NV 89008
1	G. S. Bodvarsson Head, Nuclear Waste Department Lawrence Berkeley National Laboratory 1 Cyclotron Road, MS 50E Berkeley, CA 94720
1	Steve Hanauer (RW-2) OCRWM U. S. Department of Energy 1000 Independence Ave. Washington, DC 20585

	MS	
2	1330	B. Pierson, 6811 100/12546/SAND95-1888/QA
20	1330	WMT Library, 6752
1	9018	Central Technical Files, 8523-2
5	0899	Technical Library, 4414
2	0619	Review and Approval Desk, 12630, For DOE/OSTI
1	1324	Peter Davies, 6115
1	1326	Holly Dockery, 6312
10	1324	Vincent Tidwell, 6115